Abstract

Title of dissertation: **MULTIDIMENSIONAL MICROFLUIDIC BIOSEPARATION SYSTEMS WITH SPATIAL MULTIPLEXING**

Shuang Yang, Doctor of Philosophy, 2008

Directed By: **Professor Donald DeVoe**
Department of Mechanical Engineering

Despite the refinement of liquid chromatography and peptide mass fingerprinting techniques for protein analysis, two-dimensional polyacrylamide gel electrophoresis (2-D PAGE) separations of intact proteins remain a core technology for proteomic studies due to their high peak capacities and resolving power. In 2-D PAGE, denatured intact proteins are separated on the basis of their charge state by isoelectric focusing (IEF), followed by a size-based separation using sodium dodecyl sulfate (SDS)-PAGE. While 2-D PAGE is most commonly practiced with backend analysis of proteins by mass spectrometry, 2-D PAGE expression maps alone can provide valuable insight for differential studies, including the analysis of post-translational modifications, by yielding information about the approximate isoelectric point (pI) and molecular weight (MW) of differentially expressed species within complex samples.

However, conventional slab-gel 2-D PAGE remains a labor intensive and low throughput process, which significantly constrains its utility. In this dissertation, a novel microfluidic 2-D PAGE platform is developed which employs a combination of multifunctional photopolymerized polyacrylamide (PAAm) gels and a discontinuous sodium dodecyl sulfate (SDS)-PAGE buffer system. The PAAm gel is used as a highly-

resolving separation medium for gel electrophoresis, while discrete PAAm gel plugs integrated into specific regions of the chip enable acid, base, and ampholyte solutions to be fully isolated prior to chip operation. The gel plugs allow different separation buffers to be stored within the chip, enabling the use of a discontinuous buffer system chosen to provide sample stacking during the second-dimension separation. The gel plugs are also employed as on-chip SDS containers, allowing defined volumes of SDS to be repeatably injected and complexed with the IEF-focused proteins, without the need for external intervention. The IEF channel itself possesses an angled geometry to minimize sample tailing, and the chip design employs backbiasing channels which eliminate sample leakage and enable uniform sample transfer between the separation dimensions. Validation of the full 2-D system is presented using fluorescently-labeled *E. coli* cell lysate as a model system.

**MULTIDIMENSIONAL MICROFLUIDIC BIOSEPARATION SYSTEMS
WITH SPATIAL MULTIPLEXING**

By

Shuang Yang

Dissertation submitted to the Faculty of the Graduate School of the
University of Maryland, College Park, in partial fulfillment
of the requirements for the degree of
Doctor of Philosophy
2008

Advisory Committee:

Associate Professor Donald DeVoe
Associate Professor Patrick McCluskey
Professor Gary Rubloff
Associate Professor Peter Sandborn
Assistant Professor Miao Yu

Dedication

To my wife and my sons, Zeren and Arthur, for their support and encouragement in this endeavor

To my parents for caring for this scholarly pursuit

Acknowledgements

I would like to thank my advisor, Dr. Don DeVoe, for his endeavor support and tremendous help during the course of my PhD pursuit. His open-mind way of thinking and his profound knowledge on microfluidic and analytical bio-chemistry turn me from a layman to an expert in this field. Without his advises, this research cannot be accomplished.

I thank Dr. Jikun Liu, Dr. Chia-wen Tsao, Dr. Chieu-Fu Chen, Chenren Shao, Dr. Lou Hromada, Dr. Yi Zhou, Dr. Likun Zhu, Dr. Parshant Kumar, Chun-fei Kung and Dr. Song Tao to help my experiment and research. Their suggestion and comments are significant during my course of Ph.D.

I thank my wife, Qiaoying Shen, with love for her endless support to me. With family burdened on her, I am able to fully focusing on research. Without her, I cannot go this far and achieve my goal. My lovely sons, Cliff and Arthur, are my motivation to conquer this goal to beyond.

List of Tables

List of Figures

Table of Contents

Chapter 1.   Introduction

Since the microfluidic system, or micro-total-analysis system (μ-TAS), was proposed in early 1990's,[1] the tremendous progress have been made as an analytical tool for biochemistry,[2-4] chemistry,[5] biology,[6-8] physics,[9] environmental science,[10] forensics,[11,12] and medicine.[13] Microfluidic system is small and monolithic in nature with a variety of functions built-in, such as sample cleaning-up,[14,15] pre-concentration,[16-18] mixing,[19] reaction[20,21] and separation.[22] It offers a great benefit to carry out multi-functions in a portable device with a reasonable price. Combination with other advantages,[23] microfluidic system is one of the popular bioanalytical tools.

1.1   Microfluidic 2D Separation

Microfluidic device, or chip, has been fabricated on different type of substrate materials, such as silicon, glass, and quartz.[24,25] These materials can be processed by mature silicon-based fabrication technologies for standard mass-production. They are dominant substrate materials for chip in the early 1990's due to their well-characterized surface modification chemistries, electroosmotic flow (EOF) profiles, and non-specific adsorption property on the fused silica materials.[26] Additionally, these materials possess favorable optical and thermal properties, facilitating signal detection and minimizing Joule heating during isoelectric focusing and gel electrophoresis separations.[27,28]

Polymer becomes the favorite substrate materials for chips due to a variety of advantages,[29] such as cost-effective fabrication and low material cost.[30] In general, polymer chip can be fabricated by hot embossing,[31] injection molding,[32] laser ablation,[33] and casting.[30,34] For example, hundreds of polymer chips can be fabricated using a single silicon-based template through imprinting with negligible replication error. The chemical

and optical properties of the polymer surface are tunable through modifying its macromolecular structure. For instance, polymer surfaces can be activated by high energy source, such as plasma or ultra-violet (UV)-ozone, and modified by covalently binding silane functional group onto surface, similar procedure as glass substrate surface treatment.[35-39] Additional coating layers can be performed on the top of the silanized surface so that the active acrylic groups are covalently bonded to the polymer surface for development of the desired polymer coating. Ultimately, the EOF on polymer surface is suppressed or enhanced by selecting the appropriate coating materials.[40]

The polymer chip has been used for one-dimensional and/or multidimensional separation device in the past decade.[30,35-39,41] Examples of one-dimensional separation are capillary electrophoresis (CE),[24,42] open channel CE,[43] micellar electrokinetic chromatography (MEKC),[44,45] isoelectric focusing (IEF),[46,47] and sodium dodecyl sulfate (SDS) - capillary gel electrophoresis (CGE).[47,48] However, one dimensional separation is unable to detect all species of complicated samples. For example, IEF separation cannot detect the proteins with identical pI values (isomer) but different molecular weight, and vice versa. Two-dimensional or multidimensional separation mechanisms are thus necessary in many instances. A lot of studies investigate two-dimensional separation, such as IFE-CGE,[49,50] IEF-SDS polyacrylamide gel electrophoresis (PAGE),[51] IEF-CE,[52] Membrane-CGE,[53] and CGE-MEKC.[54] The extremely high resolving power is achieved using the two-dimensional separation techniques, which make cell lysate analysis possible with over 10,000 peak capacity of slab-gel basis 2D-PAGE.

1.2   Motivation
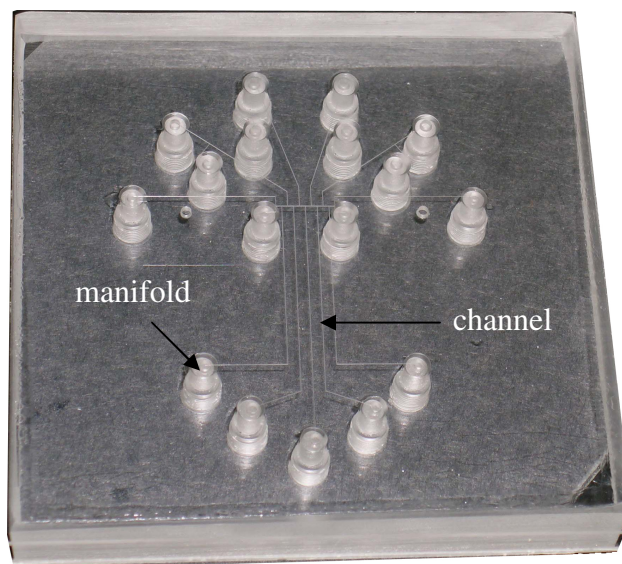
Figure 1. The image of a five-channel chip using manifold to control individual reservoirs. The manifold is sandwiched between two glass plates. The chip is made up of polycarbonate (PC) plastic.

Many multidimensional separation techniques are carried out in a serial fashion.[52,55,56] The second dimension separation is serially processed after the first dimensional separation, in which each separated bond in the first dimension is eluted one after another to the second dimension. As a result, the resolution of focused bands in the first dimension is losing while the transferred bond separates in the second dimension. The serial technique is also time-consuming and difficult for manipulation. The parallel separation approach[49,50] is studied for protein separation using IEF as the first dimension and parallel SDS gel electrophoresis as the second dimension. Griebel et al.[50] used immobilized-pH gradient (IPG) to separate the protein bands in the first dimension, and offline transferred the focused bands into the second dimension for SDS-CGE. Li et al.[49] adapted both gel and free solution IEF for the first dimension protein separation, and

online transferred the focused bands for SDS-CGE. Although the separation performance is inferior to the traditional slab-gel 2-D PAGE,[57] the separation time has been significantly decreased from several days to less than one hour and the level of system automation is greatly improved.

Several issues exist on current IEF-SDS/CGE platform. The most critical issue is how to control hydrodynamic bulk flow between the replaceable gel matrix and sample and/or buffer. Moreover, the diffusion between gel matrix and sample and/or buffer further deteriorates the separation performance. For example, 1.5% (wt) polyethylene oxide (PEO) was used as sieving matrix and conductive medium in 2-D design;[49] the low viscosity of PEO can easily diffuse into sample, or vice versa. Any hydrodynamic pressure disturbance between reservoirs can intrude PEO into IEF channel. To minimize these effects, one has to use manifold or other mechanical valves to achieve complete sealing of individual reservoirs (Figure 1).[58] The chip design becomes complex for high density of microfluidic system, not mention to the spacing occupied by manifold self. Similarly, it is difficult to prevent hydrodynamic bulk flow between acid/base tank and sample/buffer, especially for IEF separation in carrier ampholyte solution. Any disturbance of acid/base reservoir electrolyte and buffer will cause catastrophic failure of IEF separation, or at least deteriorate the separation performance. Additionally, the gel used has to be uniform and homogeneous, since gel solution may degrade after storage for a while.[59] For example, the white crystal materials can be observed in PEO in Tris-2-(Cyclohexylamino) ethanesulfonic acid (Tris-CHES) solution, which does not appear in freshly prepared solution. In addition, the chip design must be optimized to provide for uniform sample injection, asymmetric sample transfer and free of leakage. The other key

feature includes development of a gel system providing excellent resolving power and completely preventing hydrodynamic bulk flow. It is impossible to obtain the reproducible and high performance of 2-D mapping without digging in these issues.

1.3 Approach

In order to develop a chip with feasible matrix for 2-D separation, the suitable gel matrix should be capable of pressure-blocking via high viscosity or crosslinked structure, and high resolving power. The gel used should thus meet these criteria: a high-resolving power separation based on protein pI and molecular weight; a well-defined interface between gel and buffer. To this end, permanent gel and replaceable gel are investigated, and permanent gel will be used as pseudo valves for the latter case. The second objective is to develop the short gel plug for pressure-blocking between acid/base and IEF sample. These short gel plugs can prevent the hydrodynamic bulk flow during IEF separation. The gel plug is conductive so that it allows protons and hydroxides electrokinetically transport through in a short period of time.

This dissertation demonstrates a successful microfluidic 2D-IEF/CGE separation on complex protein samples. 1-D microfluidic IEF and CGE will be investigated respectively to better serve as their coupling. The factors such as chip surface property, gel interface, EOF, sidewall roughness etc will be considered. Because the surface property of polymer is an essential property for chip bonding strength, protein adsorption and EOF, surface modification will be extensively studied. The permanent surface coating is thus developed to provide strong sidewall adhesion, suppress EOF and minimize protein adsorption.

The microfluidic design is simulated using PSpice[60] and FEMLab[61] software for electrical current distribution and sample transfer. The analytical model is derived for electrical distribution. The optimized microfluidic design allows asymmetrically uniform sample injection, free of sample leakage and minimized tailing. The optimized design based on simulation will be validated by experimental work.

1.4   Dissertation Organization

The dissertation consists of nine chapters. Chapter 2 briefly reviews microfluidic relevant issues such as chip material, polymer chip surface modification, 2-D separation technique and its platform, and injection simulation. Chapter 3 describes the device fabrication process, which consists of chip milling, surface activation and modification, sidewall coating, and chip thermal bonding; additionally, photopolymerized crosslinked polyacrylamide gel fabrication is illustrated in detail. Imprinting techniques are also compared with chip milling fabrication. Chapter 4 discusses the chip design requirements for 1-D IEF, 1-D CGE and 2-D IEF-CGE separation platforms. The chip design use of replaceable gel is extensively discussed in Chapter 5, demonstrating IEF protein preparation using gel plug and 2-D IEF-CGE on FITC-labeled *E.coli* cell lysate. The drawbacks in this separation design are discussed and proposed improvement is given in Chapter 6. The proposed design is able to symmetrical sample transfer uniformly without leakage and with minimized tailing. The following chapter uses this design feature for 2-D PAGE, in which a multifunctional PAAm gel plug is used for pressure-blocking, ion-packet, buffer-container and sieving matrix. The chip density can be easily upgraded up to 64 channels in a 100 mm x 100 mm chip dimension. The *E.coli* 2-D PAGE is demonstrated using this novel 2-D platform. To achieve better separation performance,

optimization of chip design and gel matrix will be performed in the future (Chapter 8). In addition, the 3rd-D of LDI or MALDI-MS will be coupled to 2-D PAGE for protein identification.

Chapter 2.   Literature Review

Microfluidic system has been intensively studied since 1990's, especially on chip materials, fabrication and application. In this chapter, chip materials are summarized and compared on their advantages and limitations. The polymer-based substrate, polymer surface modification and coating are briefly reviewed. State of art isoelectric focusing (IEF) and capillary gel electrophoresis (CGE) 2-D is also summarized. Furthermore, the simulation work on sample injection and separation has been discussed, from which the design requirements on the multiplex separation chip is suggested.

2.1   Chip Substrate Materials

Chip has been fabricated on silicon,[62-64] glass[43] or quartz[65,66] substrate since 1990's. These materials are popular due to a variety of considerations.[30] The modification chemistries of these materials have been well-known characterized. In general, there are 4-5 silanol groups per nm^2 on the smooth and non-porous amorphous silica surface.[67,68] When base buffer contacts with the silica surface, the silanol groups hydrolyze to form $Si-O^-$ negative charge, occurrence of the EOF under the electric field. To alleviate EOF, a neutral coating must cover the fused silica surface by either covalently bonding 3-methacryloxypropyltrimethoxysilane to silanol[36,39] or dynamic coating.[35,69] Other advantages includes well-developed silicon-based fabrication technologies for standard chip production, favorably optical and thermal properties, and non-specific adsorption on the fused silica surface.[30,70]

However, silicon, glass, or quartz fabrication process is expensive and many hazardous chemicals have to be used, which drives researchers to find alternative substrate materials of inexpensive and non-hazardous. Polymers are increasingly

explored for chip substrate materials,[71-73] mainly because of their inexpensive replication fabrication technologies,[74-76] low raw material cost,[29] a variety of surface chemistry,[77-79] and good optical[80] and electrical insulation properties.[23,30,37,48,81] However, polymer chip is not flawless. In contrast to glass, polymers are not a good thermal dissipation material. To avoid heat accumulation inside chip, a small channel dimension is desirable for minimizing Joule heating. It is routine to limit the electric field strength in order to reduce Joule heating without sacrificing separation performance. In addition, polymer surface usually adsorbs analytes due to its heterogeneity,[82,83] causing sample loss and deteriorating separation performance. Polymer surface is usually modified prior to separation performed.

2.2 Polymer Chip Surface Modification

Modification polymer surface not only reduces the non-specific protein adsorption, but also alters EOF via activation of the wall by covalently-bonded coating,[37,68] most importantly improving separation reproducibility.[68] Polymer modification sometimes can tune the surface property as desired, e.g., reversed EOF by coating charged polymers such as polyamine (PA) and poly (dimethyldiallylammonium chloride) (PDMDAA).[84,85] Generally, a strongly hydrophilic coating is desirable for protein analysis. Studies on two anionic coatings indicate that polymer surface modified by hydrophilic coating exhibits better protein separation compared to that by hydrophobic coating, e.g., poly (vinyl sulfonic) (PVS) acid.[86]
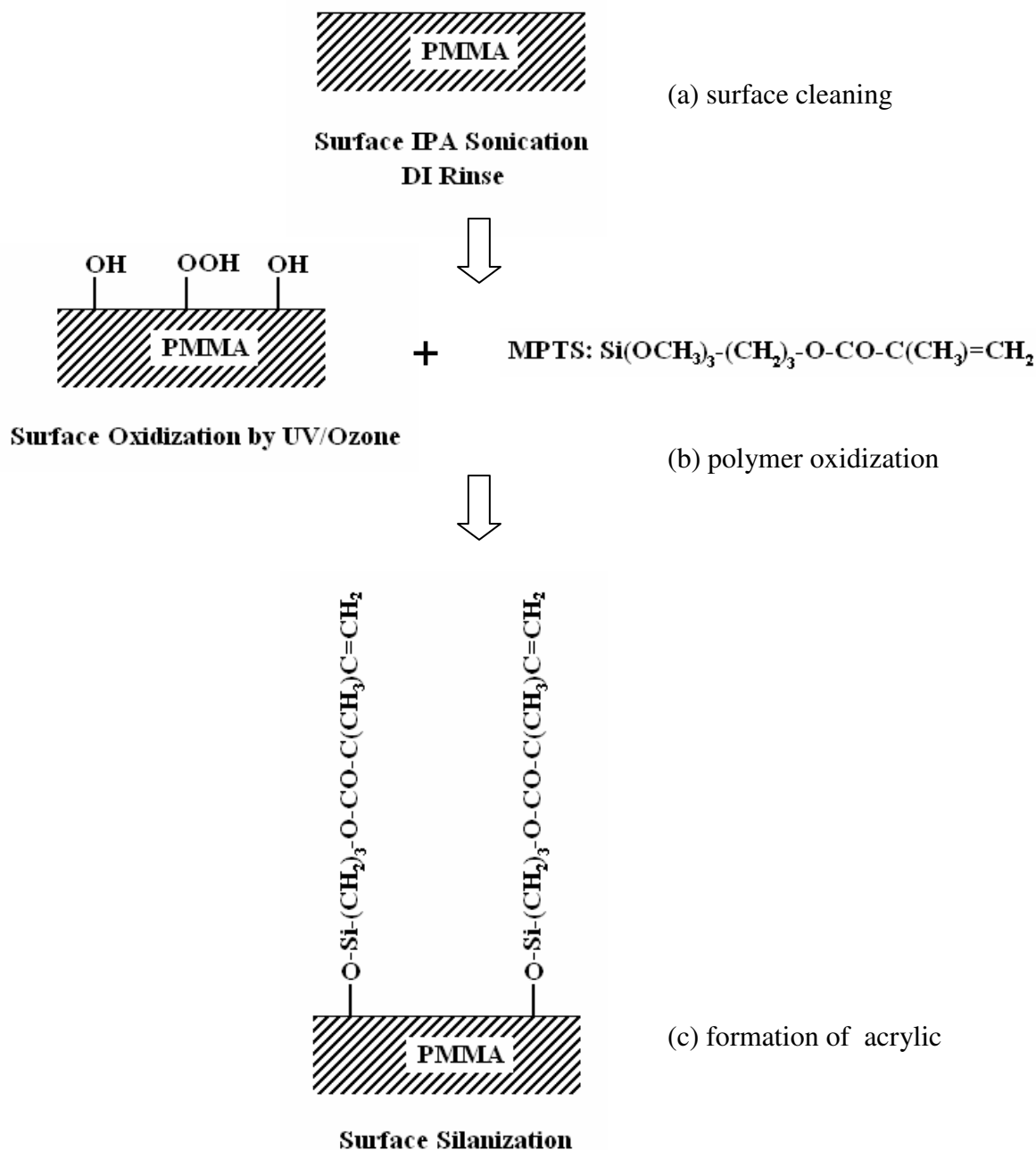
Figure 2. Schematic diagram of permanent surface modification on PMMA substrates through silanization, (a) clean PMMA surface to remove contaminants using IPA with sonication and DI water rinse; (b) oxidize PMMA by exposing to UV/O$_3$ to form –OH; (c) covalently bond 3-methacryloxypropyltrimethoxysilane (MPTS) to anchor acrylic group on PMMA surface.

Two approaches are usually employed for modifying polymer surface: dynamic coating[87,88] and permanent coating (or modification).[35,38,89] Dynamic solution contains

high molecular weight of polymer to immerse or rinse the coated substrate (polymer of capillary), such as hydroxypropylmethylcellulose (HPMC),[90] hydroxyethylcellulose (HEC) for sieving and coating,[91] and poly(diallyldimethylammonium chloride) (PDADMAC)-gold-nanoparticle.[92] The coating materials are tightly adsorbed onto the polymer surface via physical interactions, e.g., *Van der Walls* and polar-polar force. In some instance, the low concentration of coating materials is added into the separation medium to enhance the coating quality (by continuously coating surface to equilibrium). The dynamic coating is a convenient approach in that the coating solution is easy to prepare and apply. However, the weak physical interaction (compared to covalent coating) coating tends to re-dissolve into the buffer or the separation medium from polymer surface. These dissolved reagents are contaminants to analytes, especially detrimental to mass spectrometry (MS) detection.

Permanent modification,[93,94] or static coating, usually employs high energy sources to active the top surface layers, and uses specific chemicals to react with the activated polymer surfaces. The permanent surface modification typically involves three steps: surface pretreatment, double-bond formation on the pretreated surface, and polymer bonding on the double-bonds.[95] Compared to the dynamic coating, the permanent surface modification has much longer lifetime and is more robust without introducing contaminants into analytes. The surface modification process on poly methyl methacrylate (PMMA) is schematically shown in Figure 2. The surface has to be cleaned to eliminate the contamination on surface prior to coating. The polymer wafer is then immersed in isopropanol (IPA) solvent for 5~10 min sonication. It is necessary to perform this step, especially for milled channel, since the debris formed during milling

inside or along the channels may not be removed by simply methanol and IPA rinsing. It is unnecessary for the imprinted chip for no debris is produced by this process. The second step is to activate PMMA surface or anchor active functional groups. The UV-Ozone creates hydroxide and carboxyl groups (R-COOH). The 3-methacryloxypropyltrimethoxysilane (MPTS) is covalently bonded to these hydroxide group, leaving acrylic groups on the wall surface.[39] The treated surface allows for further modification to meet specific requirements, such as zero-EOF and no protein adsorption. The appropriate surface modification improves IEF separation and CGE separation with reducing bond broadening.

2.3   IEF and CGE in 2-D Separation

The IEF-gel electrophoresis two-dimensional separation is commonly used for proteomics due to its resolving power and high peak capacity. In general, the IEF is the first dimension and the gel electrophoresis the second dimension. The prerequisites capable of coupling of the discrete separation techniques include orthogonality,[96] or independently successive separation mechanism, rapid peak generation in the previous separation dimension,[97] high resolution and overall technique compatibility.[96,98]

Two types of buffer solution are suitable for IEF separation, carrier ampholyte[99] and synthetic buffer compound, or immobilized pH gradient (IPG).[100] Carrier ampholyte contains mixtures of a few hundreds different homologues of amphoteric buffers that carry both current and buffering capacity. The buffers possess both acid and basic functional groups, e.g., H+ or COO-, and are charged at the beginning. They start to migrate according to their charges to the anode or the cathode respectively under the influence of the electric field until reach zero net charge condition, or called isoelectric

point (*pI*). The carrier ampholyte suffers to the problems of pH gradient instability and irreproducibility, which were overcome by the introduction of immobilized pH gradients (IPG) for IEF in 1980's.[101] IPGs are based on the principle that the pH gradient is generated by a limited number (6-8) of well-defined chemicals (the 'Immobilines') which are co-polymerized within the acrylamide matrix. The cathodic drift is thus eliminated, reproducibility enhanced even for inter-laboratory experiments. Additionally, IPGs allow the generation of pH gradients of any desired range (broad, narrow or ultra-narrow) between pH 3 and 12. Since sample loading capacity of IPG-IEF is also higher than with CA-IEF, especially in combination with narrow (1 pH unit) or ultra-narrow (0.1 pH unit) IPGs, 2D-PAGE with IPGs is the method of choice for micro-preparative separation and spot identification.[102,103]

The IEF is generally prepared as the first dimension for several reasons. The IEF can focus quickly and the bands can halt in the IEF channel for the second dimension.[97] Because IEF takes advantages of electrical charge properties of molecules to focus them within the defined zone in the separation medium, there is no diffusion during the focusing and no interaction between the focused bands. The focused bands are predictable if the pI values, pH gradient, electric field and device geometries are known,[104,105] by using Eqn. (1),

$$\Delta(pI) = 3\sqrt{\left|\frac{D}{E}\left(\frac{d(pH)}{dx} / \frac{d\mu}{d(pH)}\right)\right|} \tag{1}$$

where p*I* is the isoelectric point value, D is the diffusion coefficient of the analyte, E is the electric field strength, pH is equal to $-\log(C_{H+})$, and μ is the buffer viscosity. Different from other separation mechanisms, the focused bond is insensitive to the injection dispersion in the initial sample plug, which otherwise has to be carefully

controlled for separation. IEF is also a technique to pre-concentrate very dilute sample and improve the detection sensitivity.[52]

Coupled with the first dimension IEF, the second dimension can be varied such as SDS/CGE,[49,50,106] SDS/PAGE (slab gel),[49,103,106-110] CE,[52,111] reverse phase liquid chromatography (RPLC),[112-115] and MS,[116,117] to list a few. Gel electrophoresis is a routine methodology to analyze proteins and peptides. Slab-gel 2-D PAGE is the most popular method for proteomics. The IEF-SDS/PAGE slab gel has many advantages, such as high peak capacity, high resolving power, capable of detection of post-translationally modified proteins, affordability and methodology maturity. However, to conduct slag gel 2-D PAGE is time-consuming, a large amount of sample required for analysis, sample loss, off-line sample transfer and SDS-protein complexation, and the system is not portable. An automatic and miniaturized separation system could build on a capillary-based substrate, such as glass capillary or plastic microfluidic.

Microfluidic two-dimensional IEF-CGE have been reported in literatures.[49,50,58,110,118] Griebel et al.[50] studied an IPG/IEF-SDS/CGE system for protein separation. In their platform, the proteins were firstly focused in immobilized-pH gradient (IPG), and transferred to 300 parallel channels in a PMMA chip. The separation on all 300 parallel channels is fairly uniform. The IEF is conducted in IPG strip and placed into the device for CGE transfer, though the IEF is offline approach, similar as[118]. An online IEF approach was investigated in single channel of spatially-multiplexed chip[49] and more effort is given in Buch's work.[58] This real-time sample transfer approach requires a strict control of gel-buffer, gel-sample surface (most difficult for carrier ampholyte used), because any hydrodynamic flow will result in diffusion between diluted (1.5%, PEO,

600,000) and buffer. Whether the short period of electrophoresis time, e.g., one minute used in Li's study,[49] is long enough for SDS migration from injection channels down to IEF (1-2 cm) and how the SDS-protein binding efficiency is are questionable. Theoretically, the focused bond in IEF will not move under electric field due to its zero net charge. This immobilized proteins can bind to SDS and will be transferred into 2nd-D as long as protein-SDS complexes are developed. However, any diffusion between sample and 2-D medium will disturb IEF separation and zero net charge condition will never be reached. Moreover, the chip design did not create uniform current in each IEF channels and CGE channels using Li's spatially-multiplexed chip design. As a result, analyte in adjacent IEF channel asymmetrically migrates into CGE channel. Without dealing with these issues, it is difficult to implement the protein analysis in microfluidic 2-D PAGE, not mention to its reproducibility.

2.4   Sample Injection and Separation Simulation

The simulation on chip is an important tool to identify chip potential issues. Computational and analytical simulation of on-chip processes can serve to dramatically reduce the time from concept to fabrication. With the aid of simulation, the effects of the chip design on separation performance can be identified and measures to improve. The simulation is important to understand the fundamental physical mechanisms, which are associated with specie transport and fluid flow in the presence of the electric fields. Moreover, it provides insight of the interactions between various physical processes and improves the design of chips, or optimization of the chip design.

2.4.1　Sample Injection Simulation

There are a variety of topologies for sample injection, such as cross, double-T, triple-T, and multiple-T.[119-123] For example, Fu et al.[119] summarized the chip design and tested the injection systems with various injection configurations. They compared each injection configuration and concluded that the cross design is only capable of providing discrete fixed-volume samples, which is superior to the multi-T design. In the latter design, the injection system can manipulate the electric field magnitude and distribution as a virtual valves; this design also combines the injection mechanisms of cross, double-T and triple-T. Use of multi-T design can increase the amount of sample and the simulation is validated by experimental results. Krishnamoorthy et al.[120] developed an implicit finite-volume numerical scheme to solve the 3D transport equations that govern the EOF and electrophoretic phenomena. They used ion transport equation and electro-neutrality condition coupled with Nervier-Stokes equations to simulate sample injection in cross channels. A large tail of the sample plug during electrokinetic injection is observed. To eliminate the tailing, Jacobson et al.[121] designed a protocol for sample loading and separation. The electric potential is only applied to sample and waste reservoirs during loading stage with separation and buffer reservoirs floating. To control the injection sample volume, a pinched injection is employed, which applies the potentials to sample and buffer reservoirs with waste reservoir floating. Experiment and simulation shows that floating sample injection causes a more diffuse injection plug due to eddy flow, and the pinched injection enables a trapezoidal sample shape, creating a temporal stability and short sample plug. The different injection approaches are summarized in Wenclawiak and Puschl.[122] Because separation performance is affected by injection technique, sample

plug shape and its length, it is more significant to design an injection scenario which can control plug both shape and length. To this end, a novel electrokinetic injection method is proposed by Zhuang et al.[123] A numerical investigation of different electrokinetic injection approaches is described. They use the parallel electric field as virtual walls to confine sample plug spreading and prevent sample leaking. A non-distorted shape and variable volume of sample plug can be delivered by electrokinetic focusing via this technique. The update simulation work on sample injection is also reviewed by Erickson.[124] More summaries will be given in Chapter 7.

2.4.2   Sample Separation Simulation

The ultimate goal to improve a chip design is obviously for better separation performance, such as higher peak capacity (n_c) and separation resolution (SR). In liquid chromatography, peak capacity is given by,

$$n_c = L/(4\sigma) \tag{2}$$

where L is the total time of sample elution, and σ is the average standard deviation of the peaks.[96,125] To achieve a high capacity factor, assuming same standard deviation, a longer channel is expected. On the other hand, achievement of high integration and portability requires fabrication of chip in a compact area. Thus, the channel turns cannot be avoided to meet such criteria as long separation length and high integration. Many efforts are given on these works.[121,126-132]

The bond-broadening is observed whenever separated bands turn in the separation channels,[126,127,133] which are attributed by the bond dispersion (skew), diffusion and non-uniform electric field. The non-uniform is caused by the high current density along the inner wall of the turn and the low current density along the outer wall. The ions on the

inside of the turn experiences a higher electric field than that on the outside, causing the fast migration of ions along the inside channel. Beyond this, the inner portion of the plug travels less distance in the turn than the outer portion.[121] Wang et al.[128] simulated the bond skew and dispersion after migration through the turn. The skew can be eliminated by using even number of turns for large diffusion analytes, which however may lead to large bond diffusion. Theoretically, if both the straight-channel dimensionless time (τ_s) (< 0.01) and the diffusion are small enough, the bond-broadening can be negligible for even number of turns. This simulation only considers factors such as diffusion and turn travel distance. It is more complicated if all dispersion factors are taken into account, e.g., field variance.[126] Molho et al.[127] and Paegel et al.[129] studied the turn geometries and used numerical models to simulate the bond dispersion. The optimized turn shape was proposed, which has reduced geometry to lengthen the inner path and constrict the outer path. The plug will undergo more equal travel distance by use of the narrowed turn geometry.

Other example to reduce the bond-broadening is use of the shaped electric field.[130] The shaped electric field can eliminate the bond expansion during separation. The channel sidewall is designed as zigzag to modify the solution flow profile, as well as solution mixing.[132] This will extensively discuss the geometry and topography of injection system, as well as 2-D chip design (Chapter 7).

2.4.3 Isoelectric Focusing Simulation

Isoelectric focusing simulation has been performed in many decades,[134-139] which is much more complicated as contrast to sample injection and separation. Sounart et al.[105,140] summarized IEF principles and numerical simulation. The simulation considers

the physiochemical processes during IEF, and combined balance laws in the model, such as ion transport and neutrality equations, unsteady electromigration-diffusion and ionogenic dissociation-association equilibrium. Different catholyte and anolyte system, including pH gradient, concentration and electric field, are simulated.

Pribyl et al.[141] presented an empirical algorithm of mesh adaptation for modeling one-dimensional reaction transport systems using FEMLab. The algorithm is able to describe the formation of large gradients of electric potential and concentrations of the electrolyte, thus it is expected to simulate IEF separation. However, this has not been done yet. Cui et al.[104] simulated the IEF separation and experimentally coupled with several stages of IEF in series. They are able to improve the resolving power by refocusing the fluorescent proteins in the second channel using a shallower pH gradient and a higher electric field gradient. They observed that the presence of T-junctions can lead to transient bond deformation and temporarily reduce resolution.

In summary, the chip geometry, anolyte and catholyte, buffer constituents, pH gradient, and electric field strength all affect the IEF separation. The IEF separation cannot be accurately simulated unless all these factors are reasonably incorporated into the model. The robust and repeatable IEF will be benefited from simulation estimation, as well as coupling with the second dimension separation.

Chapter 3.   2D Chip Fabrication

Polymer, such as polymethylmethacrylate (PMMA), cyclic olefin copolymer (COC), polycarbonate (PC), has recently become one of the dominant substrate materials for microfluidic 2-D separation due to its low cost, high optical transparency, ultra-violet (UV) transmittance, surface chemistries, excellent dielectric and mechanical properties.[142-144] PMMA is hard and stiff but brittle and notch-sensitive,[23] suitable for both milling and imprinting of high channel quality. PMMA is compatible with acid and base solvent, and can be cleaned or rinsed by solvent such as isopropanol (IPA) and methanol. It can be conveniently bonded using hot-embossing technique.

3.1   Optimization of Chip Fabrication

3.1.1   Polymer Chip Preparation

The requirements on materials are different for micro-machining or imprinting. Micro-machined chip requires the uniform thickness and strictly smooth surface in order to obtain a uniform channel depth. After milling (Roland MDX-650 CNC Milling Machine; Roland DG Corporation, Tokyo, Japan), the chip is then sonicated in IPA for 10 min to remove debris existed along channel sidewall or bottom, followed by DI water rinsing. The chip is further cleaned by methanol, IPA and DI sequentially prior to store in a room-temperature vacuum oven for future use. The tolerance of polymer chip thickness for imprinting is larger than that for milling; however, the chip should be degassed to avoid moisture trapped during imprinting, which will eventually lead to bubbled or flawed channel. In some instance, the vapor produced in high temperature imprinting (normally 10-20°C higher than its glass transition temperature) could result in

inhomogeneous channel geometry. Additionally, the cover chip containing reservoirs is also cleaned prior to thermal bonding.

3.1.1.1 Chip Milling

The PMMA wafer is milled in Roland MDX-650 CNC Milling Machine. Channel width and depth are adjustable, with width down to 50 μm. The aspect ratio can be easily adjusted, e.g., from 0 to 10, only by as-needed changing milling depth. The device used in this study is normally 125 μm by 125 μm (aspect ratio is 1).

The chip design is executed using AutoCAD (Figure 5), by which the coordinate of the plot is used to generating a program, called G-Code. As discussed before, the milled chip normally has rough channel surface (probably leading to the local electric field strength variation and protein trap inside), thus a multi-milling step can be used. The roughed surface can be further improved by linear polyacrylamide (LPA) coating to form a smooth surface.

3.1.1.2 Chip Imprinting

A silicon-based template is fabricated to imprint feature in chip. The fabrication process consists of spin coating, photolithography and deep reactive ion etching (DRIE) as shown in Figure 3. The silicon template is bonded on the stainless steel using adhesive film at 180°C for 3 hrs as described in Figure 4. The silicon template on the stainless steel is installed in the Carver Hot Press Auto Four (Carver Inc., IN). For PMMA UVT, the imprinting temperature is 125°C @ 1.4 MPa for 3 hr. In the final step, the imprinted chip is thermally bonded to the top cover with fabricated reservoirs. Same parameters are used to thermally bond the milled chip. Prior to the thermal bonding, PMMA wafer

surface is treated to eliminate the contamination and covalently bond acrylic groups as described in section 3.2.
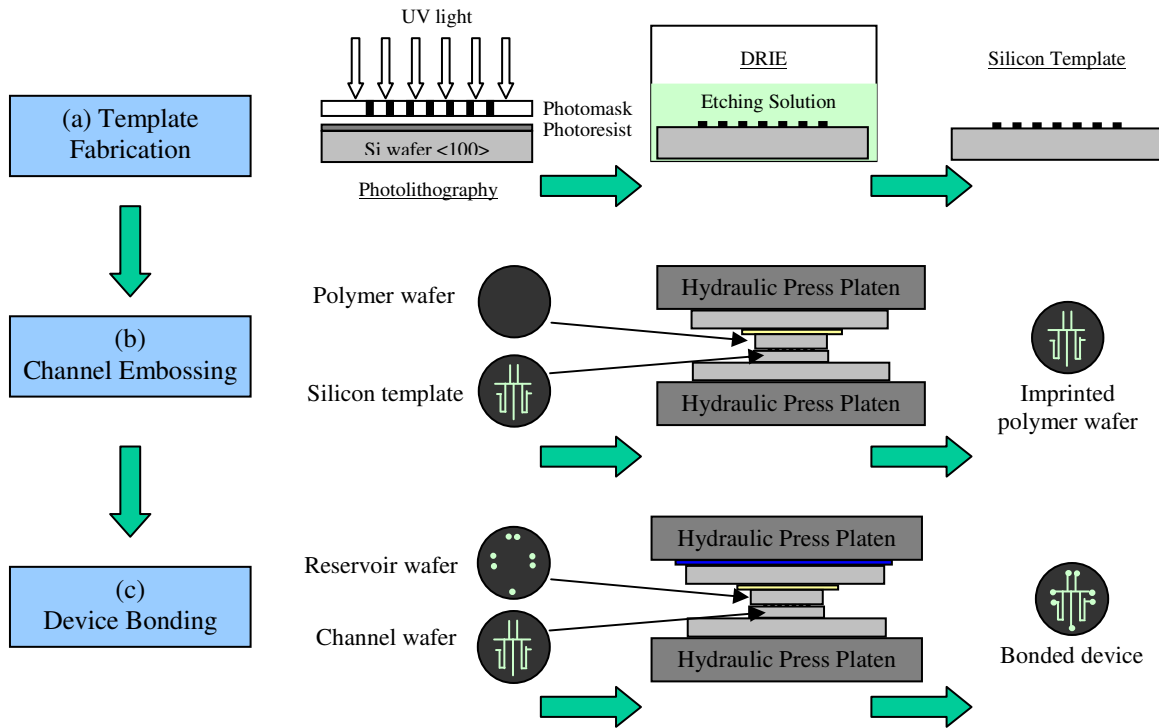
Figure 3. Schematic of chip fabrication process, (a) silicon template preparation by DRIE, (b) channel imprinting by hot embossing, and (c) chip thermal bonding by hot press
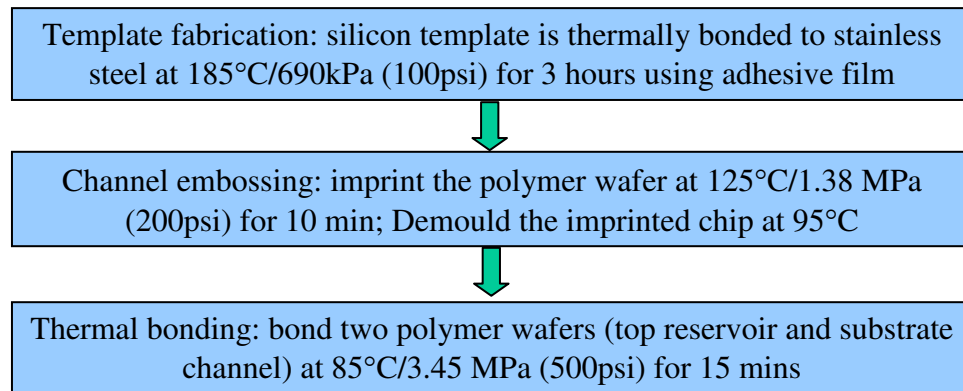
Figure 4. Process flow chart of chip fabrication and parameters used for hot embossing technique.

3.1.1.3 Milling vs. Imprinting Fabrication

The thermoplastic plastic, such as PMMA, COC, and PC, can be milled to a desired feature in a quick turnaround (from design to application). Use of milling approach for chip fabrication is mainly due to its cost-effective process and relatively short period of time to a new design. Comparatively, for imprinting fabrication, the photomask must be prepared in order to acquire silicon template through deep reactive-ion etching (DRIE), which dramatically increases the fabrication time and cost. Nevertheless, the imprinted chip produces higher channel quality, such as uniform channel feature size, smooth channel sidewall, and reproducibility imprinted by same template. The milled chip is dominantly employed in this dissertation, mainly because it can produce reasonable results and the different chip design can be easily and quickly implemented on micro-machined chip as mentioned before. The imprinting chip is more suitably applied when a new design is tested functionality and shows desired performance. The schematic process is shown in Figure 5 for chip fabrication.

3.1.2 Polymer Surface Activation and Modification

Different from glass wafer, there is no silanol (Si-OH) group on PMMA surface (similar to PC material). Direct use of 3-(Trimethoxysilyl) propyl methacrylate (MTPS) on the PMMA will not automatically result in covalent bond of acrylic group. In general, PMMA surface must be initially oxidized by high energy source, such as UV-O_3 (Novascan PSD-UV; Novascan Technologies, Inc., IA)[145] or plasma.[146-149] The O_3 can oxide side-group of PMMA to form C-OH; while the UV radiation is a process by which energy is transferred from one location to another.[150] Combination of UV and O_3 generates hydroxide or even carboxyl.
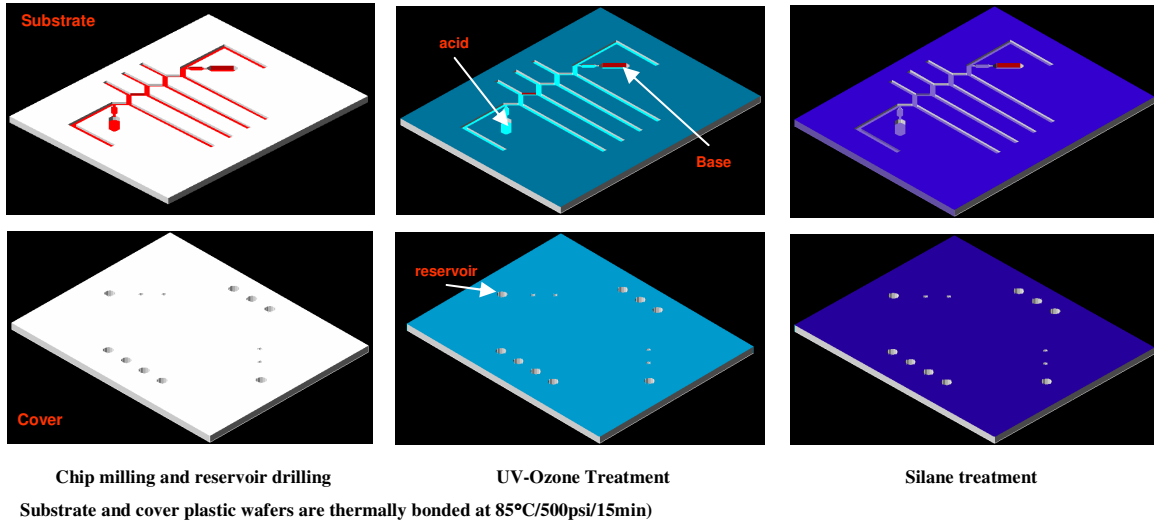
Figure 5. Schematic procedure of chip fabrication. The channel is milled in polymer substrate and reservoirs are drilled on the top cover plate.

A series of UV-O_3 exposure time is conducted, varying from 4 min to 14 min, with interval of 2 min. The contact angle, measured by Tantec CA-D Goniometer (Tantec Inc., IL), remains constant after 12 min UV-O_3 oxidation shown in Figure 6. This result indicates that the density of hydroxide on PMMA surface is saturated after 8-12 min oxidization, further exposure may undermine its under-layer; while the short oxidation period produces not enough hydroxide density. On the other hand, the longer exposure could damage bulk property of PMMA. The UV-Ozone oxidization is kept for 8 min in this dissertation unless specific. Oxidized PMMA is then immersed into silanization solution, consisting of MPTS, HCl in water, whose constituents are listed in Table 1. The silanization time varies from 30 min to 2 hr, depending on the silanization solution recipe. The contact angle and UV transmittance using HP 8452A Diode-Array UV-Vis Spectrophotometer (Hewlett-Packard Company, CA) are characterized. The results are shown from Figure 7 to Figure 12.
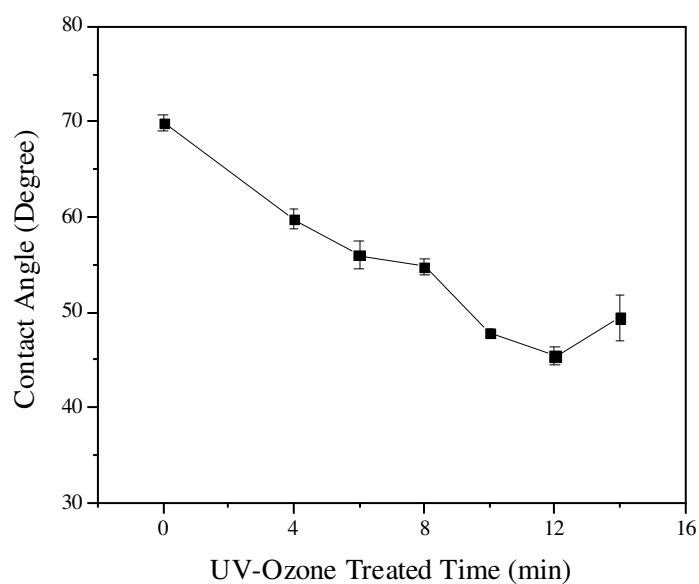
Figure 6.The contact angle of PMMA surface after UV-O$_3$ treatment. A droplet of HPLC DI water was directly deposited on the treated PMMA surface immediately after oxidization. The standard variation is estimated based on five samples.

Table 1. The recipe of silanization solution for PMMA sidewall coating

Reagent	Volume: mL (Percentage, %)						
MPTS	0.8 (0.4%)	1.2 (0.6%)	1.6 (0.8%)	2.0 (1%)	1.2 (0.6%)	1.2 (0.6%)	1.2 (0.6%)
HCl	0.2 (0.1%)	0.2 (0.1%)	0.2 (0.1%)	0.2 (0.1%)	0.4 (0.2%)	0.6 (0.3%)	0.8 (0.4%)
HPLC DI Water	200	200	200	200	200	200	200
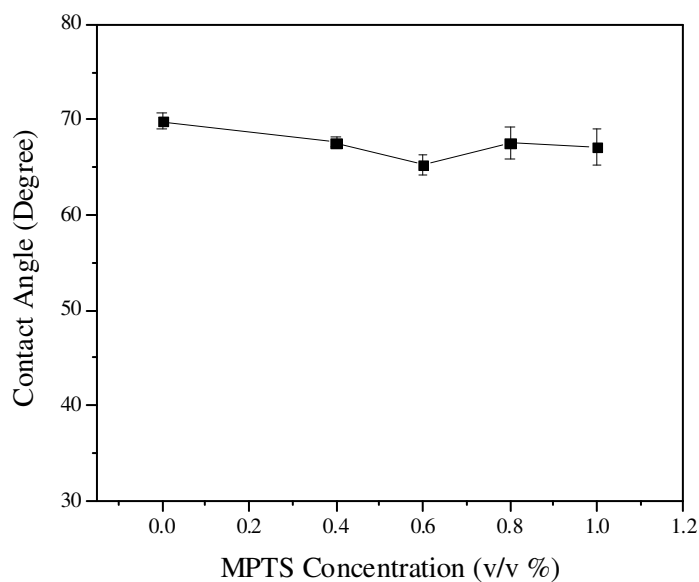
Figure 7. Contact angle change in various silanization solutions on PMMA. The PMMA was treated in UV-O$_3$ for 12 min prior to immersion in silanization solution. The HCl concentration is 0.1% and total silanization duration is 1 hr.
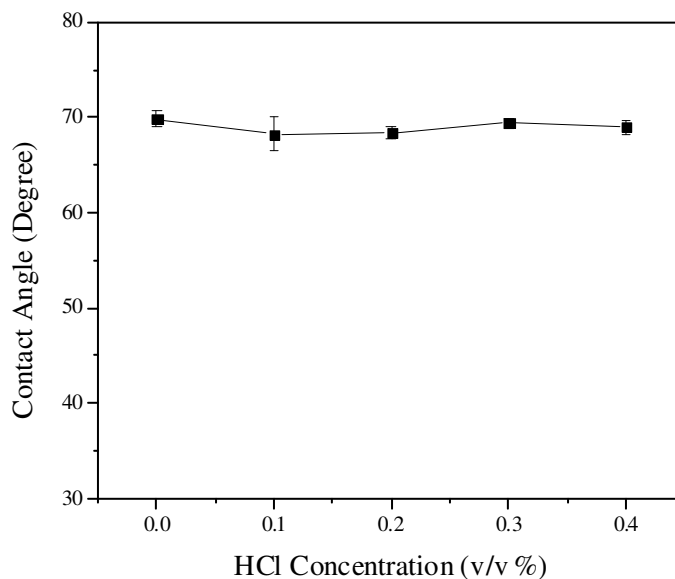
Figure 8. Contact angle change as HCl concentration in silanization solution on PMMA substrate. The PMMA was treated in UV-O$_3$ for 12 min prior to 1hr silanization. The MPTS concentration is 0.6%.
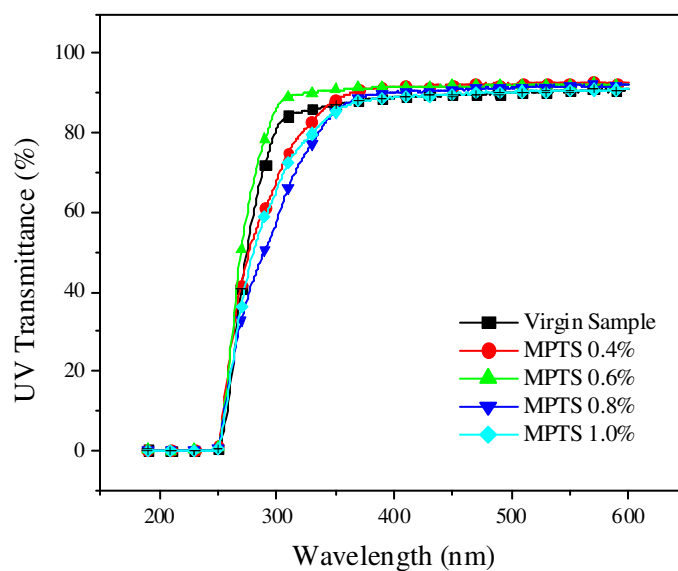
Figure 9. UV transmittance of UVT graded-PMMA under varied MPTS concentration prior to linear polyacrylamide (LPA) coating. 0.1% HCl concentration was used.
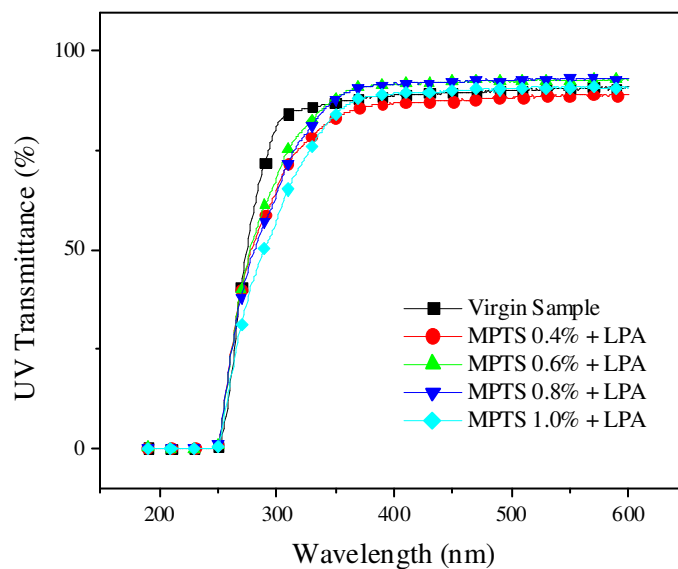
Figure 10. UV transmittance of UVT graded-PMMA under varied MPTS concentration after linear polyacrylamide (LPA) coating. 0.1% HCl concentration was used and surface was further coated by LPA solution.
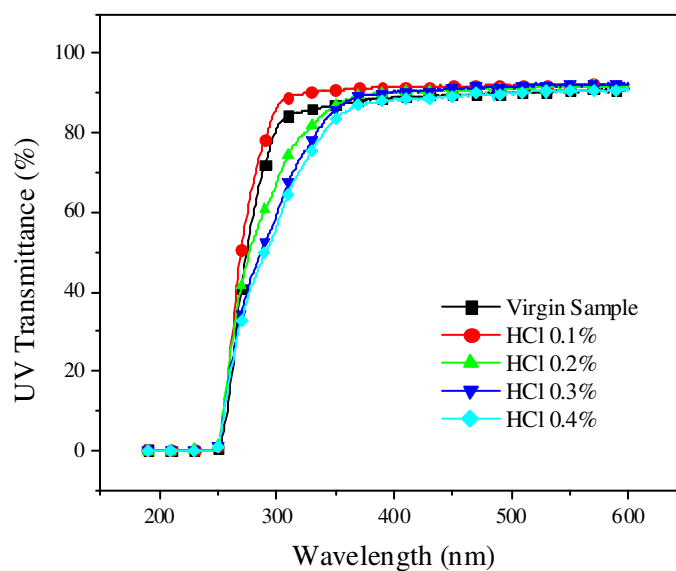
Figure 11. UV transmittance of UVT graded-PMMA under varied HCl concentration prior to linear polyacrylamide (LPA) coating. The constant MPTS (0.6%) concentration was used.
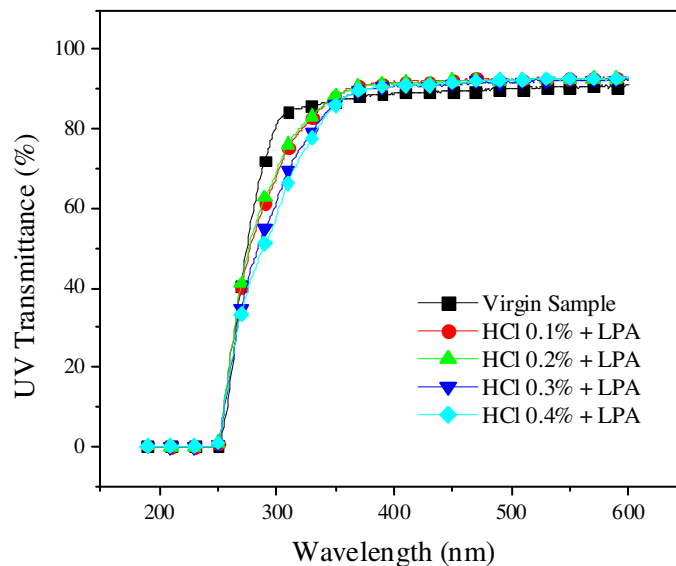
Figure 12. UV transmittance of UVT graded-PMMA under varied HCl concentration after coated by linear polyacrylamide (LPA). The silane solution contains 0.6% MPTS (wt) and LPA (6%) consists of APS and TEMED.

Figure 7 shows the MPTS concentration effect on surface contact angle of silanized PMMA substrate. The contact angle slightly decreases as MPTS concentration increasing from 0 to 1.0%. Similar results are observed on HCl concentration effects as shown in Figure 8. From these results, it seems that the concentration of MPTS and HCl does not matter the final surface condition much. However, determination of both reagents' concentration needs to consider several factors such as silanization solution stability and solubility, polymer bonding quality, LPA coating feasibility, and gel-plug fabrication. At room temperature, the silanization solution tends to be opaque in a short period of time when high MPTS and HCl concentration is used, probably due to the rapid reaction rate.

Additionally, the higher concentration of either MPTS or HCl deteriorates the UV transmittance of UVT-PMMA (UV transmitting grade) sheet as shown in Figure 9 to Figure 12. The UV transmittance for the virgin PMMA UVT sheet (0.8 mm and 1.5 mm) is above 80% at 300 nm, which decreases below 50% when MPTS increases up to 0.8%. Both MPTS and HCl show similar characteristics on UV transmittance for various concentrations. On the other hand, LPA coating layer does not change the UV transmittance properties, which can be attributed to LPA excellent its excellent optical performance if LPA layer does develop over PMMA surface. As a matter of fact, it was found that if no LPA coating is employed, the bubbles are unavoidably formed in the photopolymerized crosslinked polyacrylamide gel, especially along the gel-sidewall interface, which is extensively discussed in Chapter 7.

In this dissertation, the optimized coating protocol is: activation in UV-O_3 for 8 min, silanization for 60 min, and LPA coating for 15 min (refer to recipes listed in Table 1).

The optimized protocol is consistently used for PMMA chip surface treatment prior to thermal bonding.

3.2 *In-Situ* Photopolymerized Polyacrylamide Gel-Plug

The crosslinked polyacrylamide gel-plug is in situ fabricated inside microchannels after thermal bonding (as described in previous section). The general process is schematically shown in Figure 13, which consists of acid-base plug, linear polyacrylamide (LPA) coating, sieving gel photopolymerization, polyacrylamide plug photopolymerization in injection channel, and polyvinyl alcohol (PVA) coating in IEF channel.

(a) Acid-base plug　　**(b) LPA coating**　　**(c) Sieving gel**

(d) Injection plug　　**(e) PVA coating**
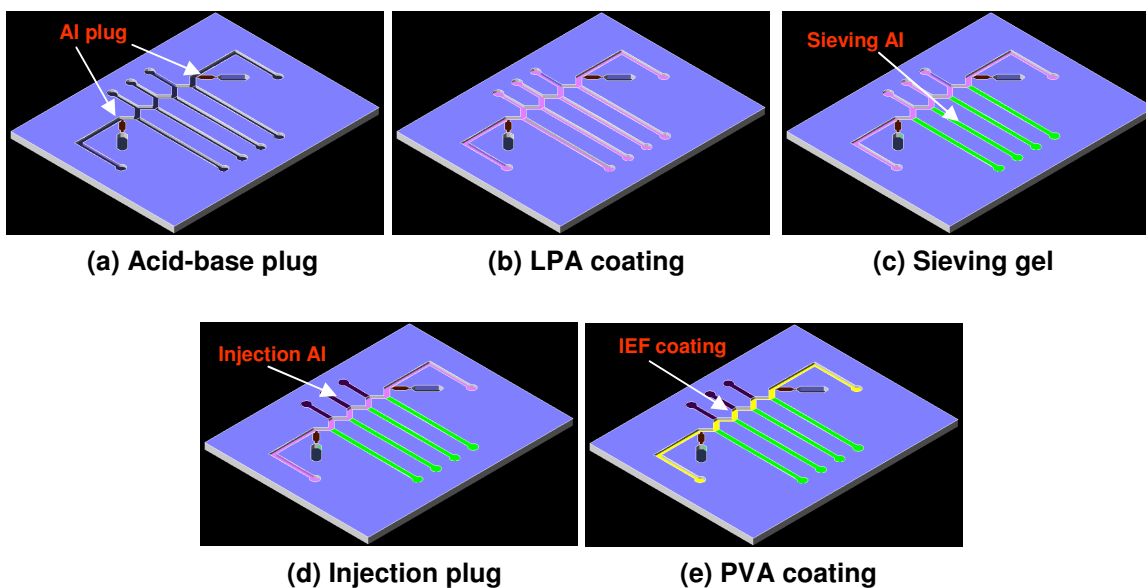
Figure 13. Schematic procedure of in-situ photopolymerization of polyacrylamide in a PMMA chip. (a) short AI plug fabrication; (b) Linear polyacrylamide (LPA) coating; (c) AI sieving matrix fabrication in separation channel; (d) AI fabrication in injection channel; (e) PVA coating of IEF channel.

3.2.1 Acid-Base Plug Fabrication.

In-situ photopolymerization is performed in chip to develop short plug and/or long gel (1 mm, compared to 10-20 mm injection plug). The short plug serves as pressure-blocking between samples and acid/base, as well as conductive path for ion transport. To achieve these goals, the pore size of the short gel plug should be larger enough so that anolyte and catholyte can be electrokinetically transported into IEF channel and the pH gradient can be established quickly during IEF separation. Otherwise, an undesired ion-transport gel plug leads to a shallow pH gradient, e.g., pH close to 5-7 along the IEF channel even using pH 3-10 ampholyte. The prepolymer recipes are shown in Table 2, from which the plug for each recipe can be quantitatively characterized.

Table 2. The prepolymer solution for the short gel plug (AI)

Reagent	AI-Bis-4-5-3* (%)	AI-Bis-4-10-3 (%)	AI-Bis-4-15-3 (%)	AI-Bis-4-20-3 (%)
Acrylamide (AI)	3.8	3.6	3.4	3.2
Bis	0.2	0.4	0.6	0.8
I2959	0.12	0.12	0.12	0.12
DI Water	95.88	95.88	95.88	95.88
Remark	√	√	×	×

*(note: the nomenclature of recipe AI-Bis-4-5-3 represents: AI, acrylamide + I2959; 4 is 4% acrylamide + Bis; 5 is 5% Bis in total acrylamide + Bis; 3 is 3% I2959 in acrylamide + Bis.

The concentration of acrylamide (AI) is the sum of the acrylamide (AAm) and Methylenebisacrylamide (Bis) (expressed as T% in literature[38]) and crosslinker

- 31 -

concentration is expressed as the amount of Bis in the total monomer (AI + Bis). The photopolymerization consists of five steps such as prepolymer preparation, injection, photomask preparation, photolithography, and DI rinsing. After at least 20 min fully oxygen extraction by sonication, prepolymer solution is filled into the chip via hydrodynamic pressure. Prior to the UV exposure, the quartz chrome mask or black tape patterns the chip to allow the desired areas exposure to UV light (Tamarack PRX-1000; Tamarack Scientific Co., Inc., Corona, CA). The exposure time is 500 sec for a power of 24.0 mW/cm^2. The remaining prepolymer in microchannel under photomask is removed from chip and flushed by DI water (DO NOT USE solvent, such as isopropanol and methanol, to flush channel after surface treatment, since it damages the treated surface and forms white film on PMMA surface) prior to LPA coating.

The photopolymerized gel of various recipes (Table 2) has been qualitatively characterized by observing gel transparency, gel electrical resistivity and flow-pressure resistance. It was found that 5% of Bis could result in the smallest pore size, below or under such concentration will slightly increase gel pore size.[151] Example is that AI-Bis-4-5-3 has stronger burst-pressure than AI-Bis-4-10-3 (The gel may not always photopolymerize with a lower concentration of AI + Bis, e.g., AI-Bis-3-5-3). The recipe of AI-Bis-4-10-3 works well, whose electrical resistance is much lower than that of AI-Bis-4-5-3 (1/3 lower). The pressure-resistance is high enough to prevent the hydrodynamic flow by use of AI-Bis-4-10-3. On the other hand, recipe of AI-Bis-4-15-3 or AI-Bis-4-20-3 shows slightly opaque even only 150 sec UV exposure performed. Overall, the recipe of AI-Bis-4-10-3 can meet both mechanical and electrical

requirements for acid and base pressure-blocking plug. More details will be discussed in Chapter 5-7.

3.2.2   Linear Polyacrylamide Sidewall Coating

This step is performed after acid-base plug fabrication due to two factors: no bubble formation on a less than 2 mm gel plug without LPA coating; weak covalent bonding strength between plug and sidewall after LPA coating. The linear long polymer chain is anchored to PMMA sidewall acrylic group and covalently connected to crosslinked polyacrylamide (after acrylamide and Bis photopolymerization). The acid-base plug is normally less than 1 mm in length. As a result, the relative high pressure during gel fabrication likely causes leakage through the acid-base plug sidewall. Therefore, chip sidewall is coated only after acid-base plug fabrication.

Through permanent surface treatment discussed in section 3.1, acrylic groups are generated on PMMA surface. Polyacrylamide (PAAm) can be covalently bonded to the acrylic groups by using either linear acrylamide (LPA)[38,152,153] or cross-linked polyacrylamide (CPA).[154,155] The free acrylic groups serves as anchors on the polymer sidewall for growing PAAm chains. As it has been pointed out,[154-158] the potential problem for LPA approach is that the coating may not completely cover the surface due to roughness and cavities on the silicon surface. Instead use of CPA can certainly improves the LPA coverage for the cavities,[155,159] but the CPA tends to clog the channel since the crosslinked gel has extremely high viscosity as polymerization progress. Besides, a comparatively complex experimental setup is needed for CPA coating. The roughness of PMMA chip surface is less than 1-2 µm and even less for imprinted channel. Therefore, LPA coating is well suitable for PMMA sidewall coating. The LPA

coating recipe is given in Table 3. The prepolymer solution is injected into microchannels by manual syringe and coated for 15 min. After vacuuming LPA polymer, the coated microchannels are flushed with DI to remove LPA residue prior to the following step.

Table 3. The acrylamide prepolymer solution for PMMA chip surface coating

Reagent	LPA-2(%)	LPA-4 (%)	LPA-6 (%)	LPA-8 (%)	LPA-10 (%)
Acrylamide (AI)	2	4	6	8	10
TEMED	0.1	0.1	0.1	0.1	0.1
APS	0.1	0.1	0.1	0.1	0.1
DI Water	97.8	95.8	93.8	91.8	89.8

APS: ammonium persulfate (Sigma-Aldrich, MO)
TEMED: N,N,N,N′-tetramethylethylenediamine (Sigma-Aldrich, MO)

The results of coating solution recipes (Table 3) show that 2% and 4% acrylamide may only form discontinuous coating layer after 30 min, especially for 2% solution. Leakage was observed along the sidewall using 2% LPA coating solution after photopolymerized polyacrylamide was developed in the channel; while 8% and 10% solution has faster reaction rate, viscous coating polymer developed in 5-10 min. 10% LPA coating solution forms strong covalent bond with sidewall and within gel, thus the LPA gel forms in the channel permanently. It turns out that 6% acrylamide solution is suitable for in-channel surface coating. After 15 min coating (reaction), the polymer solution can be vacuumed out, while more than 20 min coating will lead to channel clog and the LPA polymer cannot be vacuumed. In this dissertation, time to LPA coating is fixed to 15 min, unless specified.

3.2.3   Sieving Gel Photopolymerization

The fabrication process of sieving gel is similar to that of acid-base plug except prepolymer recipe. The buffer of sieving gel is 5 mM Tris-HCl, whose pH is 6.9 with 0.1% sodium dodecyl sulfate (SDS) mixed. The concentration of AAm and Bis suitable for protein separation is 3-10-3 or 4-10-3, where 3 denotes 3% of AAm and Bis, 10 denotes 10% of Bis in AAm and Bis, and 3 denotes 3% of I2959 in AAm and Bis. Above this concentration, AI gel shows opaque after photopolymerization; below this concentration, the prepolymer is unable to photopolymerization unless performed in nitrogen-purged glove box environment.

The prepolymer is normally filled into LPA coated microchannels, and all channels are photomasked except separation region. The UV source is turned on after at least 5 min equilibrium of prepolymer within channels (with all reservoirs sealed by blue or black tape to further prevent bulk flow during UV exposure). 150 sec to 500 sec exposure is applied to the sieving gel. Less than 150 sec UV exposure does not generate enough energy to polymerize AI-Bis-3-10-3 at power of 24.0 mW/cm^2.

It is highly possible to introduce bubbles into sieving gel during prepolymer injection. Two sources will result in bubbles in sieving gel, gel shrinkage due to shear force and bubbles flow into prepolymer during equilibrium step. The gel shrinkage will discuss elsewhere, while the bubbles caused by the second mechanism can be prevented by carefully handling prepolymer injection. Normally, a pipette with tip is employed for liquid introduction so that no bubble is trapped in the reservoirs. After filling prepolymer into sample inlet and waste reservoirs, the chip is placed on ground-level work station to allow liquid filling the entire microchannels by hydrodynamic pressure. When

prepolymer reaches injection and separation reservoirs, photomask is applied and all reservoirs, except separation reservoirs, are sealed with black or blue tape. Then the whole chip moves into PRX1000 UV system, allowing 5 min equilibrium prior to UV exposure. To obtain homogenous crosslinked gel, the liquid must be zero-flow during UV exposure. Otherwise, the partially photopolymerized gel will mobilize and opaque gel will produce in some channel.

3.2.4 Injection Gel Photopolymerization

The injection gel contains 25 mM Tris, 192 mM glycine with pH 8.3. In order to in situ denature protein by sodium dodecyl sulfate (SDS), 1.2% to 2% SDS is added into injection gel prepolymer, which is hydrodynamically introduced into injection channel. If bubbles exist inside prepolymer, use of pump under vacuum mode can easily remove them. The photomask is patterned to expose injection channels to UV light source as shown in Figure 13 (d). The base buffer requires longer exposure time and higher concentration of AI+Bis to fully polymerize,[160] thus 4-10-3 or even 6-10-3 recipe is employed for injection gel, with 500 sec exposure time (the detail energy dose is shown in Chapter 7). One potential issue is that gel could be easily damaged if the prepolymer was prepared a few weeks ago. Dissolution of oxygen inside prepolymer will retard photopolymerization so that gel quality degrades gradually.

3.2.5 IEF Channel Sidewall Coating

The IEF channel has been covalently coated a layer of LPA, which mostly reduces electroosmotic flow (EOF). In order to further decrease possible EOF and non-specific protein adsorption, the dynamic coating is necessary. The 4% polyvinyl alcohol (PVA), MW 130,000, is injected into IEF channel and coated at least 20 min (Figure 13 (e)). The

PVA can be easily vacuumed out of IEF channel which is ready for 1D or 2D separation. In some instance, PVA is mixed with sample to enhance dynamic coating during separation.

In this dissertation, the PVA coating is usually performed right before sample introduction, so that a uniform and fresh layer of PVA is on the surface. Filling with buffer or DI water after PVA coating will gradually dissolve PVA already coated on the surface. Therefore, if the chip will not be used for separation, then it can be filled with DI water in IEF channel and temporarily stored in the fridge (-20°C). The IEF channel can be re-coated using PVA after thawing prior to test.

3.2.6 Sample Introduction

One critical step is how to introduce sample into microchannel. Several approaches can be employed for this purpose, such as by automatic syringe pump, manual syringe, or vacuum. For automation application, syringe pump should be the best method for sample injection. The connection between syringe pump and chip reservoir could be Upchurch nanoport, or needle, both of which serves well. However, fabrication of nanoport and needle interface will increase total analysis time, cost and manipulation feasibility. Unless the final protocol is fixed, it is unnecessary to use neither interface connections. Instead, the quick-curing epoxy is routinely used to seal sample channel inlet and outlet reservoirs. The whole process takes only 5-10 mins without much effort needed. Besides, epoxy curing does not build up pressure to the sample channel, since difference did not observe for a chip sealing both reservoirs or leaving one reservoir open (or even using blue tape to seal both reservoirs). However, one should keep in mind that you shouldn't wait for a longer time to start IEF separation if you use replaceable gel matrix, e.g., PEO,

in that sample tends to continuously diffuse into PEO matrix. Fortunately, this issue can

be mitigated using crosslinked gel matrix.

Chapter 4.   2D Chip Design

A variety of design has been used for one-dimensional and two-dimensional separations. One-dimensional, such as CGE or IEF, and two-dimensional separation have certain design requirements, for example, a steady pH gradient during IEF separation and minimal Joule heating and no-EOF during CGE.

4.1   One Dimensional Chip Design

The requirements for CGE and IEF chips are different, such as IEF chip requires an acid reservoir and a base reservoir with capability of blocking hydrodynamic flow during IEF separation. To high throughput purpose, the CGE chip has parallel multi-channels and one common channel for sample injection.

4.1.1   Capillary Gel Electrophoresis Chip

(a) CGE design   (b) IEF design   (c) IEF-CGE coupling
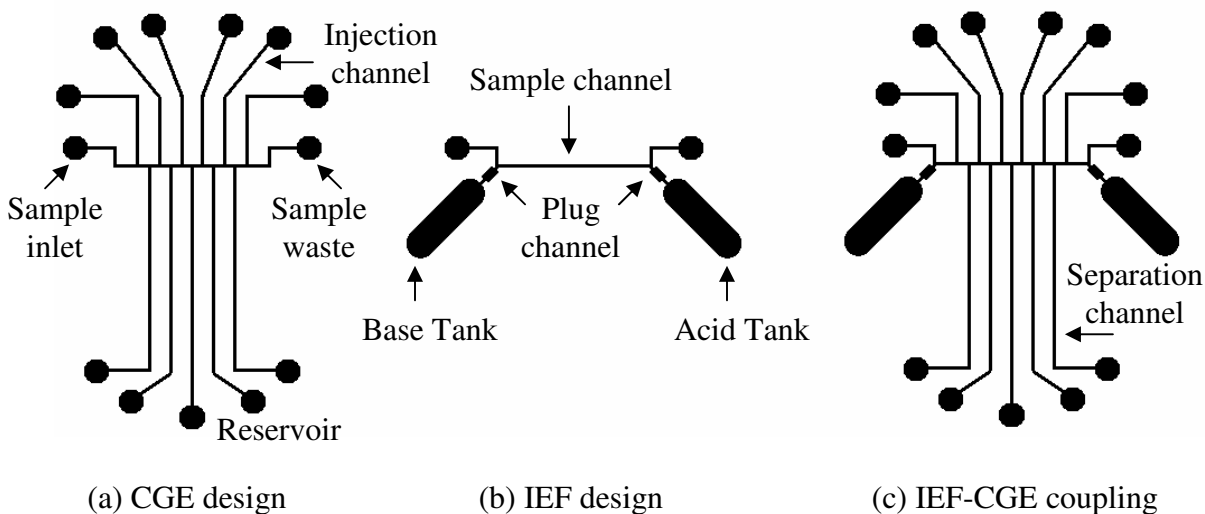
Figure 14. Schematic diagram of polymer chip design of (a) capillary electrophoresis, (b) isoelectric focusing, and (c) IEF-CGE separations

The schematic chip design for a capillary gel electrophoresis (CGE) is shown in Figure 14 (a). The design consists of injection channel, sample channel and separation channel. In order to generate a uniform current in each separation channel, the length from the injection reservoir to the separation reservoir identical, as well as each segment in 1st-D. The design allows a constant potential drop across the channel by assumption that the electrical resistivity is same in all channels. The channel resistance is thus only a function of the channel length.

To negative electrode

To positive electrode
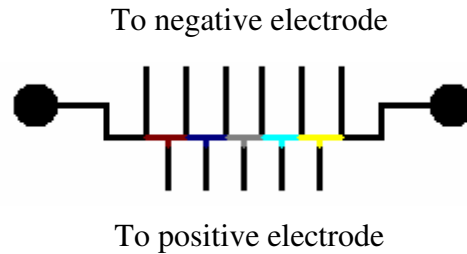
Figure 15. The transfer of all samples into the separation channel through symmetry injection channel design.

Figure 15 illustrates the sample transfer from 1st-D to 2nd-D during CGE when negative charged protein is separated. Six channels are fabricated in the upper section, each adjacent pair of channels corresponding to the common channel in the separation section. Ideally, sample in the 1st-D channel segment between two adjacent injection channels will co-elute into 2nd-D channel. However, the asymmetrical injection is expected due to un-even current distribution inside 1st-D channel segment. Besides, sample leakage will occur in the 1st-D channel between the most-left injection channel and sample inlet, same as the most-right injection channels and sample waste.

4.1.2   Capillary Isoelectric Focusing Chip

The chip design for capillary isoelectric focusing (cIEF) is performed in a single channel with two pressure-blocking barriers connecting to acid/base tank as shown in Figure 14 (b). Two reservoirs are used for sample inlet and sample waste. A partial wide-deep channel can easily constrain the short gel plug between acid/base tank and sample channel to improve gel pressure-blocking strength. The constrained structure anchors the gel plug inside the channel, avoiding plug moving either way. Without using the constrained structure, the short gel plug could be mobilized during chip LPA coating and gel preparation. The total length of the gel plug is around 1000 μm long, with around 500 μm constrained plug. The detail requirements on the short gel plug are described in Chapter 5.

4.2   Two-Dimensional Chip Design

The IEF-CGE chip combines IEF and CGE designs by adding the IEF constrained channels and acid/base reservoirs into the CGE channels as shown in Figure 14 (c). Sample is introduced from the reservoirs connecting with horizontal IEF, same as IEF chip sample introduction. Anolyte and catholyte are electrokinetically injected into the IEF through the constrained channels. After IEF separation, the CGE is conducted in the vertical channels.
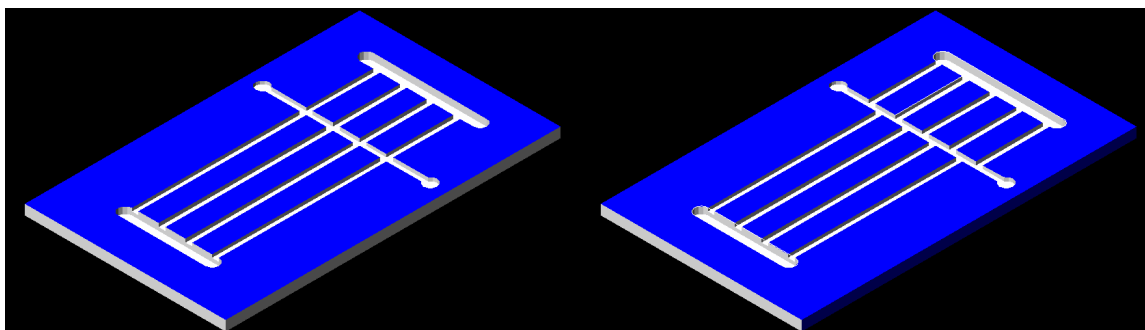
(a) Multi-cross design   (a) Multi-T design

Figure 16. Schematic diagram of spatially-multiplexed 2D chip design of (a) multi-cross and (b) multi-T.

4.2.1 Spatially-Multiplexed Multi-Cross-2D Design

Cross-T design has been widely used in a single CGE design, which provides a concise sample plug theoretically equal to cross-T area. The cross injection can be adapted to 2D chip as shown in Figure 16 (a). Sample in the cross intersection can be fully transferred into 2nd-D during electrophoresis. However, sample between cross will remain in the 1st-D channel due to zero electric potential drop between adjacent crosses. Thus the fractionationed sample after IEF cannot be transferred into 2nd-D. This intrinsic defect can be mitigated by using multi-T 2D design.

4.2.2 Spatially-Multiplexed Multi-T-2D Design

The schematic diagram of multi-T-2D design is shown in Figure 16 (b). The chip design can be simply regarded as many double-T channels connected in parallel. Obviously, the potential between adjacent injection and separation channel drives charged sample into 2nd-D. Besides, zero dead-volume is achieved by this unique design, which has been used for protein separation in several research groups.[49,110]

Nevertheless, there are several issues pertaining to this design. First, when IEF is performed in carrier ampholytes, the sample inlet and waste reservoirs are directly connected to IEF portion; no barrier between acid/base and IEF sample. Any hydrodynamic flow ruins the IEF separation and increases irreproducibility. Second, although efforts are paid to use manifold to control individual reservoirs if replaceable gel such as PEO is employed,[58] the limited spacing between reservoirs increases complexity of manipulation. It is extremely difficult to completely seal injection and separation reservoirs using manifold due to surface roughness and copolanity. To control gel-sample interface, the crosslinked polyacrylamide (PAAm) is photopolymerized in the injection and separation channel. As a result, the better interface is achieved without using manifold setup. However, during IEF separation, the injection reservoir electrophoretically connects, leading to charged sample migration into both injection and separation channel, or named crosstalk. To avoid crosstalk during IEF separation, the injection and separation reservoirs must be individually isolated. The common reservoir shown in Figure 16 is separated into one reservoir per channel (injection or separation channel)

4.3   Requirements on Sample Injection

4.3.1   Free of Leakage Injection

The transfer (or injection) of sample from 1st-D to 2nd-D is critical step for a 2D chip in that the leakage of sample from the 1st-D leads to bond-broadening and even ghost peak. It is expected that sample in the side-channel of the multi-T design (Figure 16 (b)) will leak into the two outer 2nd-D channels. The side-channel leakage will be analyzed in Chapter 6. There are major two approaches to prevent sample leakage. The first approach

employs a pull-back potential to the side-channel during sample injection (transfer). In this mean, the sample is electrokinetically migrated into sample inlet or waster reservoir. The second approach, proposed in this dissertation, fabricates channels parallel to the two outer 2nd-D channels, whose dimension will be discussed in Chapter 6. During capillary electrophoresis separation, the sample inside side-channel will certainly transfer into these two channels, namely backbiasing channel.

4.3.2 Uniform Injection

Another important aspect of sample injection is uniformity. Ideally, the potential and current distribution in the 1st-D and 2nd-D should be same. In other word, each IEF segment has equal current and potential, so does each CGE channel. The analysis of those distributions will be estimated and simulated by Pspice software.

4.3.3 Uniform Chip Geometry and Channel Surface

As discussed in Chapter 3, the chip can be fabricated easier by milling than by imprinting. It is difficult to fabricate complicated chip feature with small channel to channel dimension, e.g., 50 µm channel distance for a 150 µm deep channel, by imprinting approach. The high aspect-ratio can cause damage of imprinting template (by deep reactive ion etching (DRIE)). Because of above rationality, direct milling approach takes place for chip fabrication, which has extremely short design-to-product time.

Several issues have to been considered for chip milling. First, before starting milling, the milling machine requires calibration the z-height based on one position of milled chip. If the chip is non-uniform thickness, the channel depth will be associated with its thickness. The channel milled is deeper at those positions where chip is thick, and vice versa. Therefore, a uniform chip thickness is required for channel depth uniformity.

Second, channel sidewall roughness increases for a larger diameter of end mill. To achieve relatively smooth channel, repeat milling will be a good solution. In addition, the surface treatment, including silanization and LPA coating, further decreases channel surface roughness.
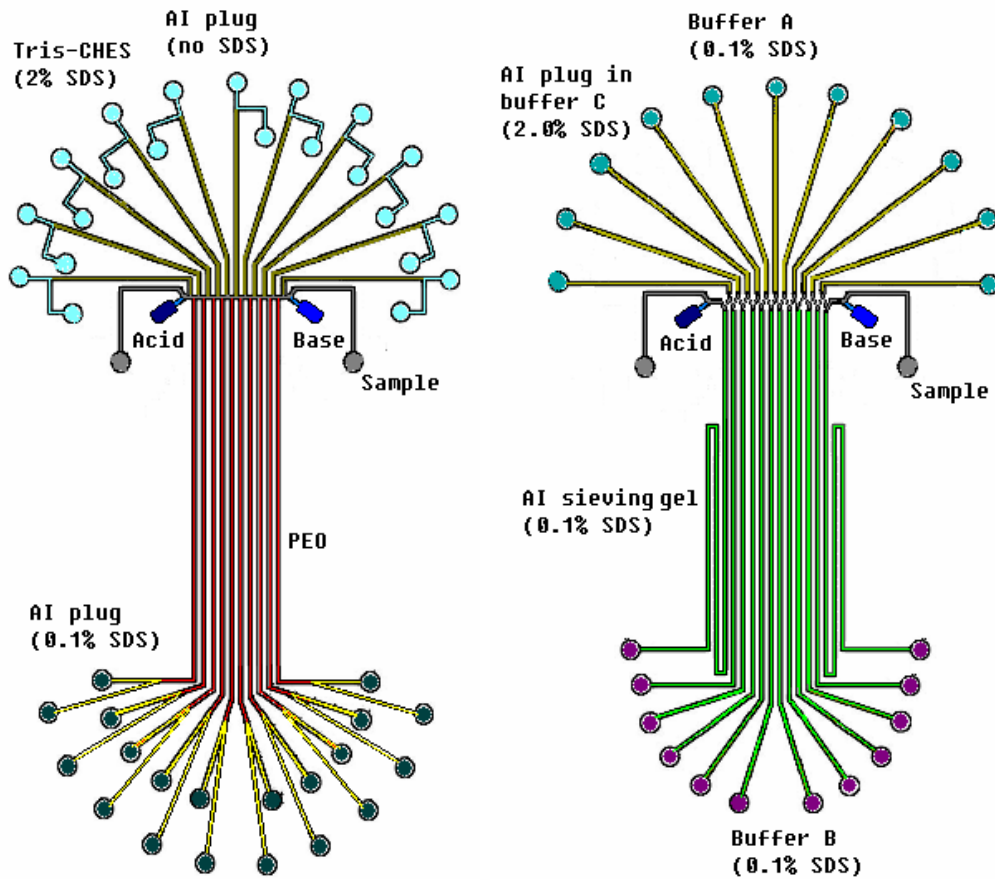
(a) Plug-enabled 2-D using PEO   (a) Plug-enabled 2-D using PAAm

Figure 17. The schematic diagram of 2-D chip designs at progressing stages, (a) manifold-enabled replaceable sieving platform; (b) PAAm-enabled acid-base replaceable sieving platform; (c) Uniform-symmetrical injection design with PAAm plug-sieving platform.

4.3.4   2-D Chip Design Summary

The 2-D chip considers all factors discussed above. To fully understand chip design and gel matrix effect on 2-D separation, two types of chip platforms are investigated as shown in Figure 17. 2-D separation of proteins on these two chip platforms are discussed in detail in Chapter 5, 9 respectively.

The previous design[49] uses common injection and separation reservoirs. It is thus expected that crosstalk occurs during IEF, in which the proteins migrate into both injection and separation channels. To avoid this, the design (a) in Figure 17 is proposed which features discrete reservoirs and employs PAAm gel plug in injection and separation channels to provide solid interface control. The PAAm gel does not contain high concentration of SDS (<0.1% SDS used), thus the SDS inside injection gel does not affect 1st-D separation, i.e., IEF, while the valve-less gel-plug maintains the replaceable PEO in the separation channels. Because the SDS is introduced after injection gel plug fabrication, the SDS isolates between sample channel and injection channel (see detail in the next chapter). The downside of this design includes increased number of reservoirs on both injection and separation channels. The reservoirs normally have 1.5-2.0 mm in diameter, which occupy majority of spacing of a chip, limiting number of channel integrated in a fixed chip size.

To reduce number of reservoirs, the crosslinked PAAm gel is required to use in both injection and separation channel. Use of PAAm in separation channel can certainly decrease number of reservoirs by half, not mention to simplification of gel fabrication process. Additionally, use of two reservoirs in each injection channel purposes introduction of high concentration of SDS after gel fabrication. It is a clever means to

mix high concentration of SDS in the PAAm gel for injection plug. The quantitation of SDS is contained in PAAm gel (by knowing channel volume and prepolymer concentration. The Figure 17 (b) shows such design to realize fully crosslinked PAAm gel system. More detail will be discussed in Chapter. 5 and Chapter. 7.

Chapter 5.   2D-IEF/CGE via Replaceable Sieving Matrix

In-situ photopolymerized PAAm gel plugs are used as hydrodynamic flow control elements in a multidimensional microfluidic system combining IEF and parallel SDS gel electrophoresis for protein separations. The PAAm gel plugs offer a simple method to reduce undesirable bulk flow and limit reagent/sample crosstalk without placing constraints on the selection of separation media, or hindering electrokinetic ion migration in the complex microchannel network. In addition to improving separation reproducibility, the discrete gel plugs integrated into critical regions of the chip enable the use of a pressure-driven sample injection approach which avoids electrokinetic injection bias. The gel plugs also serve to simplify operation of the spatially-multiplexed system by eliminating the need for complex external fluidic interfaces (Figure 1). Using an FITC-labeled E. coli cell lysate as a model system, gel plugs demonstrate to significantly enhance separation reproducibility in a chip with a five-parallel CGE array, whose average variance in peak elution time is only 4.1%.

5.1   Introduction

In this 2-D chip platform, the use of in-situ photopolymerization to generate a discrete semi-permeable PAAm gel plugs within a complex IEF-CGE separation chip is described. The gel plugs act as ion bridges within selected regions of the microfluidic system, allowing ion transport required for electrokinetic separations while preventing hydrodynamic bulk flow and unwanted mixing of ionic solutions, sample, sieving gel, and other reagents within the system. The use of in-situ gel plugs has been previously described for microfluidic applications including electrokinetic protein pre-concentration,[161,162] separation of SDS-denatured proteins,[162,163] and combined separation

and bulk flow control for 2-D separations.[110,164] Here the gel plug is further extended to its application as flow-blocking elements within discrete regions of a 2-D separation system.[58] The gel plugs eliminate bulk solution flow within both the IEF and CGE dimensions, allowing highly repeatable separation performance without substantially affecting ion mobilization during the formation of the first-dimension pH gradient, injection of SDS for the formation of SDS-protein complexes, or during the protein separations themselves. Furthermore, because the chip design allows the photopolymerized gel plugs to be defined independently from the separation channels; their integration does not add unwanted constraints upon the selection of sieving media for CGE. Advantages of this approach are discussed, with a particular focus on separation reproducibility for the 2-D platform.

5.2   Experimental Section

5.2.1   Materials

Polyethylene oxide (PEO, MW ~600,000), poly(vinyl alcohol) (PVA, MW ~130,000), acrylamide (AAm), *N,N'*-methylenebisacrylamide (Bis), ammonium persulfate (APS), *N,N,N',N"*-tetramethylethylenediamine (TEMED), 2-hydroxy-4'-(2-hydroxyethoxy)-2-methyl- propiophenone (Irgcure 2959 or I2959), 2-(cyclohexylamino)ethanesulfonic acid (CHES), 3-(trimethoxysilyl)propyl methacrylate (TPM), fluorescein isothiocyanate (FITC), DL-dithiothreitol (DTT), iodoacetamide (IAM), and ampholyte (pH 3-10) were purchased from Sigma-Aldrich Inc. (St. Louis, MO). Sodium dodecyl sulfate (SDS), urea, tris(hydroxymethyl)- aminomethane (Tris), methanol, concentrated hydrochloric acid (HCl), phosphoric acid, sodium hydroxide, sodium carbonate, and sodium bicarbonate were purchased from Fisher Scientific (Fair

Lawn, NJ). Triton X-100 nonionic surfactant was ordered from MP Biomedicals Inc. (Solon, OH). *Escherichia coli* (E. coli) protein sample was purchased from Bio-Rad Laboratories (Hercules, CA). All aqueous solutions were prepared using HPLC-grade water (Fisher Scientific) and filtered through 0.22-μm syringe filters (Fisher Scientific, Fair Lawn, NJ) before experiments.

5.2.2 Plug Integrated Chip Fabrication

The PAAm injection gel plugs and acid/base gel plugs were fabricated by first injecting a prepolymer solution composed of AAm, Bis, I2959, and 10 mM Tris-CHES buffer (pH 8.4) into the microchannel network from the sample reservoir (A). Before photopolymerization, all reservoirs were sealed to reduce bulk flow, and an optical mask was aligned to the chip to define exposure windows in the desired plug regions. The chip was then placed into a PRX-1000 UV system (Tamarack Scientific, Corona, CA) and exposed to UV radiation for 500 sec at 22 mW/cm^2 to *in situ* synthesize the injection gel plugs (B), acid gel plug (C), and base gel plug (D). After photopolymerization, the IEF channel (E) and the separation CGE channels (F) were rinsed with deionized water. Unreacted monomer solution in the injection channels (G) was replaced with 10 mM Tris-CHES buffer by flushing from the SDS reservoirs (H) to the SDS waste reservoirs (I). Unreacted monomer within the acid (J) and base (K) reservoirs was replaced with deionized water.

To depress the nonspecific adsorption of proteins to the channel surface of the IEF and the lower CGE channels, a double layer of LPA and PVA coating was then performed. To coat the channels with LPA, 30 μL of 10% (w/v) APS solution and 30 μL of 10% (v/v) TEMED solution were added to a vial containing 2.5 mL of 6% (w/v) AAm

aqueous solution, which had been degassed for at least 15 min by sonication. The mixture was vigorously vortexed for 10 s and quickly injected to the channels. After 15 min, the channels were rinsed with 10 mM Tris-CHES buffer to remove the unpolymerized acrylamide. In followed PVA coating step, 4% (w/v) PVA was injected to the channels from the sample inlet (A) and kept undisturbed for 20 min. Excess PVA was removed by rinsing the channels with 10 mM Tris-CHES buffer.

Following the channel coating steps, a sieving matrix containing 2% PEO, 0.1% SDS, and 10 mM Tris-CHES buffer in HPLC DI water was introduced from the sample reservoir (A) until the lower CGE channels (F) were filled. To prevent the hydrodynamic flow of the PEO matrix, a second set of PAAm gel plugs (L) were prepared in the channel sections located between the CGE waste reservoirs (M) and lower gel plug waste reservoirs (N). Vacuum was applied to the CGE waste reservoirs to remove the PEO sieving gel in the channel sections between (M) and (N), followed by vacuum introduction of acrylamide monomer solution from the CGE waste reservoirs (N). Finally, the introduced monomer solution in the lower channel regions was *in situ* photopolymerized by 500 sec UV exposure to form the PAAm gel plugs (L) at the terminus of the lower CGE microchannels (F).

5.2.3 Protein Sample Preparation

A 1 mL solution of 100 mM sodium carbonate/sodium bicarbonate buffer (pH 9.6) containing 1.3 mg/mL of FITC was used to reconstitute the E. coli protein sample, which contained approximately 2.7 mg of solid. The reaction was allowed to proceed in the dark overnight at room temperature. A PD-10 size exclusion chromatography desalting column (GE Healthcare Bio-Sciences Corp., Piscataway, NJ) was used to remove free

FITC from the FITC-labeled proteins and exchange the highly conductive carbonate buffer in the protein sample for 10 mM Tris-HCl (pH 8.2) buffer. The total protein concentration of the FITC-labeled protein sample was determined to be 0.44 mg/mL by a standard Bradford assay.[165]

To denature and reduce the FITC-labeled E. coli protein sample, urea and DTT were thoroughly mixed with 1 mL of the sample solution in a vial with final concentration of 8 M and 100 mM respectively. The reaction was allowed to proceed in the dark overnight at room temperature. Subsequently, IAM was added to the solution to a concentration of 120 mM to alkylate the denatured proteins and the vial was kept in the dark for 1 h at room temperature. Before IEF-CGE experiment, the E. coli protein sample was diluted 20 times using a solution of urea, Triton X-100, and ampholyte (pH 3-10). Their final concentrations in the diluted sample were 8 M, 2% (w/v), and 4% (v/v) respectively.

Protein sample was introduced into the chip using a negative-pressure sample injection method. Before sample introduction, PEO sieving matrix in the sample and sample waste reservoirs was removed, and 1.5 μL of protein sample was pipetted into the sample reservoir. Sample was then loaded into the IEF channel by applying vacuum to the sample waste reservoir through a pippet tip to carefully draw the sample through the IEF channel.

5.2.4   1st-D and 2nd-D Separation Setup

Following the sample injection process, liquid remaining within the sample and sample waste reservoirs was removed, and two 30 μL drops of pre-mixed epoxy (ITW Devcon, Danvers, MA) were applied to each reservoir and allowed to dry for 1-2 min. This step not only enhances separation repeatability by completely and irreversibly

sealing the reservoirs, but, most importantly, it simplifies the chip preparation process. Or other sealing methods, such as nanoport (Upchurch), are also desirable for elegant platform. The DI water in the acid and base reservoirs was then replaced with 0.5 M phosphoric acid and 0.5 M NaOH respectively, and the 10 mM Tris-CHES buffer in the SDS channels was changed to 10 mM Tris-CHES buffer containing 2% (w/v) SDS. To perform IEF, the chip was positioned on the stage of a TE-2000 S inverted epi-fluorescence microscope (Nikon, Melville, NY), and a CZE 1000R high-voltage power supply (Spellman High-Voltage Electronics, Plainview, NY) controlled by a HP E3630A triple output DC power supply (Agilent, Santa Clara, CA) was used to apply a voltage of 240V to the 1.2 cm long IEF channel through two platinum wires inserted in the acid and base reservoirs. After focusing for 3 min, platinum electrode was inserted in the injection SDS reservoirs and lower CGE waste reservoirs, and 1000 V was applied to the lower electrode with the injection grounded. The resulting electric field mobilizes SDS from the upper microchannels, through the SDS gel plugs, and into the IEF microchannel were the SDS rapidly complexes with the focused proteins. The SDS-protein complexes are thus transferred into the array of second dimension microchannels where CGE is proceeded. Fluorescence from the separated protein bands was monitored within a downstream detection region (see Figure 18). The detection channel spacing was intentionally narrowed for detection purpose. An excitation wavelength of 465~495 nm was employed using a B-2E/C blue filter (Nikon) to detect FITC-labeled proteins and a 4 x, 0.20 N.A. objective was used for simultaneous imaging and detection from all CGE channels. Data recording was performed using a Spot RT monochrome CCD camera (Diagnostic Instruments; Sterling Heights, MI) installed on the microscope. ImageJ

(http://rsb.info.nih.gov/ij) and MATLAB 6.5 (MathWorks; Natick, MA) software were used to construct the electropherograms.

5.3   Gel-Plug Enabled PEO 2-D Separation

5.3.1   In-Situ PAAm Gel-Plug

In the original demonstration of a spatially-multiplexed 2-D IEF-CGE protein separation chip, each of the second-dimension CGE channels terminated in a common reservoir,[49] yielding a substantially simpler design compared to the present case. However, this design was found to yield low and unpredictable focusing resolution and high sample loss during IEF, due to the shunting of electric current and sample ions through the low-resistance paths defined by the interconnecting reservoirs. To avoid this issue, each injection and CGE channel shown in Figure 18 terminate in a single isolated reservoir. For the design with 5 CGE separation channels described here, this approach requires a total of 26 individual reservoirs, each of which serves to increase the chance of generating an unwanted on-chip pressure gradient. Despite this large number of reservoirs, the PAAm gel plugs are successfully eliminating all observable bulk fluid flow in the chips. In contrast to previous efforts to integrate pressure-blocking gel plus into microfluidic separation chips,[110,164] discrete gel plugs were fabricated only in relatively short regions of the chip where pressure blocking is critical, using a chip design which allowed the gel plugs to be formed separately from the separation media used for IEF and CGE. The PAAm plugs were fabricated in three sections of the 2-D microchannel network, namely in the injection channels proximal to the IEF channel, in the channel segments connecting the ends of the IEF channel to the acid and base

reservoirs, and the ends of the lower CGE channels distal from the IEF channel (Figure 18).
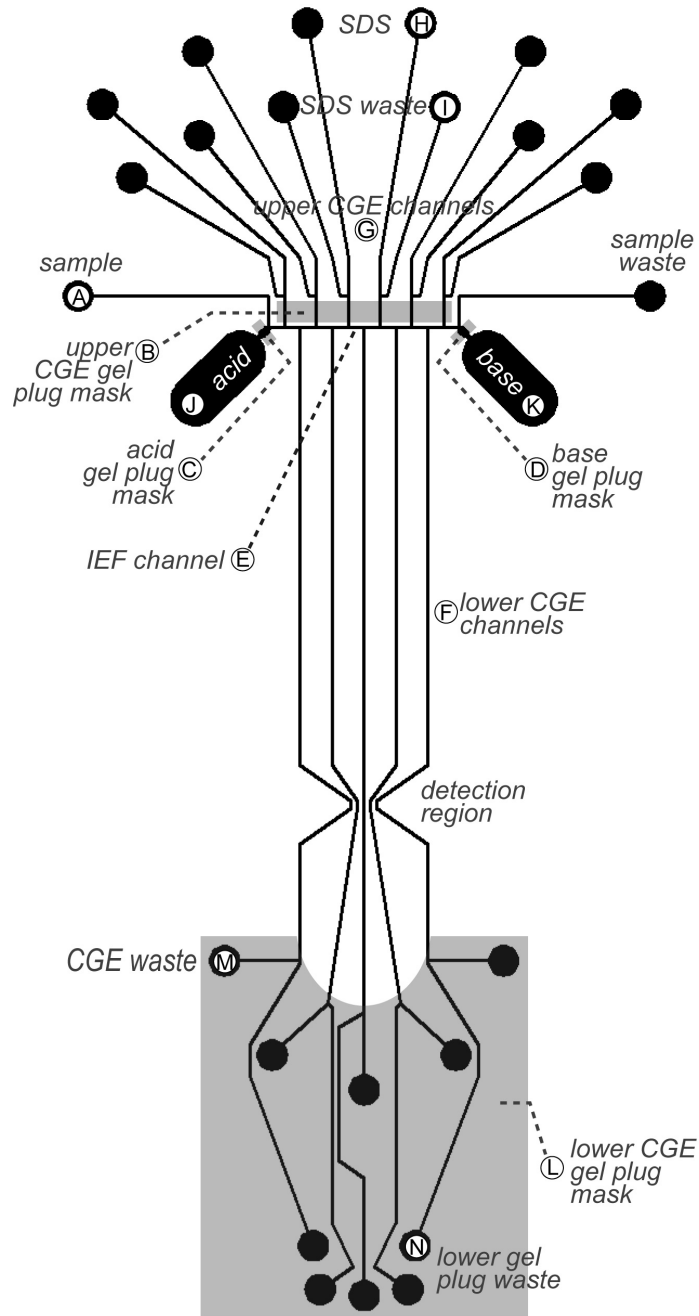
Figure 18. Schematic diagram of a microfluidic 2-D chip. Regions exposed to UV light source during AAm photopolymerization (B, C, D, and L) are shown in gray (in multiple UV exposure steps).

One potential concern for the pressure-blocking plugs is the possibility of ion depletion, with differential ion mobility through the gel resulting in depletion of ions at one end, and ion enrichment at the opposing end. To determine whether this phenomenon poses an issue in the optimized PAAm gel recipe, a 1 mm long gel plug was fabricated in the center of a 2.1 cm long microchannel, with a 10 mM Tris-CHES background buffer. A 500 V bias was applied across the channel for 30 min. No significant current variations were observed during this period, indicating the absence of ion depletion in this system.
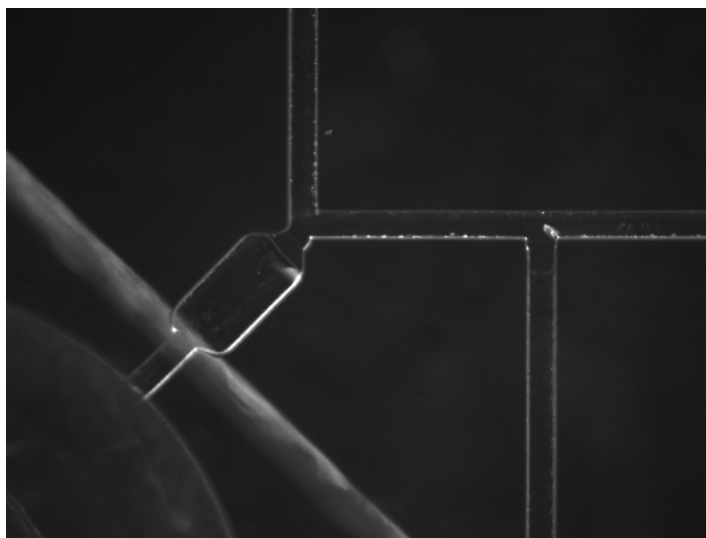
Figure 19. Image of acid/base gel plug connecting to sample channel and acid/base tank in a spatially multiplexed 2-D chip (channel width, 150 μm).

Resistivity of the PAAm gel was characterized by measuring current through a gel-filled channel 170 μm wide, 100 μm deep and 80 μm long, with a background buffer of 10mM Tris-CHES. To avoid electrolysis, a low voltage (140 V) was applied across the reservoirs, generating a stable current of 0.84 μA for a measured resistivity of 3.6 kΩ cm. Pressure resistance of the gel plugs was measured using at least five chips containing

photolithographically-patterned 300 μm long PAAm gel plugs. A syringe was connected vertically to one reservoir, and increasing weights were applied to the syringe plunger until bulk fluid flow was observed within the channel. Using this approach, an average burst pressure of 490 kPa was determined for the short 300 μm plugs.

The 2 mm long PAAm gel plugs fabricated in the injection channels served to prevent the highly conductive SDS buffer from entering the IEF channel and interfering with IEF separation, while allowing SDS to electro-migrate through the gel plugs and complex with the focused protein bands upon application of an electric field along the CGE microchannels. Similarly, the discrete PAAm gel plugs at the acid/base reservoirs (Figure 19) prevented bulk flow of anolyte/catholyte solution within the IEF channel due to EOF, unleveled reservoir heights, or trapped bubbles within the reservoirs. In a typical experiment without acid/base gel plugs, pressure gradients disturb the pH gradient and sweep protein bands along the IEF channel, preventing effective focusing. After introduction of the PAAm gel plugs, observable bulk flow was eliminated. A key feature of the chip design is that the connecting channels linking the acid/base reservoirs to the IEF channel are twice as wide as other microchannels on the chip. This provides a physical constraint to increase the mechanical resistance of the gel plugs to pressures generated during the introduction of sample and sieving matrix solutions, while also reducing the electrical resistance of the gel plugs to ensure a higher electric field along the IEF channel during protein focusing.
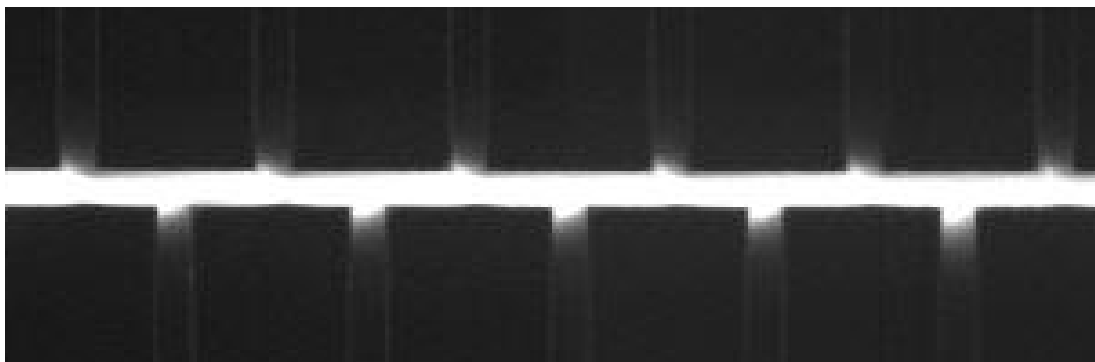
Figure 20. Sample injection in the IEF channel showing minimal intermixing with PEO sieving matrix due to use of PAAm gel plugs in injection and end of separation channels

The PAAm gel plugs located in the lower CGE channels prevent bulk flow of the relatively low-viscosity PEO sieving matrix, allowing a well-defined and stable interface between the sieving gel and the free-solution IEF channel to be established, as seen in Figure 20. This is a critical aspect of the chip design, since intrusion of gel into the IEF channel can change the local electric field and disturb the focused bands during IEF, resulting in lower separation resolution and irreproducible parallel CGE separations. The gel interfaces are also desirable to encourage sample stacking at the IEF/CGE channel intersections. The previous efforts to form defined PEO gel boundaries at the heads of parallel CGE channels required laborious manual injection of gel from each of the injection and lower CGE channels while simultaneously flowing buffer solution through the IEF channel at a high rate to flush gel intruding from the CGE channels.[58,166] Acceptable interfaces could only be generated by tuning the flow rates of gel in each CGE channel independently. In contrast, the PAAm gel plugs provided hydrodynamic resistance in the lower CGE channels, allowing ampholyte/sample solution to be rapidly injected through the IEF channel without disturbing the PEO gel, resulting in highly

repeatable gel interfaces at each channel intersection. While similar results within the CGE channels could have been achieved by filling the entire second dimension channels with photopolymerized PAAm as a sieving gel,[58,110] the discrete plugs used here provide flexibility in the choice of separation medium for CGE. It is a significant feature in that replaceable gels such as PEO are often preferred due to the challenges involved in realizing uniform photopolymerization and repeatable sieving properties for *in situ* PAAm.

The gel plugs also served to greatly simplify external interconnects to the chip. In order to limit the shunting of electrical current during IEF, individual reservoirs are necessary at the terminus of each injection and lower microchannel used for the parallel CGE separations. Without gel plugs, each reservoir required a cumbersome fluidic interface including external low-dead-volume valves, capillaries, Upchurch nanoport connectors, and multiple syringe pumps were required to introduce sample and other reagents while attempting to limit the bulk flow throughout the chip. Operation of the system was difficult, time consuming, and not amenable to automation. Furthermore, it was difficult to remove the bubbles from the complex network due to the large numbers of reservoirs and off-chip connections. As a result, the system could not entirely eliminate bulk flow, resulting in consistently poor separation repeatability. In contrast, the integrated PAAm gel plug device offers the potential for repeatable and automated operation using a standard robotic autosampler platform.
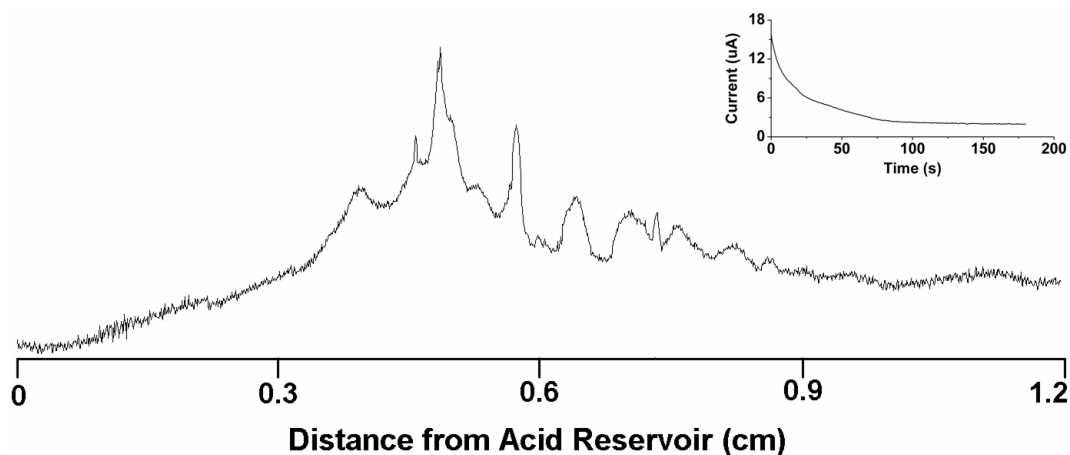
Figure 21. IEF of FITC-labeled E. coli protein sample. The inset is the electric current-time profile during the IEF separation

5.3.2 2D Separation of E.coli Cell Lysate

A typical electropherogram following focusing of the FITC-labeled E. coli proteins in the first dimension microchannel is shown in Figure 21. While it appears that the majority of the focused proteins are located towards the basic end of the IEF channel, it should be noted that FITC is sensitive to pH and exhibits reduced fluorescence intensity at pH below 4.[167] Thus proteins focused near the acid reservoir cannot be detected due to the quenching of FITC fluorescence. For the more prominent peaks in the electropherogram, an average peak width around 250 μm is estimated, suggesting a peak capacity of 48 for the IEF separation.

It is a common practice in 2-D gel electrophoresis experiments to equilibrate the IEF dimension with a solution containing SDS to ensure complete SDS-protein complexation before performing gel electrophoresis. It has been suggested that during 2-D gel electrophoresis with carrier ampholytes, SDS equilibration is unnecessary if the effective gel diameter is less than 1 mm.[168] Similarly, due to the small diffusion lengths in the

microfluidic system, the complexation reaction occurs rapidly so that equilibration is unnecessary. Same separation performance was observed when 5 min equilibration was used, except for diffusion-induced broadening of the focused bands. Thus, SDS was electrokinetically injected through injection channel gel plugs and across the IEF channel without an equilibration step. The process of SDS injection and protein mobilization into the CGE microchannels is depicted in Figure 22. When the CGE voltage was applied, SDS ions migrated through the 2-mm-long PAAm gel plugs in injection channels and continuously bound to the denatured proteins in the IEF channel to form negatively-charged SDS-protein complexes, which were then swept towards the entrance of the nearest lower CGE channel. The real-time complexation process results in a stacking front, in which bright bands were formed and migrated towards the lower CGE channels. As a result, the charged SDS-protein complexes are concentrated during the injection process. However, significant bond broadening was observed during transfer due to inhomogeneities in the electric field lines around the 90 degree channel bend, as apparent in Figure 22 (d-e).

When attempting to perform repeated 2-D separation runs on a single chip, it was observed that residual SDS within the device resulted in poor IEF performance, eventually leading to the formation of a single sample bond which continuously migrated toward the anode in the acid reservoir. While residual SDS was reduced by aggressively flushing the chip with solvent, carryover could not be fully eliminated. In addition, leakage across the PAAm gel plug at the base reservoir often occurred in re-used chips, presumably due to the high concentration of hydroxyl ions present on the channel walls near the base reservoir during the previous IEF separation. Under basic conditions, Si-O-

C bonds linking the gel plugs to the surface were hydrolyzed, and adhesion of the gel plug to the channel surface was compromised. As a result of these factors, the polymer chips are not re-usable, and separations reported here were performed with virgin chips.
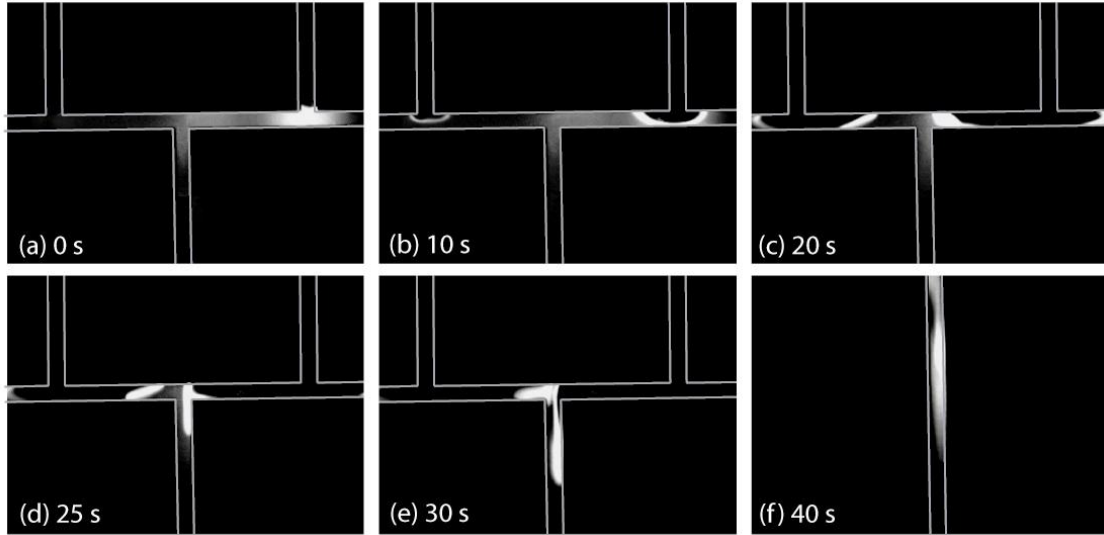
Figure 22. Sequential images depicting the real-time SDS-protein complexation and stacking process during transfer of protein bands from the IEF channel to a single CGE channel.
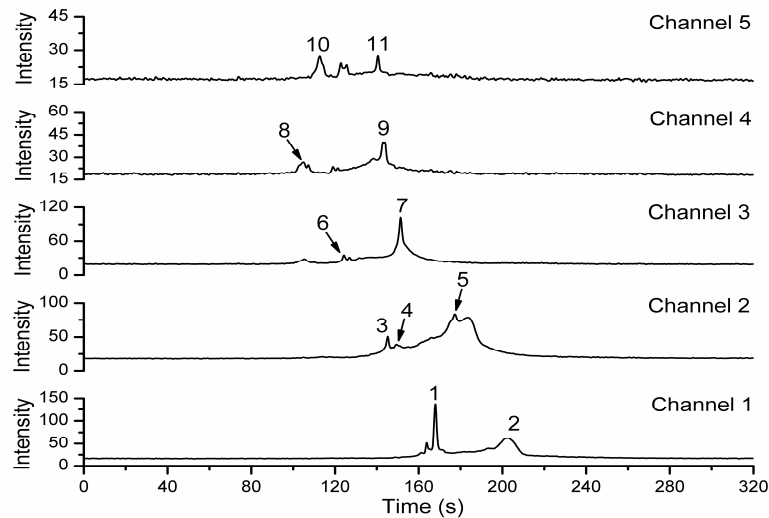
Figure 23. Parallel CGE separation of IEF-separated FITC-labeled E. coli proteins. Channel 1 corresponds to acid side and channel 5 to base side.

(1)
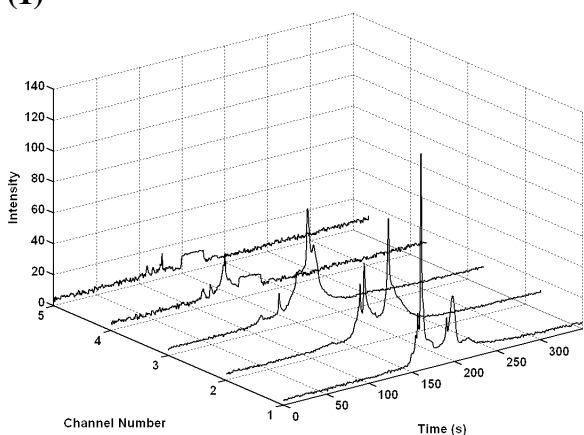
(2)
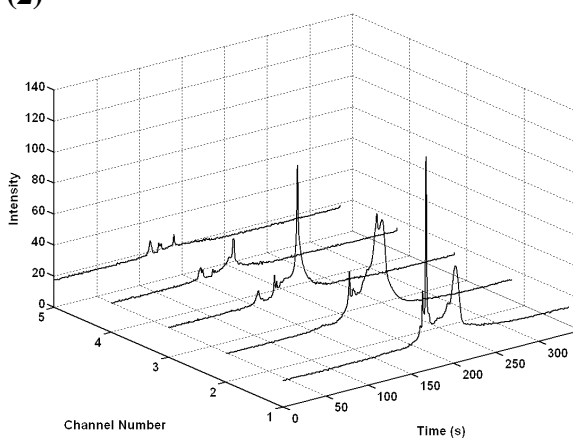
(3)
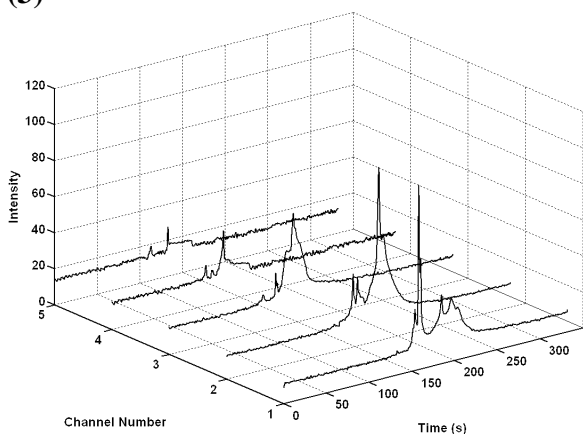
(4)
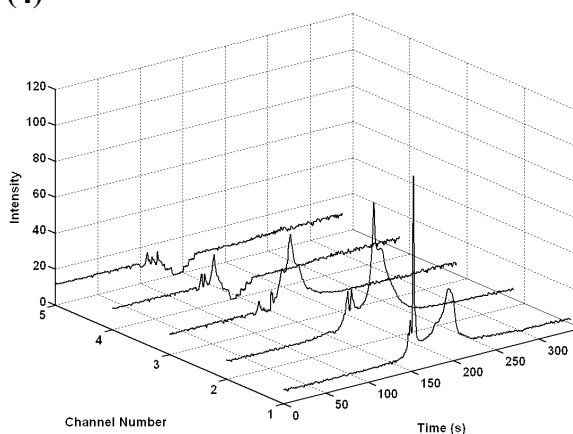
Figure 24. Four consecutive runs of parallel five-CGE separation used for evaluation of separation reproducibility

A typical set of electropherogram resulting from a full 2-D separation of FITC-labeled E. coli protein sample is shown in Figure 23. The parallel CGE separation was completed within 4 min, and a complete 2-D separation is less than 10 min following initial sample injection. To evaluate the separation reproducibility of the on-line IEF-CGE devices, a sequence of runs was performed using four virgin chips, with the resulting electropherogram shown in Figure 24. The elution times of 11 resolved peaks were used to estimate the separation reproducibility, with the results listed in Table 4. The relative standard deviation (%RSD) values of all peaks are between 1.6% and 7.7% ,

with an average of 4.1% and only three peaks showing variations greater than 5%. These results compare favorably with conventional 2-D PAGE gels, particularly when using carrier ampholytes in the first IEF dimension.[169,170]

Table 4. Relative standard deviation (%RSD) of peak elution time

Channel #	Peak Number										
	1	2	3	4	5	6	7	8	9	10	11
1	4.0%	1.6%									
2			4.2%	4.3%	3.9%						
3						2.8%	5.9%				
4								2.3%	7.5%		
5										2.1%	6.6%

5.3.3 Improvement on Separation Medium

The PEO sieving gel produces a very promising 2-D separation. However, the PEO self is fluidic due to its low viscosity at low concentration. The higher concentration of PEO (>4%) can be used for 2-D chip, but it is very difficult to introduce viscous PEO into 2-D chip. For example, use of syringe pump to injection PEO may cause acid-base gel plug damage; vacuum force is too weak to introduce PEO gel. Additionally, during PAAm gel fabrication for separation channels, the PEO in adjacent channel tends to flow into IEF channel under vacuum. As pointed out that methanol is used to clean remainder of PEO in separation channel for PAAm fabrication, the covalent bonded LPA may break down after methanol rinsing, leading to weak sidewall binding. To completely prevent sieving matrix intrusion into IEF, it will be wise to use crosslinked sieving matrix in the CGE channel. There is a variety of approach to improve the separation medium, examples including PEO-PAAm, and photopolymerized PAAm system. The latter

sieving matrix can withstand a much higher pumping and hydraulic pressure during gel preparation. It is unrealistic to use PAAm for sieving matrix unless polyacrylamide can be photolithographily polymerized inside microchannel without generating bubbles. Other hydrogel polymers, such as poly (ethylene glycol) (PEG), can be used as protein separation sieving matrix, as long as they are inert and do not adsorb to proteins.[171,172] These issues will be studied in Chapter 7 and 8.

5.4   Summary and conclusion remarks

In-situ photopolymerized PAAm gel plugs offer a simple, valve-less approach for controlling bulk hydrodynamic flow and isolating reagents in microfluidic systems, without hindering the mobility of electromigrating ions. This approach is particularly attractive for complex electrokinetic systems where precise control over interfacial sample/reagent boundaries is critical for effective and repeatable operation. For the case of the integrated IEF-CGE platform, the use of short PAAm gel plugs provided effective isolation of sample and ampholytes in the IEF channel, acid and base solutions within the individual IEF channel reservoirs, SDS in the upper injection channels, and PEO sieving gel in the lower CGE channels. The gel plugs also provided for efficient injection of SDS into the IEF channel post-focusing for real-time SDS-protein complexation. These features collectively enabled separation repeatability comparable to traditional 2-D gel electrophoresis. More generally, the use of *in-situ* gel plugs can substantially reduce the challenges associated with off-chip interfacing to electrokinetic microfluidics by making systems more robust to unavoidable pressure gradients. Ultimately, integrated PAAm gel plugs can make separation platforms such as the 2-D IEF-CGE chips more amenable to automation through the use of standard dispensing robotics. The need for such simple

approaches to automation becomes increasingly important as higher-dimensional microfluidic separation chips are developed, such as a proposed concept for a 4-dimensional platform combining IEF, ITP, SDS-PAGE, and RPLC [173] or depletion, IEF, 1-DE and RP to MS/MS.[174] With the gel plug technology established, future developments will focus on improving the overall resolving power of the IEF-CGE microfluidic system, which is affected by a host of factors such as sample labeling, choice of sieving matrix, channel intersection geometry, and channel density.

Chapter 6.   Electrokinetic Design Optimization

As observed in the previous chapter that 2D microfluidic design (Figure 17(a)) does not avoid sample leakage, and PEO sieving matrix is incapable of preventing sample-PEO inter-intrusion even use of PAAm gel plugs. By such microfluidic platform, less than 30 bands can be resolved for *E.coli* cell lysate (Figure 24). To improve separation performance, sample injection has to be investigated via both simulation and experiments. In this chapter, an approach is introduced for microfluidic electric and electrophoretic simulation.

6.1   Introduction to Electrokinetic Simulation

6.1.1   PSpice Simulation

The chip can be regarded as the resistor connected in series and parallel. The potential and current distribution is determined by the electrical diagram, as well as its resistance values. To simply the simulation, the medium in each channel is replaced with a resistor. The electric resistance of each channel is based on its physical geometry and associated resistivity of the medium used, e.g., buffer (Tris-CHES) for IEF, gel (PEO) for injection and CGE channels. The schematic diagram of a five-channel 1-D chip is shown in Figure 25. The injection channels have same channel length and cross-section area, thus the electric resistance is R_i. Similarly, the resistance of each segment of the 1st dimension channel is R_1; the resistance of the 2nd dimension channel is R_2. The resistance of the 1st-D consists of 10 R_1, adjacent pair of which will co-elute into the common 2nd-D channel (R_2). The migration velocity of the charged species will be related to the magnitude of current and potential through the R_1. Use of PEO as sieving matrix platform, for example, the measured resistance is,

$R_i = 60Mohm$, $R_1 = 0.3Mohm$, $R_2 = 150Mohm$
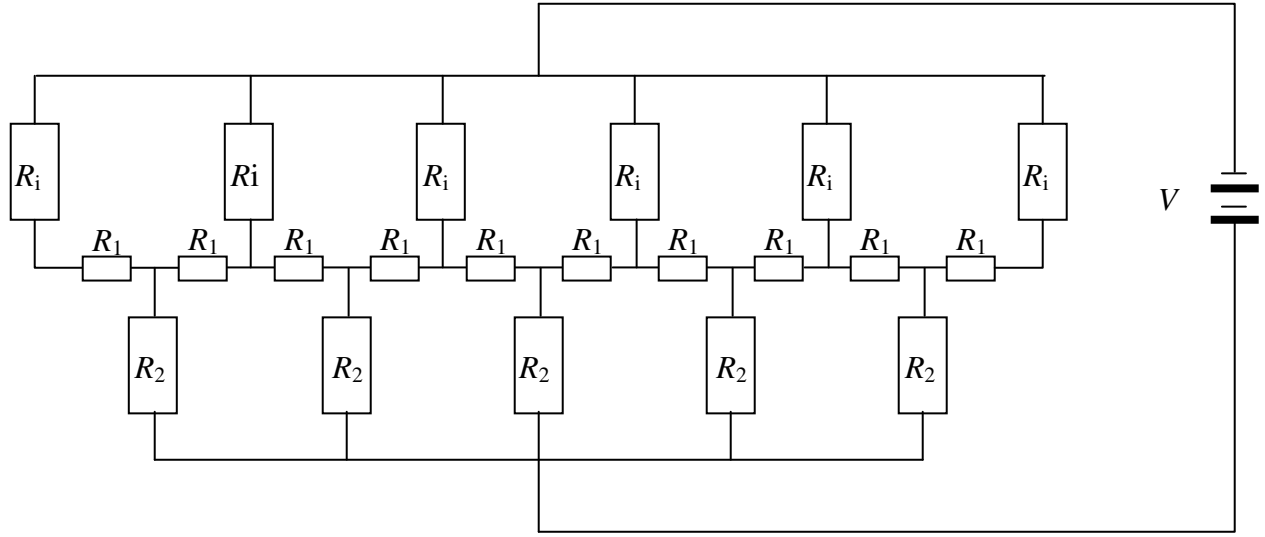
Figure 25. The equivalent electric diagram of a five-channel chip. The R_i represents for the resistance of the injection channels; the R_1 for individual segment of the 1st-D channel; the R_2 for individual separation channel, assuming constant electrical resistivity on all channels.
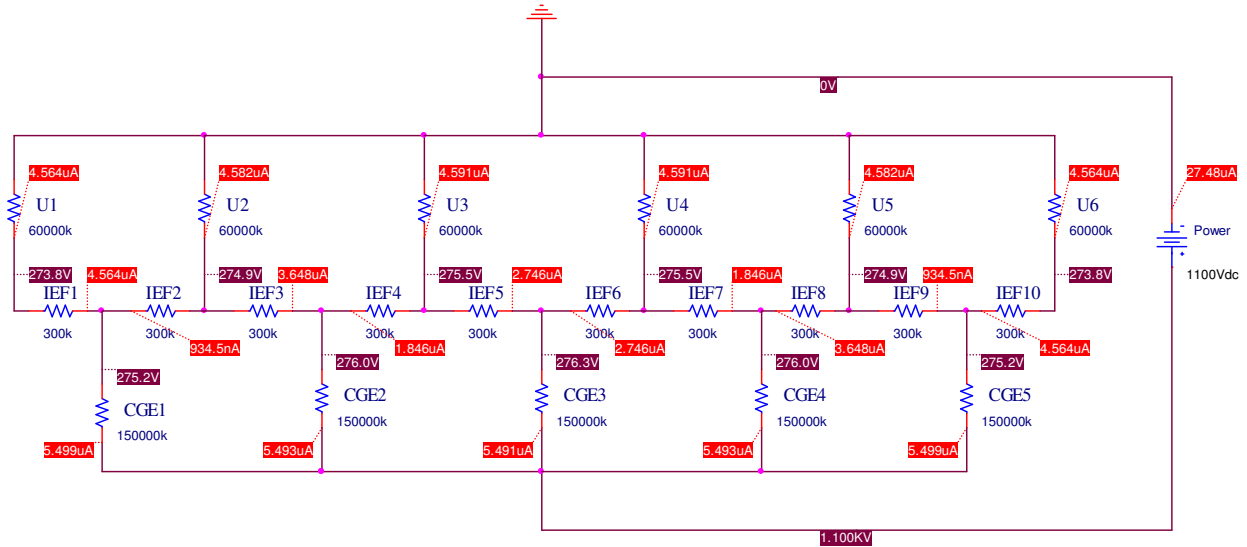
Figure 26. The electric potential and current distribution in a five-channel chip by Pspice simulation. The injection resistor is grounded and separation resistor positive.

During gel electrophoresis, the total potential of 1100V is applied between injection and separation channel reservoirs, with ground on the injection terminus. Taking the resistance into account, Pspice simulates voltage and current distribution in the circuitry (Figure 25) and the results are given in Figure 26. The current in the injection channels are approximately equal, and similar results for the separation channel, e.g., 5.499 µA in the most-outer separation channel, and 5.493 µA in the adjacent separation channel. However, both current and voltage are significantly different in the adjacent pair of segment in the 1st-D, such as 4.554 µA in IEF1 and 0.934 µA in IEF2, respectively. This pair of segment has nearly five-time of variation. The impact of the current difference on sample transfer is so large that sample transfers much faster in higher current segment than its counterpart. The slower velocity is expected in the counter-pair segment, leading to the bond dispersion and broadening.
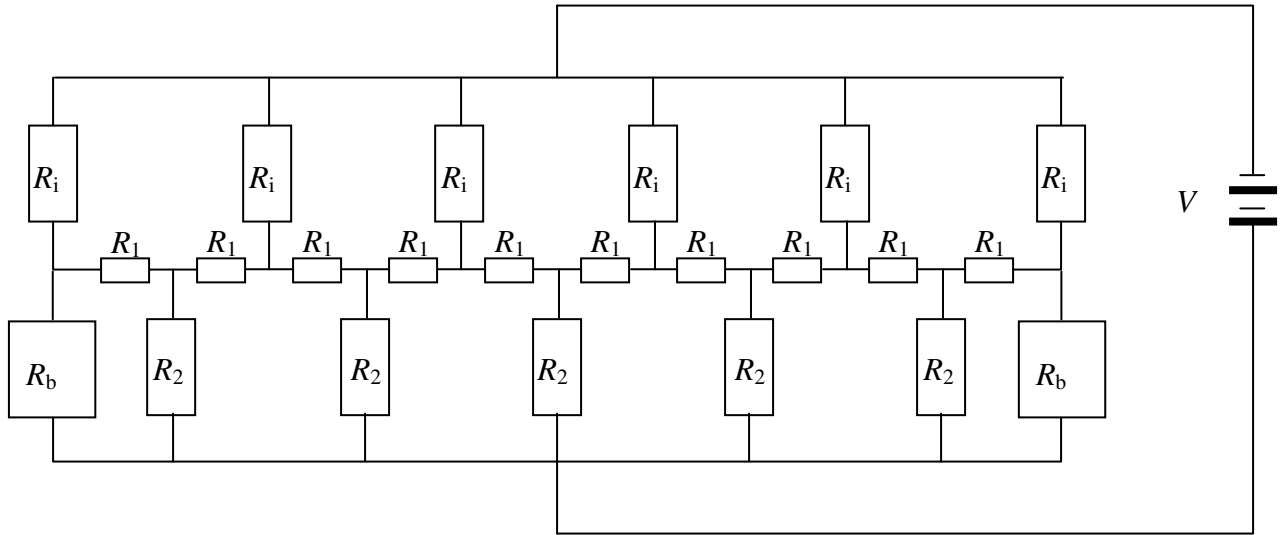
Figure 27. The equivalent electric diagram of a five-channel chip with addition of two-backbiasing channels. The R_i represents the resistance of the injection channel; the R_1 individual segment of the 1st-D channel; the R_2 individual separation channel; R_b backbiasing channel, assuming constant electrical resistivity on all channels.
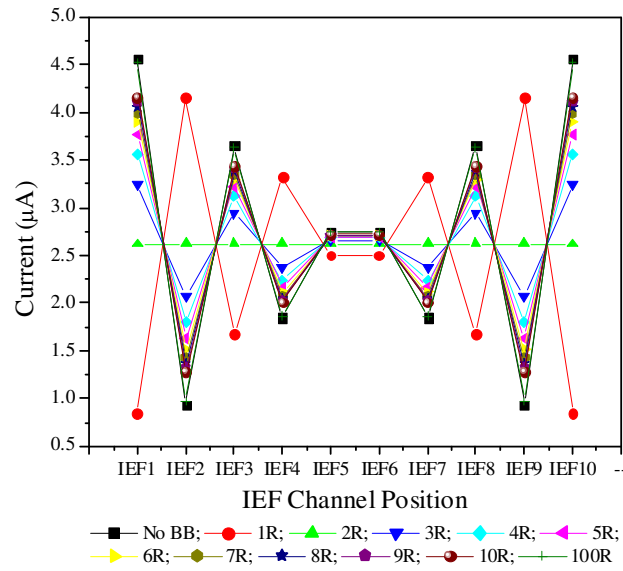
Figure 28. The current distribution in 1st-D segment of a five-channel chip using backbiasing channels with different resistance ratio over separation channel. The backbiasing resistance is infinite when no backbiasing channel is employed.
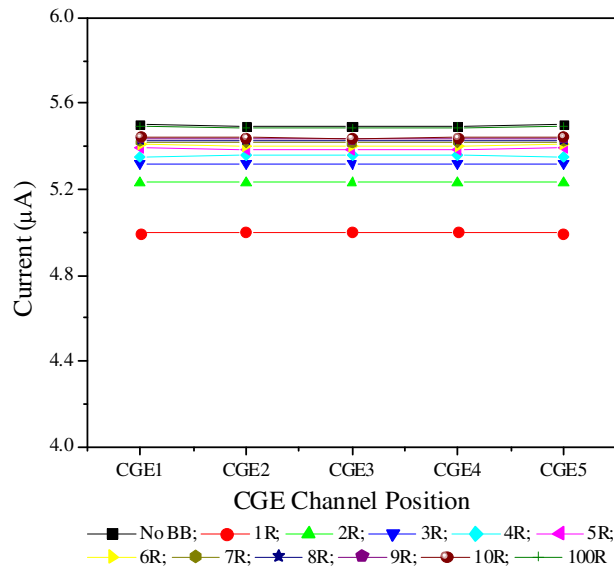
Figure 29. The current distribution in 2nd-D channel of a five-channel chip using backbiasing channels with different resistance ratio over separation channel.

An ideal design should be able to bear uniform current (and/or potential) distribution in respective channels, such as equal current in 1st-D segment. Besides, the leakage from side-channel into 2nd-D has to be prevented during sample transfer. The straightforward approach to prevent leakage is to add two 2nd-D channels parallel to two outer 2nd-D separation channels, as seen in Figure 27. In order to understand the effect of these channels on current distribution, a series of channel resistance is simulated. Current and potential in each channel are summarized in Figure 28 and Figure 29. As discussed before, without these two channels, the current variation in the 1st-D segment is enormous, up to 5 time of adjacent segment in the outer 1st-D channel. On the other hand, use of small channel length, e.g., same length as of the separation channel, leads to current variation in opposing direction. The current is lower in IEF1 than IEF2, compared to higher in IEF1 than IEF2 for a chip without leakage-protected channel. There is one special case where the current distribution is uniform in either 1st-D or 2nd-D. The two-fold resistance of channel is the design optimization to eliminate current (and/or) variation. It is also true for varied number of the separation channels, e.g., two-channel to ten-channel chip. With assumption of same electrical resistivity, the potential distribution is also uniform. This special channel can not only avoid sample leakage, but also regulate current distribution. Because this channel serves as backbiasing purpose, it is termed as backbiasing channel.

6.1.2 FEMLab Simulation

Sample injection is a critical step of gel electrophoresis separation. A well-defined sample plug from sample channel can improve the separation resolution. Several sources, such as sample leakage, sample tailing and diffusion, deteriorate injection plug length. To

minimize the skew and bond-broadening, many studies investigated various channel design and geometry [120-132] to obtain regular short sample plug. The effect of those factors can be easily observed by FEMLab simulation.

6.1.2.1 Introduction to FEMLab

One of useful simulation tools, FEMLab is capable of simulating sample plug transfer from horizontal channel to vertical channel. Two physical models are used: conductive media and electrokinetic flow (Nernst-Planck), whose equations manifest them as Physic modes in FEMLab simulation. To develop a FEMLab model for electrophoresis simulation, the physic models are created by selecting conductive media and electrokinetic flow under Multiphysics tab.

The next step is to define the model system, such as constants and variables. Under Options menu, click Constants, the constant can be added by inputting the name of interest and value; or click Expressions to compile variables, e.g., a Gaussian distribution plug equation. The constant used includes initial sample concentration (C_0), diffusion coefficient (D_0), sample mobility (u_0), medium conductivity (ρ), voltage (V), sigma (σ) and plug center position (μ). The expression for the plug distribution is

$$Plug\_Gafu = C_0 \exp[-0.5 \times ((x-\mu)/\sigma)^2] \tag{3}$$

Above equation only gives the Gaussian distribution of plug in the x-direction. Thus it is not considered that a plug is inside a channel, whose width will confine plug in y-direction. For this purpose, a restriction expression is added into above equation, as follows,

$$Plug\_Gafu = C_0\{abs(y <= y_0) \times \exp[-0.5 \times ((x-\mu)/\sigma)^2]\} \tag{4}$$
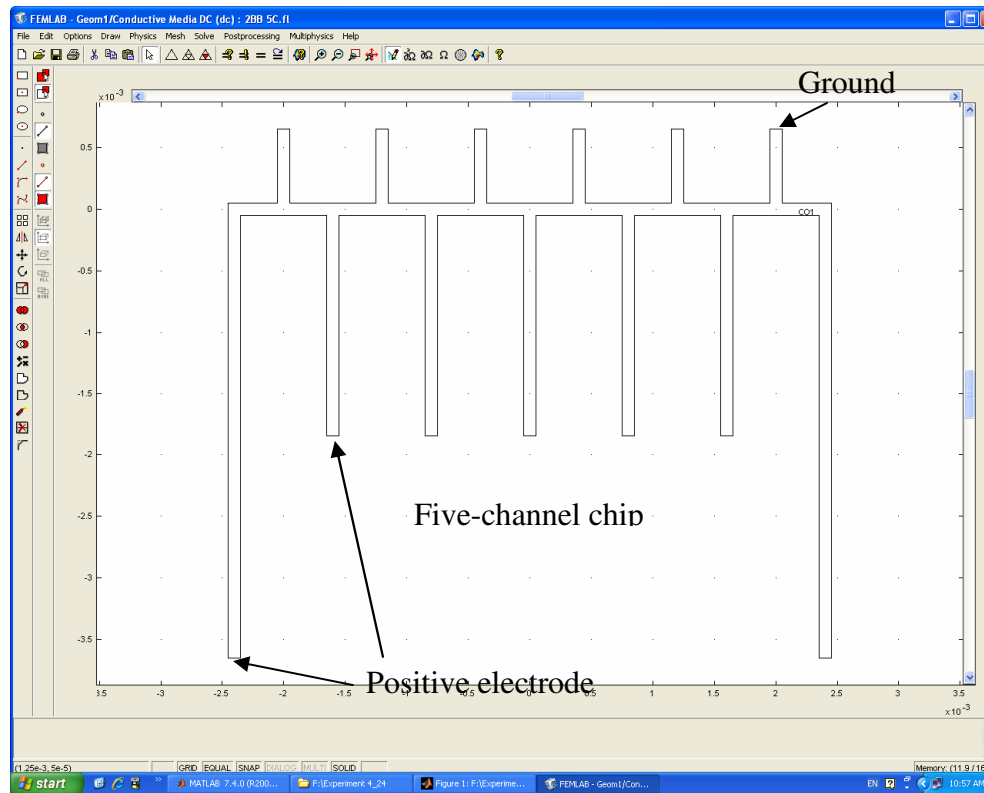
Figure 30. A typical five-channel chip layout in FEMLab simulation platform. The boundary conditions and mesh size can be readily manipulated.

The next step is to draw a schematic diagram of chip, which can be easily done in FEMLab with a variety of drawing options. A typical 2-D chip is shown in Figure 30. The boundary conditions for both conductive media and electrokinetic flow are manipulated according to the application. For example, for gel electrophoresis, the horizontal boundary in injection channel is grounded and the horizontal boundary in separation channel is positive electrode. All other boundaries are insulation.

6.1.2.2 Sample Transfer Simulation

It is almost impossible to simulate chip system with identical geometry as real case. To do so, it requires much longer time to perform a single simulation run, not mention to the requirements on capacious memory and CPU system. In order to facilitate the

simulation, the miniature design structure and scaling boundary conditions are adopted instead of the actual chip dimension. Besides, sample transfer and initial electrophoresis inside 2nd-D channel is of interest. In a five-channel 1D test chip, the injection channel length is 10 mm, separation channel 60 mm, 1st-D segment 0.4 mm, and applied potential 1100 VDc. The voltage used in simulation is scaled to 5 V, and injection channel is grounded and lower CGE is positive electrode by 220 fold (1100/5 = 220). Simulation results of a simple sample transfer from 1st-D to 2nd-D in non-biased and backbiasing chip are given in Figure 31 and Figure 32. From FEMLab simulation, the difference between these chip designs can be clearly distinguished, i.e., sample leakage is observed from the side-channel and the sample injection velocity is varied in non-biasing design, while leakage is mitigated in backbiasing design. Non-uniformity injection is also observed for non-biasing chip, and uniform injection is expected in two-fold backbiasing device. These results are consistent with the current distribution obtained from Pspice simulation as shown in Figure 28.
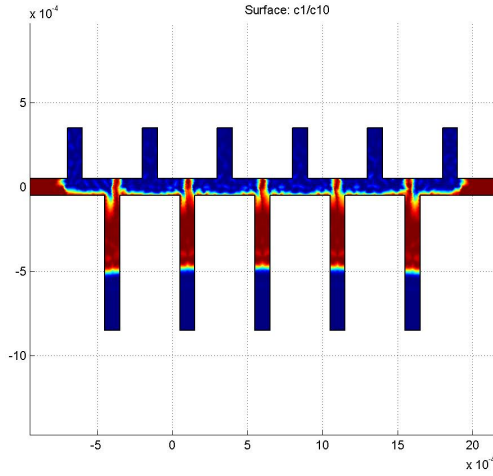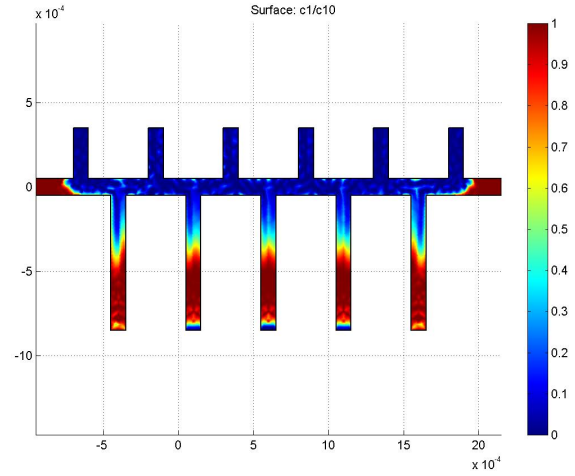
(a) Transfer from 1st to 2nd-D   (b) 2nd-D electrophoresis

Figure 31. FEMLab simulation of sample transfer in a five-lane chip without backbiasing channels. (a) Sample transfer from 1st-D to 2nd-D channel; (b) Varied migration velocity in the progress of sample transfer.
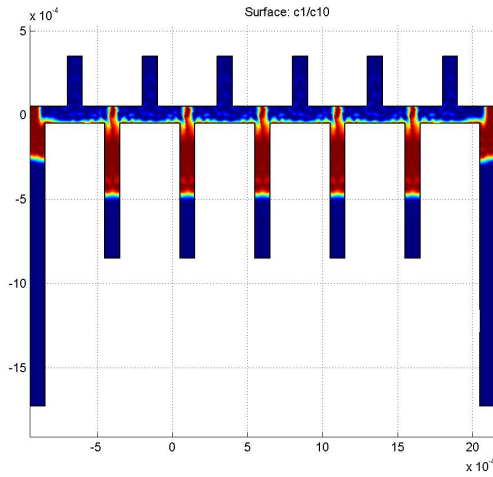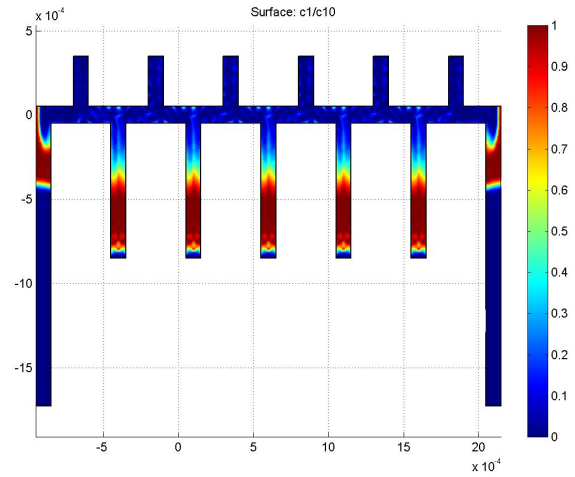
(a) Transfer from 1st to 2nd-D   (b) 2nd-D electrophoresis

Figure 32. FEMLab simulation of sample transfer in a five-lane chip with backbiasing channels. (a) Sample transfer from 1st-D to 2nd-D channel; (b) Uniform migration velocity in the progress of sample transfer.

The separation velocity in individual 2nd-D channel of non-biasing channels is also varied (Figure 29 and Figure 31). The center channel of 2nd-D shows the lowest velocity

and the two outer channels migrate comparatively faster. Asymmetrical injection is observed in each pair of the 1st-D segments, especially for the outer pair of segments as shown in Figure 31. The root cause has been demonstrated in the electrical simulation, in which the current in the segment of the 1st-D is nearly several-fold to its pair segment (Figure 28). This injection scenario leads to the bond-broadening, deteriorating the separation performance. It is expected that chip with backbiasing channels will offer a better sample injection and benefit of separation. The simulation in Figure 32 verifies that the uniform sample injection occurs on five channel chip, and the electrophoretic velocity in the 2nd-D is exactly identical. The backbiasing chip exhibits a well-defined length of sample injected, as well as the sample electrophoretic velocity on multiplex lane chip design.

(a) Transfer from 1st to 2nd-D　　　　　　(b) 2nd-D electrophoresis
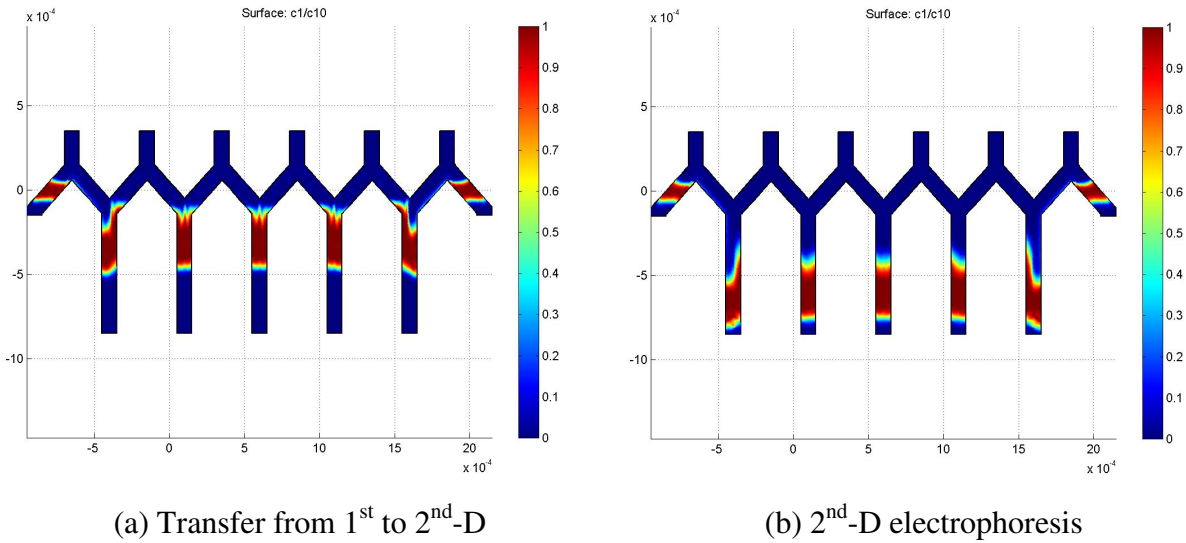
Figure 33. The sample injection and separation simulation on five-lane zigzag chip without backbiasing channels, (a) sample transfer and (b) continuation.

The backbiasing chip with straight 1st-D is not without defection, since it creates sample tailing during injection (same phenomenon exists in non-biasing chips) as shown

in Figure 31 and Figure 32, which can be clearly identified by FEMLab simulation. Further modification is made to the backbiasing chip by using angled 1st-D channel geometry, while remaining other parameters such as channel width and depth, and boundary conditions. The simulation results are given in Figure 33 and Figure 34. The sample tailing has been significantly minimized, although asymmetrical injection exists in the non-biasing chip. It is expected that the backbiasing chip performs better during sample injection and separation (Figure 34). The improvement of sample tailing is attributed to the change of the electric field distribution in the IEF. In addition, the leakage is also minimized even for non-biasing chip. More details will be discussed in section 6.2.

(a) Transfer from 1st to 2nd-D   (b) 2nd-D electrophoresis
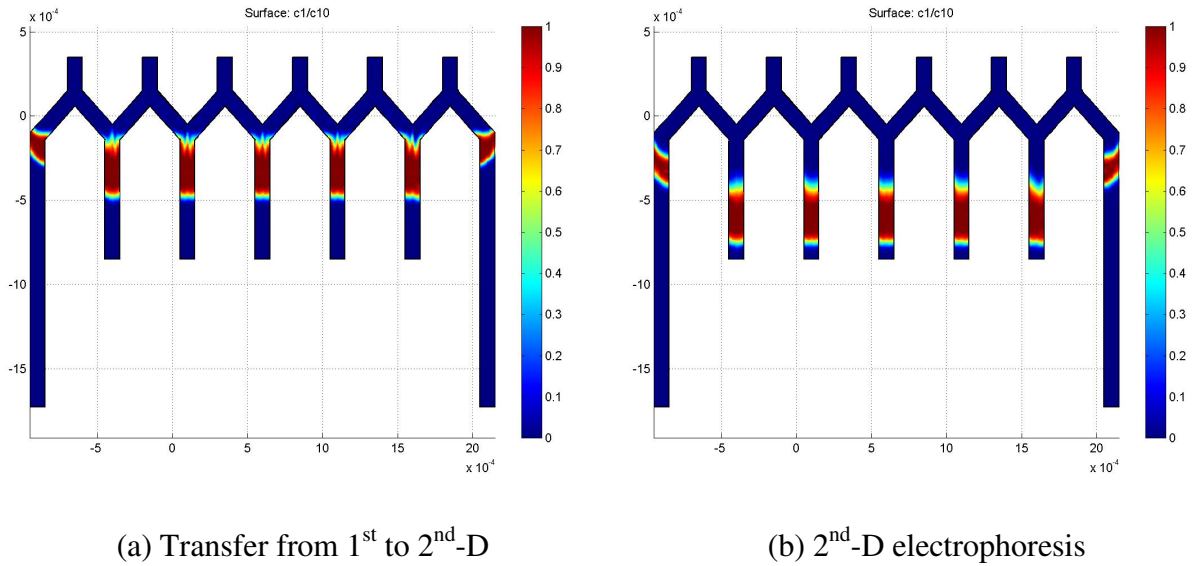
Figure 34. The sample injection and separation simulation on five-lane zigzag chip with backbiasing channels, (a) sample transfer; (b) electrophoresis in 2nd-D.

6.2   Optimization of Spatially-Multiplexed 2D Chip

6.2.1   Potential Issues of 2D Chip

There has been considerable progress in the development of microfluidic systems for biomolecular separations based on a variety of single-dimension electrokinetic separation mechanisms.[30,46,48,175] For the analysis of complex biological samples, single dimension separations typically cannot provide sufficient resolving power for effective analysis of these complex mixtures. Thus, microfluidic systems employing multidimensional separations such as isoelectric focusing (IEF) – sodium dodecyl sulfate (SDS)/capillary gel electrophoresis (CGE),[47,49,50] IEF – capillary zone electrophoresis (CZE),[52] and CZE – micellar electrokinetic chromatography (MEKC),[54] have been developed for achieving higher peak capacity than single dimension systems, while leveraging the inherent advantages of microfluidics to seamlessly couple the multiple separation dimensions on-chip.

Microfluidic platforms for multidimensional separations can be either the time-multiplexed, with second dimension separations performed serially,[52,176,177] or spatially-multiplexed, with multiple parallel second dimension separations performed simultaneously.[49,118,178] In time-multiplexing, sample fractions from the first separation dimension are sequentially sampled and separated within the second dimension. To enable reasonable sampling of analyte from the first dimension while limiting sample loss and bond broadening between sequential sampling steps, the second dimension separation must be substantially faster than the first. This constraint limits the available separation modes which may be employed in time-multiplexed systems.
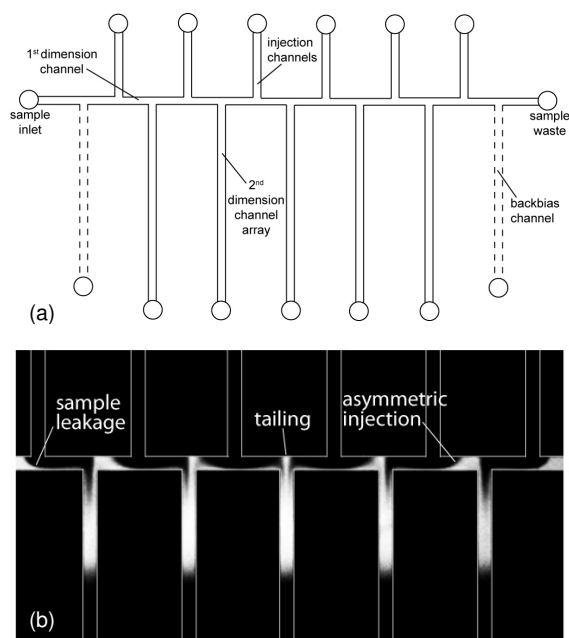
Figure 35. (a) Simplified schematic of a spatially-multiplexed 2-D separation chip with five 2nd dimension microchannels, and (b) image during the sample transfer process using a fabricated chip without backbias channels.

In contrast, spatially multiplexed separations relax this requirement by allowing the first separation dimension to be fully sampled in a single step, thus enabling access to a wider range of high-resolution separation modes.[179] Spatially multiplexed microfluidic systems for intact protein separations based on IEF-CGE has been an area of particular focus in recent years.[49,110,118,179] While the peak capacity of chip-based IEF-CGE systems remains lower than traditional slab gel two-dimensional (2-D) polyacrylamide gel electrophoresis (PAGE), microfluidics technology has been used to reduce the overall separation time by 2 orders of magnitude,[49,179] with substantially lower sample loading requirements and improved separation repeatability comparable to slab gels.[179]

In spatial multiplexing, efficient transfer of sample between the dimensions plays a critical role in achieving good separation performance. Repeatability and uniformity of

sample plug injection into each of the parallel second dimension channels are important metrics. For example, if the injection dynamics differ between the second dimension channels, a large sample bond which co-elutes into adjacent channels will exhibit different migration times at the downstream detector and appear as two or more separate bands, rather than a single bond spread over multiple channels. Avoiding dispersion of analyte plugs during the injection process is another important concern. If the initial injected sample plug length is larger than the characteristic analyte diffusion length during the second dimension separation, the system will not be capable to reaching its optimal diffusion-limited separation efficiency.[179]

The electrokinetic injection of defined sample plugs within single-dimension microfluidic systems has been extensively studied, with the most widely used injector configurations including the cross,[180] double-T,[181] and triple-T[119] topologies, and extended configurations employing continuous sample injection[182] leveraging flow switching techniques.[183] Floating-injection and pinched-injection methods have been employed in simple cross-injectors for the controlled definition of small sample plugs,[121] while double- and triple-T designs are generally employed for the introduction of larger sample volumes.[119] Regardless of the injector topology and injection method, sample leakage is a central issue which can dictate the effective injection plug length. After the desired sample plug has been transferred to the separation channel, additional sample can enter the injection region due to diffusion and fringing of the electrical field during the electrokinetic transfer process. This excess sample results in tailing of the injected sample plug which degrades separation performance. Backbiasing is a commonly-used method for eliminating sample leakage. In this approach, bias voltages are applied at the sample

inlet and waste reservoirs in order to electrokinetically pull back excess sample from the injection zone. When suitable bias voltages are selected, backbiasing is effective at eliminating sample leakage for single-channel separation devices.

Just as with single-dimension separation systems, efficient injection of sample plugs is a critical consideration in multidimensional systems when transferring analyte from the first to the second dimensions. While several groups have proposed 2-D chip designs consisting of an array of 2nd dimension separation channels aligned with an identical number of injection channels on the opposite side of the 1st dimension microchannel,[118,178] a more efficient design for spatially-multiplexed 2-D separation chips is shown in Figure 35(a). The design consists of a single first-dimension separation channel intersected by *n* second dimension separation channels on one side, and *n+1* sample injection channels on the opposite side, with the injection channels staggered with respect to the separation channels to ensure complete and simultaneous sampling of the first dimension channel.[49,179] Additional channels for multidimensional backbiasing, introduced in this dissertation, are also shown in the figure proximal to the sample inlet and sample waste reservoirs (dashed lines). In this staggered design, the parallel second dimension microchannels may be regarded as an array of double-T injectors operating in parallel. However, unlike the single-channel case, the double-T injectors are not electrically isolated in the multidimensional system. This interconnected design can result in significant variations in performance between the different injectors, as depicted in Figure 35(b). In this image, sample initially within the 1st dimension channel is being electrokinetically transferred into the second dimension channel array by applying a uniform bias voltage in the injection channel reservoirs while grounding the second

dimension reservoirs. Three main features are evident in this injection process. First, substantial tailing of sample occurs at the head of each 2nd dimension channel, resulting in sample dispersion during transfer. Second, in all but the center 2nd dimension channel, the injection is highly asymmetric, reflecting a non-uniform electric field distribution within the 1st dimension channel. Third, sample from the outermost regions of the 1st dimension channel continually leaks into the 2nd dimension array due to a combination of diffusion and electric field fringing, leading to additional tailing which can continue long after sample from the center region of the first dimension channel has been fully transferred.

In the following, the causes of these performance issues are identified and evaluated through a combination of analytical modeling, numerical simulations, and experimental validation. Based on the results, a new chip design is proposed which employs multidimensional backbiasing channels, as depicted in Figure 35 (a), and a modified geometry for the first dimension microchannel. The resulting design eliminates injection asymmetry and sample leakage, while minimizing sample tailing issues which have previously limited performance of the staggered 2-D chip design.

6.2.2 Materials and Experimental Setup

6.2.2.1 Reagents

To minimize diffusion during experimental validation, bovine serum albumin (BSA) prelabeled by Alexa Fluor-555 (Invitrogen; Calsbad, CA) was used as a low-diffusivity analyte. Acrylamide (AAm), *N,N'*-methylenebisacrylamide (Bis), ammonium persulfate (APS), N,N,N′,N′-tetramethylenediamine (TEMED), 3-(trimethoxysilyl)propyl methacrylate (TPM) and poly(vinyl alcohol) (PVA) were purchased from Sigma-Aldrich

Inc. (St. Louis, MO). Sodium dodecyl sulfate (SDS), urea, dithiothreitol (DTT), tris(hydroxymethyl)-aminomethane (Tris), methanol, isopropyl alcohol (IPA), concentrated hydrochloride acid (HCl) were purchased from Fisher Scientific (Fair Law, NJ). HPLC-grade DI water was used for sample and prepolymer solution preparation.

6.2.2.2 Sample Preparation

Sample buffer was prepared by adding 0.25 mL 0.5 M Tris-HCl (pH 6.8), 0.4 mL 10% SDS in DI water, 0.2 mL glycerol, and 0.031 g DTT in sequence. DI water was added for final concentrations of 4% SDS, 20% glycerol, 0.2 M DTT and 0.125 M Tris-HCl. Lyophilized BSA was added to the buffer solution at 1 mg/mL in a tube, and denatured by placing the tube in a water bath at 100°C for 90 sec. Prior to use, the final sample was diluted to 10 μg/mL with DI water.

6.2.2.3 Chip Fabrication

Microchannels were fabricated in a 1.5 mm thick sheet of polymethylmethacrylate (PMMA), using a standard PMMA containing UV stabilizers (FF grade; Cyro; West Paterson, NJ). Reservoirs were formed in a cover plate fabricated from a UV-transparent grade of PMMA (UVT grade; Spartech; Clayton, MO). The channels were directly patterned by computer numerical control (CNC) milling (MDX-650A; Roland ADS; Lake Forest, CA) using a 100 µm diameter end mill. The nominal geometry of each channel is 100 µm wide and 100 µm deep. The reservoirs were drilled by the same CNC milling machine, using a tool diameter of 1.8 mm. After machining, both PMMA wafers are cleaned by methanol, IPA and DI water sequentially in a class 1,000 cleanroom environment, followed by aggressive drying with an N_2 gun.

To ensure uniform and repeatable experimental results, it was necessary to minimize both diffusion and hydrodynamic flow within the polymer chips. To this end, ~1 cm long plugs of polyacrylamide gel were formed within the injection channels and 2nd dimension channels. The wafers were first oxidized using a UV-ozone system (Novascan Technologies; Ames, IA) for 8 min. After oxidization, the PMMA wafers were immediately immersed in a silanization solution consisting of 6:1:1000 TPM:HCl:DI water v/v/v for 1 h, following the method described by Zangmeister and Tarlov.[36] After drying, the TPM-treated wafers were thermally bonded in a hot press (Auto Four; Carver Inc.; Wabash, IN) at 85 °C and 3.45 MPa for 15 min. The bonded chip was next filled with a solution of 4% (wt) acrylamide in DI water with 0.1% SDS mixed with 10% APS in DI water and TEMED 100:1:1 v/v/v. The solution was sonicated for 1 min prior to injection into microchannels. After 5 min polymerization time, the prepolymer remaining in the 1st dimension channel was vacuumed and replaced with 4% acrylamide + bis prepolymer, which diffuses into the APS/TEMED-containing prepolymer within the injection and 2nd dimension channels to form a crosslinked polyacrylamide interface following a 2 hr polymerization step. Because the prepolymer solution within the 1st dimension channel does not contain APS/TEMED, no photopolymerization occurs within this channel, while linear polyacrylamide (LPA) forms within the injection and 2nd dimension channels beyond the diffusion length ~1 cm from the 1st dimension channel. The resulting gels provide a well-defined hydrodynamic barrier to limit sample dispersion out of the 1st dimension channel due to unavoidable pressure gradients. Finally, BSA sample at a concentration of 10 μg/ml was introduced into the 1st dimension channel by capillary action immediately prior to testing.

One of reasons to use of LPA in both injection and sieving matrix is that LPA approach provides more uniform gel geometry in individual channels than that of CPA. The black tape is actually used to block UV during photopolymerization. Unless application of film mask, the interface of gel and sample in the 1st-D could be asymmetry if the black tape does not perfectly align. This is not the issue with LPA gel, since it forms CPA along the interface uniformly by vacuuming AAm + Bis into 1st-D channel.

6.2.2.4 Detection Setup

Optical detection was performed using an inverted fluorescence microscope (Nikon Eclipse TE2000s; Nikon Inc.; Melville, NY) with a 4x objective and a low-noise CCD camera (Coolsnap HQ2; Roper Scientific; Tucson, AZ) with a frame rate of 10 fps.

6.2.3   Sample Transfer in Various Chip Design

6.2.3.1 First Dimension Current Variations

Consider the inter-dimensional injection region of a five-channel staggered chip design depicted in Figure 36. Sample transfer is performed by applying equal bias voltages at each of the lower separation channel reservoirs, with all upper injection channel reservoirs grounded. Upon biasing, the ith injection channel exhibits an average current I_i, and the jth 2nd dimension separation channel exhibits an average current I_{Sj}. The average current within the segment of the 1st dimension microchannel between the ith injection channel and j^{th} separation channel is defined as $I_{i,j}$, with positive orientations defined in Figure 36. Using PSpice circuit analysis software (Cadence Design Systems Inc., San Jose, CA), the average currents can be readily determined. Using lengths of L_i = 1 cm for each injection channel, L_1 = 400 μm for each 1st dimension microchannel segment and L_2 = 5 cm for the 2nd dimension separation channels, and equal cross-

sectional dimensions for all channels, normalized current variations within the ten segments of the 1st dimension channel are given in Figure 37. In this simulation, equal resistivity was assumed within the injection and 2nd dimension channels, while 4x lower resistivity was assumed within the 1st dimension channel to account for typical conductivity differences resulting from the high sample concentration within this channel before transfer.
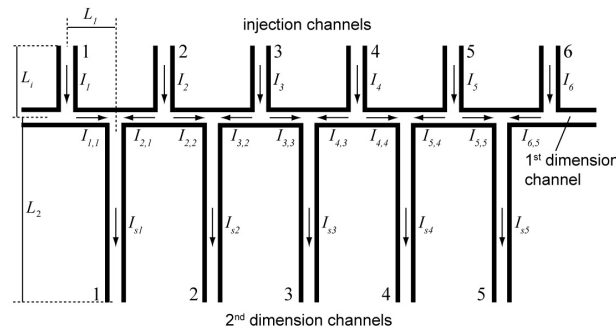
Figure 36. Schematic diagram of the five-channel chip design indicating nomenclature for currents in the ith injection channel (I_i), the jth 2nd dimension separation channel (I_{sj}), and segments of the 1st dimension microchannel between adjacent injection and separation channels ($I_{i,j}$).
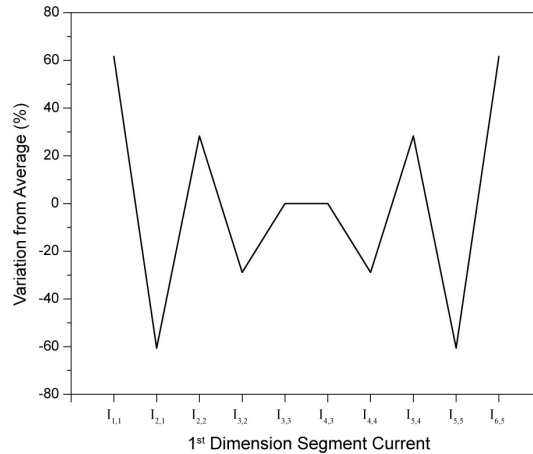
Figure 37. Normalized current variations between the 1st dimension channel segments within a staggered injection chip containing five 2nd dimension channels.

For an ideal injection process, the currents should be equal within all segments to ensure simultaneous sample transfer. However, as seen from the results in Figure 37, the actual currents vary substantially. While the two center segments which feed into the middle 2nd dimension separation channel have the same magnitude ($I_{3,3} = I_{4,3}$) equal to the average current across all segments, deviations increase for channels further from the center. For the assumed geometry in this case, the outermost segments exhibit ~60% higher currents than the average, and ~400% higher than the adjacent segments closer to the center channel, i.e. $I_{1,1} \approx 4I_{2,1}$ and $I_{6,5} \approx 4I_{5,5}$. This large degree of non-uniformity results from variations in the electrical resistance seen at the end of each injection channel. This can be more clearly seen by considering a chip containing three injection channels and two 2nd dimension separation channels. Following the nomenclature defined in Figure 36, the 1st dimension channel comprises 4 segments with currents $I_{1,1}$, $I_{2,1}$, $I_{2,2}$, and $I_{3,2}$. In the following analysis, the resistances of each injection channel, 1st dimension channel segment, and 2nd dimension channel are denoted R_i, R_1, and R_2, respectively. Due to symmetry, only half of the circuit need be analyzed. Focusing on the first 2nd dimension channel and noting that the voltage drop from the injection reservoirs to the channel inlet must be equal for both the first and second injection channel, thus

$$I_1 R_i + I_{1,1} R_1 = I_2 R_i + I_{2,1} R_1 \tag{5}$$

The current through each injection channel and its connected first dimension segment must also be equal, so that $I_{1,1} = I_1$ and $I_{2,1} = I_2/2$. The latter equality results from symmetry, since exactly half of I_2 is channeled towards the first 2nd dimension microchannel. Inserting both equalities into Eqn.(5) and solving for the ratio of currents in the 1st dimension segments results in

$$\frac{I_{1,1}}{I_{2,1}} = \frac{2R_i + R_1}{R_i + R_1} \qquad (6)$$

In general, the injection channels are substantially longer than the first dimension channel segments. With this assumption, $R_i \gg R_1$ and Eqn.(6) reduces to the simple equality $I_{1,1} = 2I_{2,1}$, i.e. a 100% variation in injection current for the case of a simple 2-D chip with only two 2nd dimension channels.
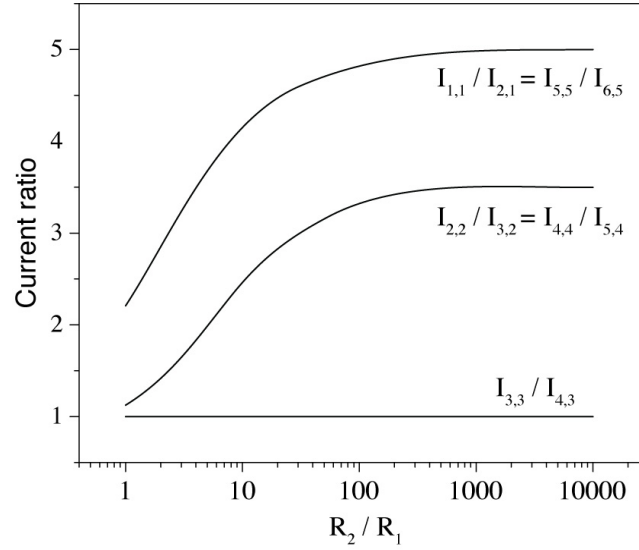
Figure 38. Effect of increasing 2nd dimension channel resistance on current asymmetry between adjacent 1st dimension channel segments for a 5-channel chip design.

To evaluate injection non-uniformity in chips containing greater numbers of 2nd dimension channels, PSpice was used as a modeling tool. Simulation results for the case of a chip with five 2nd dimension channels are shown in Figure 38. In this figure, the ratios of current within each pair of 1st dimension segments connecting to a single 2nd dimension channel is plotted against R_2/R_1, with the injection channel resistance held constant at $R_i = 50\,R_1$. The maximum current ratio occurs within the outermost pairs of 1st dimension segments. Furthermore, the current ratio increases with the 2nd dimension

resistance, approaching a value of 5 as R_2 increases towards infinity. Indeed, for any staggered chip design with n 2nd dimension channels and $n+1$ injection channels, the maximum current ratio will approach n in the limit. This fact can be seen by considering that for $R_2 \gg R_i \gg R_1$, the injection currents can be approximated as pure current sources applied to zero-resistance nodes between each 2nd dimension channel. For the outermost 1st dimension segment, the full current from the outer injection channel (Ii) must pass through the first node, with a fraction 1/n entering the outer 2nd dimension channel and $(n-1)/n$ continuing through the second node to feed the remaining 2nd dimension channels. In the other direction, each of the remaining n injection channels feeds $1/n$ of their total currents through the second node and into the outer 2nd dimension channel, for a total current of I_i. Thus the maximum current ratio becomes

$$\lim_{R_2 \to \infty} \left(\frac{I_{1,1}}{I_{2,1}} \right) = \frac{I_i}{I_i[1-(n-1)/n]} = n \tag{7}$$

From Eqn.(7) injection uniformity clearly deteriorates as the density of the 2nd dimension array is increased. However, higher density arrays are desirable to prevent under-sampling of the 1st dimension separation and to provide increased peak capacity for the overall 2-D separation. Hence there is a need for methods to reduce or eliminate current asymmetries without constraining the number of 2nd dimension channels.

6.2.3.2 Multidimensional Backbiasing

One potential solution to the challenge of injection uniformity is to individually adjust voltages applied within each of the injection reservoirs shown in Figure 35(a) to achieve equal currents within each 1st dimension channel segment. However, in addition to adding system complexity, this approach would require accurate and real-time knowledge of the resistivity within the various sections of the chip, and a feedback method for

adjusting the voltages in response to any resistance variations resulting from changes in sample and buffer concentrations during the injection and separation processes.

A more practical solution is to modify the microchannel network to compensate for the variable network input resistance seen in an uncompensated staggered injection design. Here it is considered to the use of backbias channels intersecting the outer regions of the 1st dimension channel, as shown in Figure 35(a). These channels are named following the terminology from single-dimension microfluidics, since the backbias channels serve a similar purpose in shunting current out of the ends of the sample transfer region during the injection process. Indeed, in addition to eliminating current non-uniformities during injection, the backbiasing channels also serve the same function as their single-dimension counterparts by preventing sample leakage from the outer regions of the 1st dimension channel.

Consider the case where backbiasing channels are added to the simple design consisting of three injection channels and two 2nd dimension channels. To simplify their integration, the backbias channels terminate at reservoirs biased at the same voltage as the 2nd dimension microchannel reservoirs. Given backbiasing channels with equal resistances R_b and average currents I_b, the value of R_b which minimizes injection non-uniformity is found as follows. Noting that $R_1 << R_2$, and $R_i << R_b$ and referring again to Figure 36 and summing currents into the node connecting the first backbiasing channel with the 1st dimension channel yields

$$I_1 = I_{1,1} + I_b \tag{8}$$

Inserting this into Eqn.(8), together with the previously-noted relationship $I_{2,1} = I_2/2$, gives

$$I_{1,1}(R_i + R_1) + I_b R_i = I_{2,1}(2R_i + R_1) \tag{9}$$

For symmetric injection, the currents in both segments of the 1st dimension channel must be equal ($I_{1,1} = I_{2,1}$). In this case, solving Eqn.(9) for I_b yields

$$I_b = I_{1,1} = I_{2,1} = I_2/2 \tag{10}$$

Also note that the voltage drop across the backbias channel is equal to the combined drop across the first 1st dimension segment and the first 2nd dimension channel, i.e.

$$I_b R_b + I_b R_i = I_{1,1} R_i + I_{s1} R_2 \tag{11}$$

Additionally, the current in the first 2nd dimension separation channel (I_{s1}) is simply the sum of the current through the first and second 1st dimension segments, with the latter quantity equal to half the current from the second injection channel, that is $I_{s1} = I_{1,1} + I_{2/2}$. Inserting this expression together with the equalities derived from 0Eqn.(10), Eqn.(11) reduces to:

$$R_b = 2R_2 \tag{12}$$

Thus a backbias channel with twice the nominal resistance of a 2nd dimension separation channel will result in a perfectly balanced injection process, with equal currents within all 1st dimension channel segments.

Eqn.(12) was derived for the case of a staggered injection chip with only two 2nd dimension channels. To optimize backbiasing for chip designs containing larger numbers of 2nd dimension channels, lumped-parameter numerical models were evaluated using PSpice. All analyses were performed with $R_i = 0.2R_2$ and 4x lower resistivity within the 1st dimension channel to simulate a high concentration of analyte ions immediately following sample introduction. Designs containing up to nine 2nd dimension channels were considered, with backbiasing resistances varying from $0.1R_2$ to infinity (i.e. no

backbiasing). As a model case, the injection, 1st dimension, and 2nd dimension channel lengths were maintained at L_i = 1 cm, L_1 = 0.04 cm and L_2 = 5 cm, respectively. The resulting maximum current ratios between adjacent 1st dimension segments are shown in Figure 39 (a). Without backbiasing ($R_b/R_2 = \infty$), significant current asymmetries are revealed, and found to increase with the density of channels in the 2nd dimension array. Even with the conservative selection of channel lengths used in this example, maximum current ratios are greater than half the asymptotic approximation given by Eqn.(7) for R2 $\rightarrow \infty$. However, when the backbiasing channel resistance is increased to twice that of the 2nd dimension channels ($R_b = 2R_2$), balanced injection is achieved and the current ratio is equal to unity, independent of the number of 2nd dimension channels.
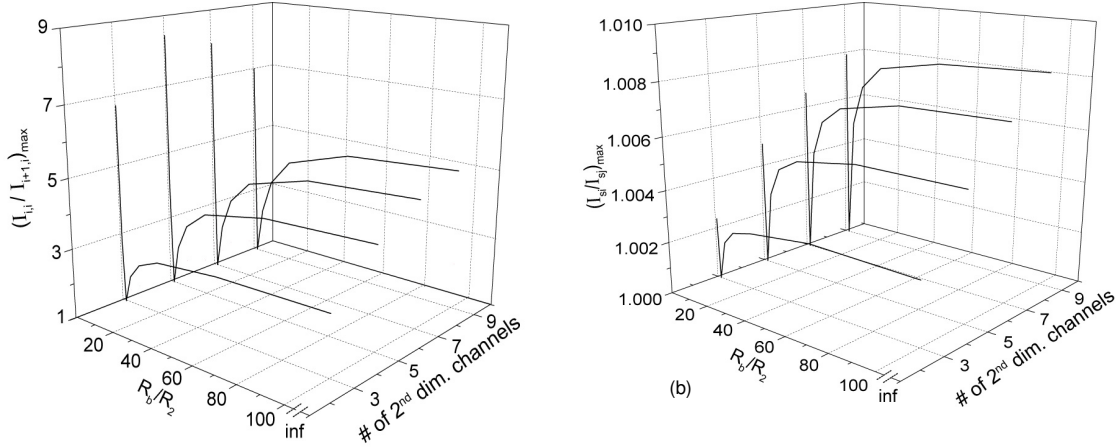
Figure 39. Maximum current ratios (a) among all pairs of adjacent 1st dimension channel segments, and (b) among all 2nd dimension channels. In both cases, the current ratios are unity when $R_b = 2R_2$.

In addition to eliminating current asymmetry in the 1st dimension channel segments, backbiasing can also serve to reduce current variations within the parallel 2nd dimension channels themselves. As seen from Figure 37, current variations within adjacent 1st

dimension segments which feed a single 2nd dimension channel approximately balance each other, such that a higher current in one segment is nearly offset by a correspondingly lower current in the adjacent channel. Thus, despite the large current ratios between adjacent 1st dimension segments, current variations within the 2nd dimension channels are relatively small. Regardless, these variations are entirely eliminated when $2x$ backbiasing is used. This is evident from Figure 39 (b), which shows the maximum ratio of currents across all 2nd dimension channels as a function of the backbias channel resistance and number of 2nd dimension channels. Without backbiasing, the current variation is less than 0.3% for a 3-channel design, and increases gradually as additional channels are added to the array. The introduction of backbiasing channels with $R_b = 2R_2$ eliminates the 2nd dimension current variations, regardless of the number of 2nd dimension channels in the array.

6.2.3.3 Sample Transfer Simulation and Experimental Validation

To evaluate the full sample injection process for a staggered 2-D chip design with and without backbiasing, numerical simulations were performed using FEMLab software (COMSOL AB, Stockholm, Sweden). In addition, multidimensional chips were fabricated, and sample transfer experiments were performed to provide validation of the simulation results.

For both simulations and experiments, the nominal system parameters are shown in Table 1. The sample mobility and buffer resistivity values given in this table were measured experimentally to provide parity between simulations and experiments. The diffusion constant for SDS-complexed BSA was taken from the literature. Note that mobility of the SDS-complexed BSA sample used for experimental validation was found

to be nearly identical within both free solution and LPA gel media, and so a single value was used for simulations. Note also that the analyte possesses a negative charge, requiring a negative bias to be applied to the injection channel reservoirs and reversing the current directions in Figure 36.

Table 5. Nominal system parameters for simulations and experimental validation

Parameter	Value
Injection channel length (L_i)	1 cm
1st dimension channel segment length (L_1)	400 μm
2nd dimension channel length (L_2)	5 cm
Channel cross-section dimensions	100 μm × 100 μm
Applied injection bias	1100 V
Injection channel resistivity	1475 Ω•cm
1st dimension resistivity	378 Ω•cm
2nd dimension resistivity	1475 Ω•cm
Sample electrokinetic mobility	3×10^{-4} cm^{2}V^{-1}s^{-1}
Sample diffusion constant[184]	6×10^{-7} cm^2/s

Simulation results using a staggered chip design without backbiasing are shown in Figure 40(a). Non-uniformities for the uncompensated chip can be seen clearly 3 sec after applying the injection bias. For each pair of 1st dimension channel segments feeding a given 2nd dimension channel, sample within the segment further from the chip center mobilizes into the 2nd dimension more rapidly than the segments closer to the center, as

expected from the electrical network model results (Figure 37). The degree of asymmetry is so severe that even after 5 sec (not shown), sample continues to gradually elute into the 2nd dimension, resulting in long and poorly defined injection plugs. In addition, a small amount of sample continually leaks into the outermost 2nd dimension channels due to diffusion and electromigration of excess sample from the ends of the 1st dimension channel. In contrast, simulation results using a chip design employing 2x backbiasing are shown in Figure 40(b). In this case, uniform injection is observed within each 2nd dimension channel, with well-defined and equal-length injection plugs, and no leakage from into the outermost channels.
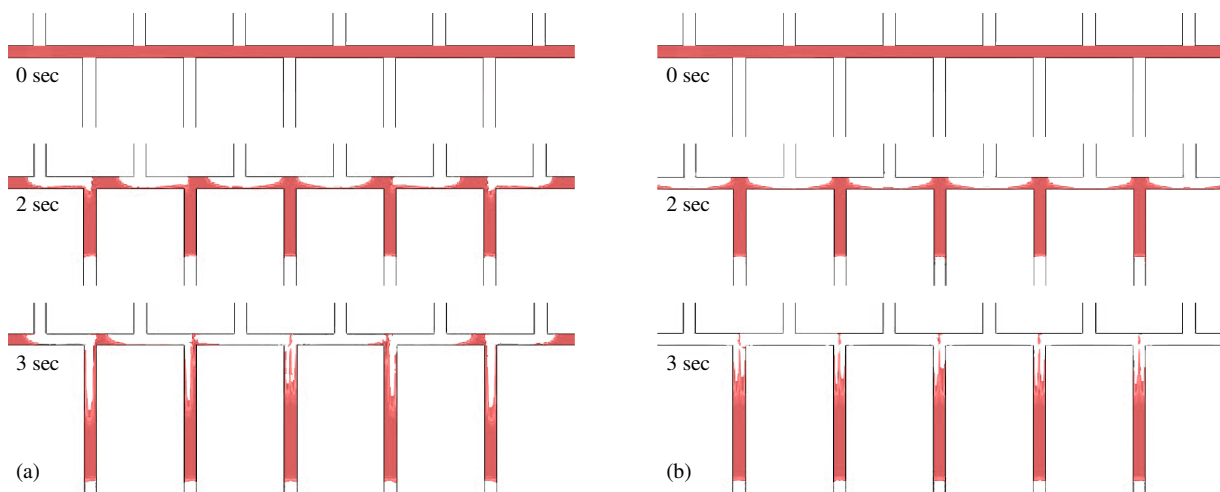
Figure 40. Electrokinetic sample transfer simulations in a staggered 2-D chip (a) without backbiasing, and (b) with 2x backbiasing. Injection asymmetry is clearly evident when backbiasing is absent, while the use of 2x backbiasing results in balanced sample transfer in all channels. Leakage is also eliminated by the removal of sample from the ends of the 1st dimension channel. Backbiasing channels are not shown.

Experimental validation was performed using a 2-D chip fabricated with the same geometry used for simulations. Analyte consisting of pre-labeled BSA complexed with

negatively-charged SDS was used to evaluate injection performance due to its relatively low diffusivity. Fluorescent images acquired during the sample transfer process are presented without backbiasing in Figure 41(a), and with $2x$ backbiasing in Figure 41(b). These experimental results, which are highly repeatable, match well to the simulation results for both cases, with 2x backbiasing providing highly uniform sample transfer between the dimensions.
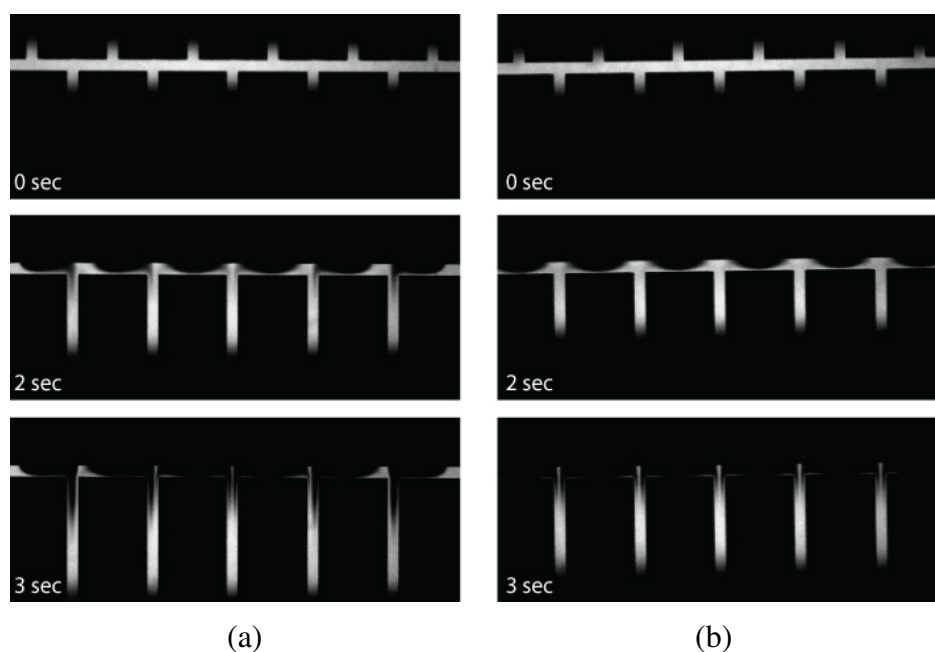
Figure 41. Experimental sample transfer results using a staggered 2-D chip (a) without backbiasing, and (b) with 2x backbiasing. Backbiasing channels are not shown.

6.2.3.4 Angled Channel Design For Reduced Sample Tailing

Although the elimination of injection non-uniformity using 2x backbiasing leads to a reduction in effective sample plug length within the 2nd dimension channel array, the injected plugs still exhibit long tails which can impact the minimum achievable plug

length. The tails visible in the last panels of Figure 40(b) and Figure 41(b) result from the geometry of the interdimensional intersections, which produce large gradients in the vertical component of the electric field within the 1st dimension channel. These gradients in turn generate variations in sample velocity during injection. Modification of the intersection geometry to minimize electric field gradients is one approach towards reduced sample tailing. While there are several ways to achieve this goal, here a simple modification is considered based on rotating each 1st dimension channel segment by an angle α from the original channel orientation (see inset in Figure 42). The benefit of the angled channel design can also be seen from Figure 42, which plots the normalized electric field profiles along the y-axis defined in the inset. Without the angled geometry ($\alpha = 0^{o}$), the electric field varies by a factor of 65, with the lowest value at the point furthest from the 2nd dimension channel inlet (y = 0). This value drops to less than 5 when the channel angle is increased to 45°. As a result, a 2-D chip employing a 45° angled channel design will exhibit significantly reduced tailing.
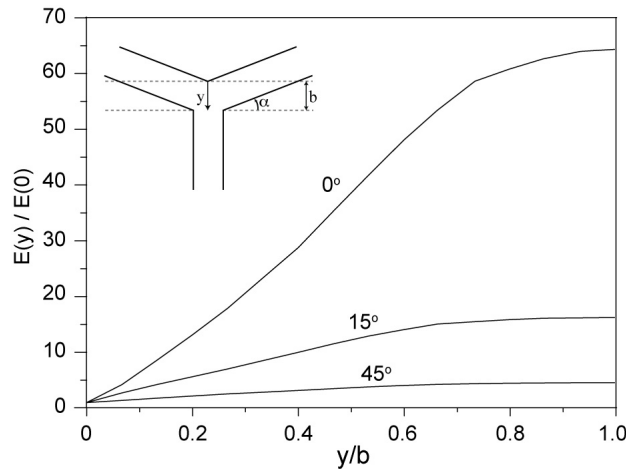
Figure 42. Electric field strength profile within 1st dimension channel along center line of 2nd dimension channel with varying channel angle (α). Channel geometry is shown inset.
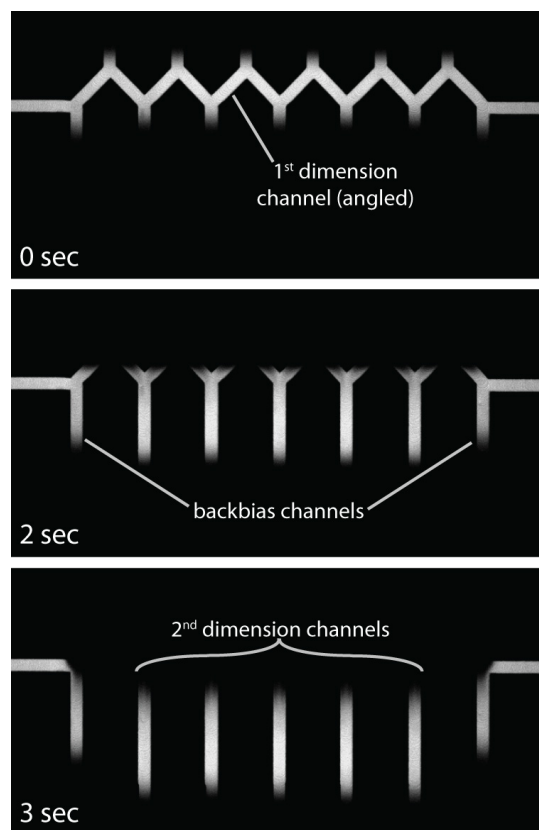
Figure 43. Minimized sample tailing using a 45° angled channel design.

Experimental results validating this statement are shown in Figure 43. This test was performed using a chip with $2x$ backbiasing channels to ensure uniform sample transfer during injection. The backbias channels were designed with the same cross-sectional channel dimensions and gel medium as the 2nd dimension channels, but with twice the length. Compared with the straight channel case (Figure 41), sample tailing is negligible for the angled channel design due to the more uniform electric field. The improved electric field uniformity also provides faster sample transfer and smaller plug lengths at the heads of the 2nd dimension channels. When taking into account the tailing observed

using the straight channel design, sample plug length was reduced an average of 34% using the angled channel design.

While tailing can be further minimized by increasing the angle of the 1st dimension channel segments, other factors including electric field uniformity and sample dispersion during the 1st dimension separation must also be considered. Increasing the angle may also impact the ease of initial sample injection and lead to unwanted extrusion of sample out of the 1st dimension channel during sample introduction. For cases where large channel angles may unduly affect the 1st dimension separation performance, smaller angles can still provide measurable benefits during sample transfer while minimizing the impact on the 1st dimension separation.

6.3   2D Chip Platform Design Summary

`Microfluidic technology is unique in its ability to seamlessly integrate large numbers of fluidic elements into a single compact package. As the complexity of microfluidic separation systems grows, it is important to consider design issues which set these platforms apart from traditional capillary or slab gel systems. The staggered two-dimensional chip design evaluated here is largely based on multidimensional slab gel platforms, but with very different design considerations resulting from the discretized nature of the microfluidic elements. In particular, the combination of $2x$ backbiasing and angled 1st dimension channel segments has been shown to substantially improve sample transfer performance in these systems.

Proper backbiasing can completely eliminate non-uniformities during both sample transfer and 2nd dimension separations, and also prevent leakage of residual sample from the outer regions of the 1st dimension channel. Optimized backbiasing channels, with

twice the resistance of a single 2nd dimension channel, can be realized in a number of ways. In the present work, all channels used the same cross-sectional dimensions, and so the length of the backbiasing channels was doubled to realize $2x$ backbiasing. Alternately, channel width or depth could have been reduced by half while maintaining identical lengths between the backbiasing and 2nd dimension channels. Backbiasing can also be performed by directly applying appropriate biases to each reservoir at the ends of the 1st dimension microchannel. However, this approach requires accurate knowledge of buffer conductivities within both dimensions and thus adds unnecessary uncertainty compared to on-chip backbiasing channels, which ensure uniform injection regardless of the buffer conditions or separation media used in each dimension.

Angled 1st dimension channel segments are also a valuable design element for realizing optimized sample transfer in staggered 2-D microfluidic chips. The angled channel design provides a simple approach for minimizing sample plug tailing and initial sample plug length within the 2nd dimension channels, thereby offering improved peak capacities for the overall system. While this work has focused on the sample transfer process using a single homogeneous analyte, full 2-D separations are performed by using chips combining both $2x$ backbiasing and angled channel design elements, using microfluidic isoelectric focusing (μIEF) in the 1st dimension and gel electrophoresis in the 2nd dimension. While this work is ongoing, it is worth noting that the angled channel design does not substantially affect focusing resolution during μIEF. Moreover, the uniform injection and minimized tailing provided by this design feature is providing improvements in the full 2-D separation performance even for relatively complex samples such as cell lysates.

Although electrokinetic injection was assumed in this work, the same conclusions apply to hydrodynamic injection. This can be seen by considering pressures and flow velocities as analogs of electrical voltages and currents, respectively, in the provided derivations. Thus, if pressure-driven separations such as liquid chromatography were employed within the second dimension, the use of $2x$ backbiasing and angled 1st dimension segments would still provide optimal sample transfer. In this sense the proposed design modifications represent a universal approach for improving sample transfer performance, and thus separation efficiency, for any combination of separation mechanisms used within a staggered 2-D chip.

Chapter 7.   PAAm-Enabled 2-D PAGE with Discontinuous Buffers

Despite the refinement of liquid chromatography and peptide mass fingerprinting techniques for protein analysis, 2-D PAGE separations of *intact proteins* remains a core technology for proteomic studies. In addition to enabling quantitative analysis of global protein levels, 2-D PAGE offers theoretical peak capacities around 10,000,[96,185] with real-world detection of several thousand proteins commonly achieved in a single run.[186] In 2-D PAGE, denatured intact proteins are separated on the basis of their charge state by isoelectric focusing (IEF), followed by a size-based separation using SDS-PAGE. While 2-D PAGE is most commonly practiced with backend analysis of proteins by mass spectrometry, 2-D PAGE expression maps alone can provide valuable insight for differential studies, including the analysis of post-translational modifications, by yielding information about the approximate isoelectric point (pI) and molecular weight (MW) of differentially expressed species within complex samples.

Overall, 2-D PAGE remains a labor intensive and low throughput process, with typical analysis times on the order of 1-2 days per run.[160,185] This throughput limitation significantly constrains the utility of 2-D PAGE. In recent years, a number of efforts have targeted the development of microfluidic systems which mimic the functionality of 2-D PAGE in a miniaturized format, while promising significantly shorter analysis times and higher levels of automation.[49,50,110,118,164,179] A common feature of these systems is the combination of a single microchannel for performing a first-dimension IEF separation, and an array of discrete second-dimension microchannels for capillary gel electrophoresis (CGE), with the second-dimension array replacing the traditional slab gel format for gel electrophoresis. Although the peak capacities of chip-based IEF/SDS-CGE systems

remain lower than traditional 2-D PAGE, the application of microfluidics technology has successful reduced separation times by 2 orders of magnitude, with substantially lower sample loading requirements than slab gels.[110,179] Furthermore, recent advances including the demonstration of on-chip differential gel electrophoresis[187] and separation repeatability comparable to slab gel analysis[179] suggest that further developments may allow microfluidic 2-D separations to emerge as a viable high-throughput alternative to slab-gel 2-D PAGE.

To this end, a microfluidic IEF/SDS-PAGE separation system which employs a combination of multifunctional polyacrylamide (PAAm) gels and a discontinuous SDS-PAGE buffer system are described here. The PAAm gel is used as a highly-resolving separation medium for gel electrophoresis, while discrete PAAm gel plugs integrated into specific regions of the chip enable acid, base, and ampholyte solutions to be fully isolated prior to chip operation. The gel plugs also allow different separation buffers to be stored within the chip, allowing the use of a discontinuous buffer system chosen to provide sample stacking during the second-dimension separation. The gel plugs are also employed as on-chip SDS containers, allowing defined volumes of SDS to be reapeatably injected and complexed with the IEF-focused proteins, without the need for external intervention. The IEF channel itself possesses an angled geometry which has been shown to minimize sample tailing in multidimensional microfluidic systems.[188] Additionally, the chip design employs optimized backbiasing channels which eliminate sample leakage and enable uniform sample transfer between the separation dimensions. This last feature is essential for eliminating injection current variations which have previously degraded the overall separation resolution and the uniformity of sample bands within the second

dimension. Finally, improved SDS-PAGE separation resolution is achieved using a discontinuous buffer system enabled by the multifunctional gels which results in efficient sample stacking near the inlets of the second-dimension microchannels. Validation of the full 2-D system is presented using fluorescently-labeled *E. coli* cell lysate, including a critical comparison between chip designs containing 10 and 20 parallel SDS-PAGE microchannels.

7.1   Experimental Section

7.1.1   Chemical and Materials

Acrylamide (AAm), ammonium persulfate (APS), *N,N′*-methylenebisacrylamide (Bis), *N,N,N′,N′*-tetramethylenediamine (TEMED), 3-(trimethoxysilyl)propyl methacrylate (TPM), poly(vinyl alcohol) (PVA, MW ~130,000), 2-(cyclohexylamino)ethanesulfonic acid (CHES), glycine, fluorescein isothiocyanate (FITC), DL-dithiothreitol (DTT), iodoacetamide (IAM), triton X-100, and ampholyte (pH 3-10) were purchased from Sigma-Aldrich Inc. (St. Louis, MO). *N,N′*-dimethylformamide (DMF) was purchased from EMD Chemicals Inc. (Gibbstown, NJ). Irgacure 2959 (I2959) was purchased from Ciba Corporation (Tarrytow, NY). Sodium dodecyl sulfate (SDS), urea, tris(hydroxymethyl)-aminomethane (Tris), methanol, isopropyl alcohol (IPA), concentrated sodium hydroxide, and concentrated hydrochloride acid (HCl, 36~38%) were purchased from Fisher Scientific (Pittsburgh, PA). High performance liquid chromatography grade DI water, purchased from Fisher Scientific, was used for sample and prepolymer solution preparation. The microfluidic chip substrate was fabricated from polymethylmethacrylate (PMMA) sheet (FF grade; Cyro, West Paterson, NJ), while the chip cover layer was fabricated using an ultraviolet-

transmitting grade PMMA sheet (UVT grade; Spartech, Clayton, MO). Alexa-Fluor 488 model proteins, parvalbumin (MW 12 kDa), trypsin inhibitor (MW 21 kDa), ovalbumin (MW 45 kDa), and bovine serum albumin (BSA) (MW 66 kDa), were purchased from Invitrogen Corporation (Carlsbad, CA). *Escherichia coli* (*E. coli*) sample was purchased from Bio-Rad Laboratories (Hercules, CA).

7.1.2   2-D Chip Fabrication

Channels and access reservoirs were directly machined into the chip substrate and cover layer, respectively, by a computer numerical control (CNC) milling machine (MDX-650A; Roland Corp., Lake Forest, CA). Acid and base reservoirs were first machined in the substrate layer using a 3 mm diameter end mill prior to channel fabrication. All channels were machined using a 125 μm diameter end mill, with final channel geometries of 150 ± 3 μm width by 140 ± 5 μm depth. The length of the IEF channel between the two outer backbiasing channels is 1.1 cm, with each IEF channel segment 500 μm long. The length of the CGE channels from the IEF channel to the detection region is 4 cm. Access reservoirs were fabricated in the cover layer using a 1.8 mm diameter drill bit. Both PMMA plates were sequentially cleaned by methanol, IPA and DI water in a cleanroom environment prior to UV/ozone oxidization for 8 min using a commercial UV/ozone system (Novascan Technologies, Ames, IA). Following the process described by Zangmeister and Tarlov,[36] the oxidized PMMA wafers were immediately immersed into a silanization solution consisting of 1.2 mL TPM and 0.2 mL HCl in 200 mL DI water, and sonicated within this solution for 1 hr. After nitrogen drying, the TPM-treated substrate and cover plates were thermally bonded using a hot press (Auto Four; Carver Inc., Wabash, IN) at 85°C under a pressure of 3.45 MPa for 15

min. The reservoirs of the resulting chips were sealed with blue semiconductor tape to avoid contamination prior to use.

7.1.3 Polyacrylamide Gel Fabrication.
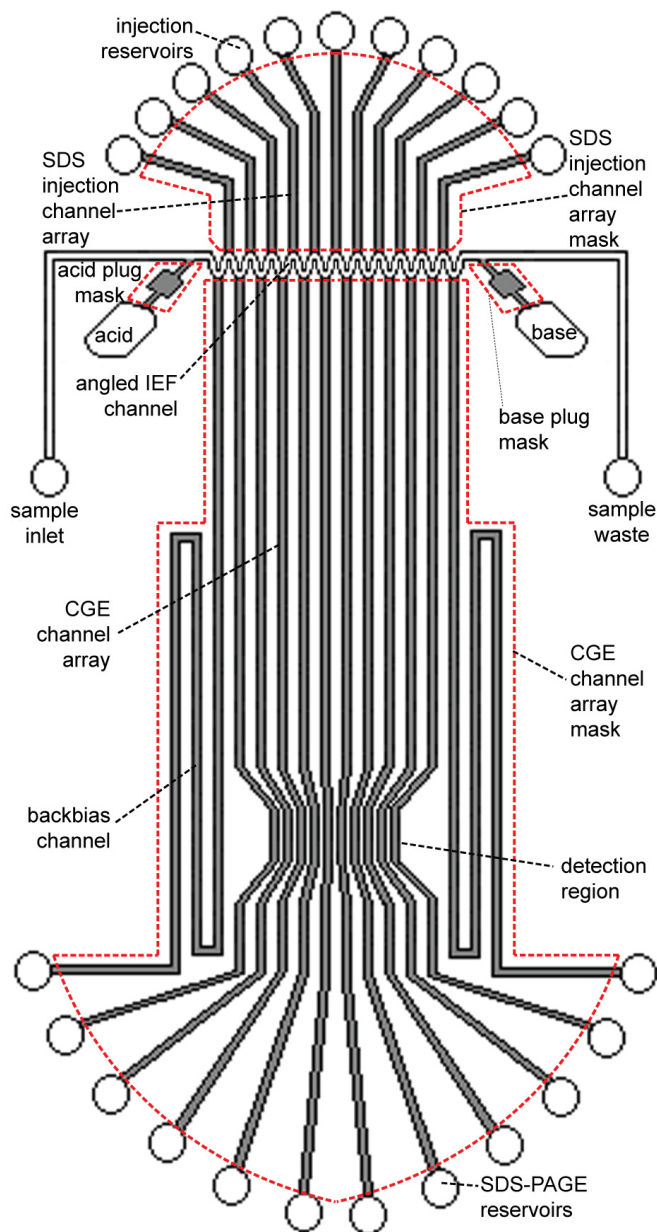
Figure 44. Schematic of an IEF/SDS-PAGE separation chip combining PAAm sieving gel and gel plugs, an angled IEF channel design, and back-biasing channels. Photolithography masks used for patterning each of the gel regions are shown (dashed contours).

A schematic image of the chip design is shown in Figure 44. Crosslinked PAAm gels were fabricated within three different regions of the chip by sequential photopolymerization steps, using different acrylamide prepolymer solutions and individual photolithography masks to define each gel. Masking was performed using black tape applied to the chip surface prior to UV exposure. A summary of conditions used for gel fabrication, including prepolymer composition, is provided in Table 6, together with details of the buffers used in the injection channel and SDS-PAGE reservoirs during second-dimension separations. Referring to Figure 44, acid and base plug masks were used to pattern pressure-blocking gel plugs from a prepolymer solution consisting of AAm, Bis, and I2959 photoinitiator dissolved in 5 mM Tris-HCl buffer. After photopolymerization with a total UV dose of 11 J/cm^2 delivered using a UV flood exposure instrument (PRX-1000; Tamarack Scientific Co., Corona, CA), unexposed prepolymer solution was removed by vacuum, and an acrylamide coating solution consisting of 6% AAm, 10% APS, and 10% TEMED in DI water at a volume ratio of 100:1:1 was injected into the microchannel network. This coating solution was used to provide stress release at the gel/channel interface and prevent the formation of voids. After 15 min, the coating solution was removed, followed by flushing with DI water. Next, the separation gel defined by the CGE channel array mask (Figure 44) was fabricated using the same recipe as the acid and base gel plugs, but with SDS added to the buffer solution to yield a 0.1 % background SDS concentration within the separation medium. After photopolymerization using a lower UV dose of 5.5 J/cm^2, the chip was again flushed with DI water to remove unreacted prepolymer. Finally, the gels defined by the SDS injection channel array mask were fabricated. The injection channel gels

employed the same prepolymer recipe as the acid and base gel plugs, but using a different buffer with a higher concentration of SDS (1.2 %), allowing the gel plugs to serve as containers for defined quantities of SDS (see Table 6). These SDS packets are stored for later injection into the IEF channel for SDS-protein complexation following sample focusing. After the final UV exposure of the injection channel gels, the IEF channel was flushed and refilled with 4% PVA for at least 30 min prior to sample introduction. The PVA coating served to minimize electroosmotic flow and protein adsorption during IEF.

7.1.4 Sample Preparation.

E. coli sample was prepared by dissolving 1 mg FITC into 100 µL DMF and mixing with reconstituted *E. coli* protein sample, which contained approximately 2.7 mg of solid in 500 µL DI water. The reaction was allowed to proceed in the dark overnight at room temperature. The total protein concentration of the fluorescein-labeled protein sample was determined to be 0.44 mg/mL using a standard Bradford assay.[165] To denature and reduce the *E. coli* sample, urea and DTT were thoroughly mixed with 1 mL of the sample solution in a vial with final concentrations of 8 M and 100 mM, respectively. The reaction was allowed to proceed in the dark overnight at room temperature. Subsequently, IAM was added to the solution to a concentration of 120 mM to alkylate the denatured proteins, and the vial was placed in the dark for 1 h at room temperature. The resulting solution was diluted 20 times using a solution of urea, Triton X-100, and ampholytes, for final concentrations of 8 M, 10% (w/v), and 4% (v/v) respectively.

Model proteins pre-labeled with Alexa-Fluor 488 were prepared in a similar manner. A total of 2 mg protein sample (0.5 mg per protein) was dissolved into 400 µL DI water, and 0.48 g urea and 15.4 mg DTT were added into 100 µL DI water. Both solutions were

mixed and placed in a dark room overnight, followed by the addition of 0.277 g IAM. Finally, 100 µL Triton X-100 was added into the denatured sample. For capillary gel electrophoresis (CGE), no ampholytes were employed, while for 2-D separations 4% ampholytes were added. In each case, the concentrated proteins were diluted to 25 µg/mL by 8 M urea and 10% triton X-100 in DI water.

7.1.5 Optical Detection.

Optical detection was performed using an inverted fluorescence microscope (Nikon Eclipse TE2000s; Nikon Inc.; Melville, NY) with a 4x objective and a low-noise CCD camera (Coolsnap HQ2; Roper Scientific; Tucson, AZ) with a frame rate of 10 fps. The detection region shown in Figure 44 is 40 mm away from IEF channel.

7.2 Multifunctional Polyacrylamide Gel and 2D-PAGE

7.2.1 PAAm Sieving Gel.

While the previous efforts focused on using replaceable gel, such as polyethylene oxide (PEO),[49,179] pullulan,[189] and dextran,[190] as a sieving matrix in IEF/SDS-CGE chips, there are several disadvantages to this approach. At lower gel concentrations (~2%), PEO can mobilize due to small on-chip pressure gradients, resulting in unstable interfaces between the first and second dimension channels, but filling the CGE separation channel array at higher PEO concentrations (>4%) is challenging due to the gel's high viscosity. Even when an ideal interface between the IEF and CGE separation media is initially achieved, inter-diffusion between PEO and sample/ampholytes can rapidly deteriorate the interface, resulting in poor IEF resolution, sample loss, and irreproducible separation results. Furthermore, PEO separation performance is dependent on the operation temperature,[59] with crystallization of the on-chip PEO solution typically observed

following a single day of room-temperature storage. Both of these latter issues can further impact separation reproducibility.

Crosslinked PAAm fabricated by *in situ* photopolymerization is a sieving matrix which possesses a well-defined and tunable pore structure determining by the ratio of the monomer (AAm) and crosslinker (Bis) within the prepolymer solution.[191] Originally explored for capillary separations,[39,89] crosslinked PAAm has been widely used as a gel electrophoresis sieving medium in microfluidic platforms.[110,163,192-194] The fabrication of long PAAm separation zones can result in voids along the gel-sidewall interface in silica capillaries due to shrinkage of the polymer chains during photopolymerization.[38,152,155] To eliminate bubble formation, a layer of linear polyacrylamide (LPA) may be formed by bonding pedant methacrylate groups within the LPA to acrylic groups grown on the silica surface via TPM. The resulting LPA layer serves to relax interfacial shear forces produced due to gel shrinkage during polymerization, thereby preventing the formation of voids. Because native PMMA does not offer suitable functional groups for LPA attachment, UV-Ozone treatment was used here to oxidize the PMMA surface and generate hydroxide groups, which are further covalently bonded to methacryloxypropyltrimethoxysilane following the method of Zangmeister and Tarlov, enabling LPA to be anchored to the oxidized and MTP-treated PMMA surface.[36,38,194] Even with this LPA surface coating, voids were consistently observed when using a reported PAAm recipe[110,163] based on a prepolymer solution of 8 % AAm, 0.03 % Bis, and 0.24 % I2959. However, by using LPA coating together with a modified gel recipe consisting of 4 % AAm, 0.4 % Bis, and 0.12 % I2959, no voids were observed for gel

plugs up to 8 cm long in the PMMA chips. Use of the optimized recipe without the LPA stress release layer resulted in voids for any PAAm gel longer than around 2 cm.

7.2.2 PAAm Pseudo-Valves.

In addition to the PAAm sieving medium, gel plugs fabricated adjacent to the acid/base reservoirs and within the injection channel array serve as pseudo-valves to prevent hydrodynamic flow of bulk solutions within the chip. Due to the small gel pore size, which is on the order of the protein molecules themselves,[195,196] hydrodynamic flow through the PAAm gel pores is negligible. Although the PAAm is covalently linked to the channel sidewalls, bulk flow of solution can potentially occur by failure of the gel/wall interface, or structural failure of the highly crosslinked gel network. The pressure resistance of the gel plugs was characterized using a set of five single-channel chips with channels 110 μm wide and 80 μm deep containing a 300 μm long PAAm gel plug. With one end of the channel connected to a syringe, a series of weights was applied to the syringe plunger until bulk flow was observed within the channel. Using this approach, an average burst pressure of 490 kPa was determined. Considering the substantially longer gel plugs used in the IEF/SDS-PAGE chip, even higher pressure resistance is expected. In addition, pressure resistance of the shorter pseudo-valves fabricated adjacent to the acid/base reservoirs (Figure 44) was enhanced by increasing the local channel depth from 50 μm to 140 μm, while also increasing the channel width from 150 μm to 300 μm to provide a mechanical constraint for these gel plugs (Figure 45). After injecting sample into the IEF channel and sealing the sample inlet and waste reservoirs, no bulk flow was observed even after 10 min equilibration, with stable and well-defined sample/gel

interfaces maintained between the IEF channel and all injection and SDS-PAGE channels.

7.2.3 SDS Gel Packets.

Another important use of the PAAm gel plugs is for reagent containers in the 2-D chip. In particular, the gel plugs formed in the injection microchannel array are photopolymerized with 1.2% SDS, which remains constrained within the gel until being mobilized by electrophoresis. This approach allows well-defined and uniform quantities of SDS to be dispensed during the initial stage of SDS-PAGE, with SDS injected into the IEF channel complexing with focused proteins in real-time. Because complete binding of SDS with denatured proteins requires a 1.4:1 SDS:protein ratio,[197] the total protein loading dictates the minimum amount of SDS which must be loaded into the gel packet. To avoid precipitation of proteins during IEF, sample concentration should be maintained below around 2 mg/mL. In the present design, the IEF channel volume is 0.225 μL, thus a maximum sample loading of around 0.5 μg is reasonable for the microfluidic chip, and a total SDS amount of 0.7 μg is desired. Based on the SDS concentration and plug volume, the total amount of SDS within all eleven injection channels is approximately 28 μg, substantially more than the required 0.7 μg. The excess SDS ensures its high availability for protein binding, allowing the complexation process to occur in real-time without the need for incubation.[179]
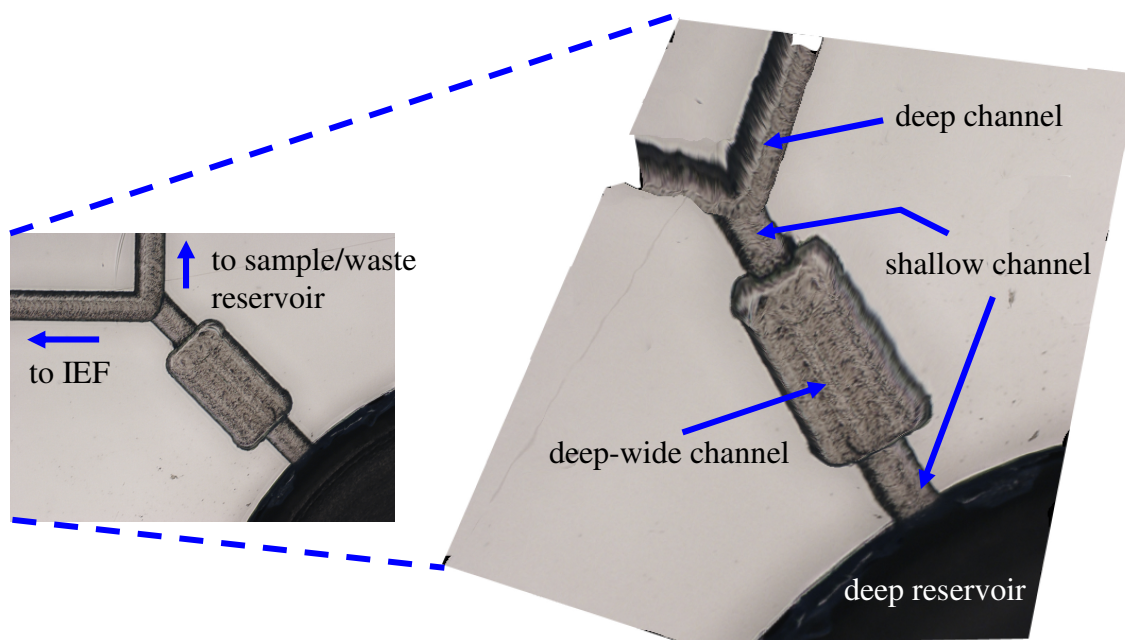
Figure 45. The schematic 3D view of acid and/or base gel plug channel. The shallow channel segments connect to both IEF and deep reservoirs, and the deep-wide channel creates mechanically anchored gel plug so that AI plug is permanently confined inside the channel. The dimension of the channel is: shallow segment 50μm × 150 μm, deep-wide segment 140μm × 150μm.

7.2.4 IEF and Sample Transfer.

Integrated in-situ PAAm gels have been previously used as pressure-blocking elements for 2-D separation chips, enabling sample to be loaded into the first-dimension microchannel with minimal intrusion into the second dimension channel array.[110,179] In particular, PAAm gel plugs have been shown to prevent hydrodynamic flow within the acid/base reservoirs, injection channels, and second-dimension separation channels, enabling highly-repeatable separations with less than 5% variation in peak elution time for a chip containing five SDS-CGE microchannels.[179] However, non-uniform injection of sample from the IEF channel to the SDS-CGE channel array remains problematic, resulting in significant broadening of the injected sample bands. Most critically, large electric field gradients across the width of a straight IEF channel can produce long

sample tails during the injection process, preventing effective stacking following transfer to the second dimension and resulting in poor separation resolution. To provide a substantially more uniform electric field during sample transfer, each IEF channel segment was angled 45° relative to its adjacent second dimension separation and injection channels (Figure 44). This design can reduce electric field variations during sample transfer by a factor of 13 compared to a straight IEF channel.[188]
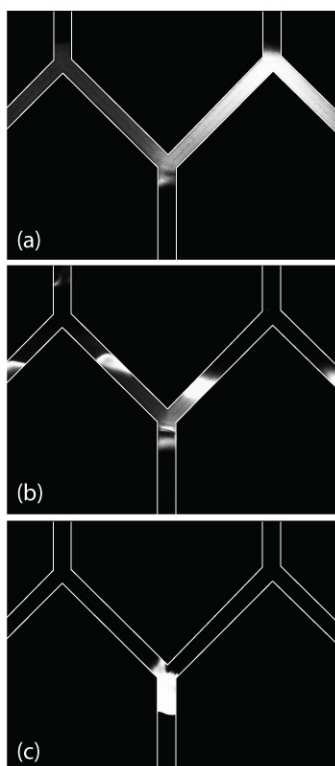
Figure 46. Transfer of focused proteins showing (a) initial mobilization of SDS from the injection channels into the IEF channel, (b) real-time SDS-protein complexation, and (c) complete and uniform transfer of SDS-protein complexes to the SDS-PAGE dimension (channel width: 150 μm).

A detailed view of the sample transfer process following IEF is shown in Figure 46. After the initial focusing step in Figure 46 (a), a negative bias is applied to the upper injection reservoirs with the lower SDS-PAGE reservoirs grounded, for an average

electric field strength of 200 V/cm during sample transfer. As SDS from the injection channel gel plugs enters the IEF channel, real-time complexation with the denatured proteins occurs, mobilizing the proteins towards the lower separation channels in Figure 46 (b). Even for complex samples, only minimal variations in migration speed of the SDS-protein complexes are typically observed among the different IEF channel segments. More importantly, as shown in Figure 46 (c), the entire sample is transferred into the SDS-PAGE channels, with no significant residual sample remaining within the IEF channel within 10 s of the initial SDS front reaching the proteins. This result compares favorably with previous 2-D separations performed using a straight IEF channel, where long sample tails up to several mm long were formed during sample transfer, severely degrading separation resolution.[179]
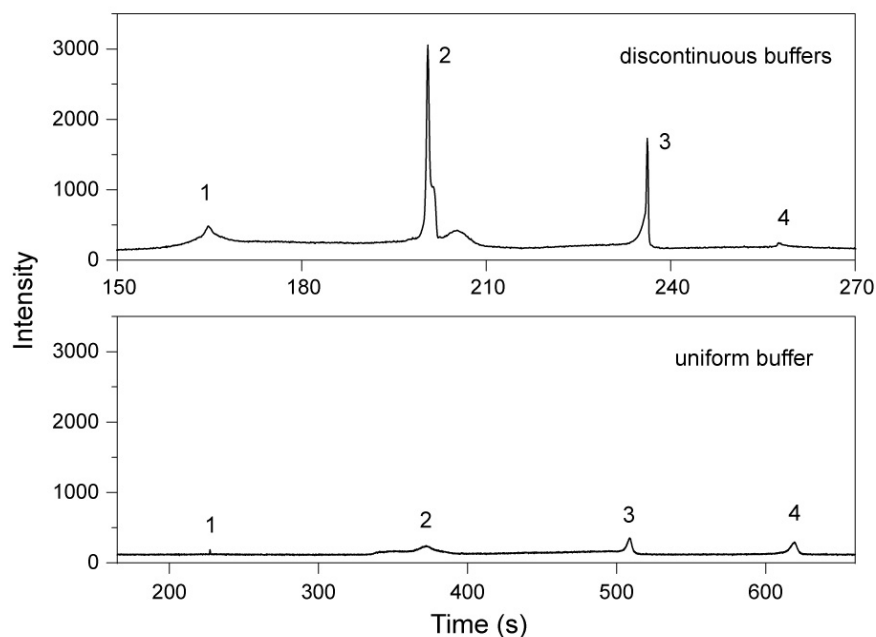
Figure 47. On-chip SDS-PAGE of urea-denatured proteins in uniform and discontinuous buffer systems. The labeled electropherogram peaks correspond to (1) parvalbumin, 12 kDa; (2) trypsin inhibitor, 21 kDa; (3) ovalbumin, 45 kDa; (4) BSA, 66 kDa. Length to detector = 4 cm, E = 100 V/cm. The uniform buffer is 5 mM Tris-HCl, pH6.9, 0.1% SDS.

As shown in Figure 44, the chip design also includes a long microchannel on either side of the second dimension array. These two channels, which are twice the length of the second dimension channels and filled with the same PAAm gel and buffer, are used to back-bias the IEF channel during sample transfer and SDS-PAGE separations. Back-biasing in the 2-D chip serves to eliminate injection non-uniformities, ensuring that sample bands enter the second dimension channel array simultaneously, while also preventing leakage of sample into the outermost separation channels within the array.[188]

7.2.5 SDS-PAGE Separation Performance.

In the commonly-used buffer system reported by Laemmli[198] for slab gel SDS-PAGE, which extends the discontinuous buffer system originally developed by Ornstein[199] and Davis,[200] proteins are concentrated isotachephoretically within a large-pore stacking gel before being separated within an adjacent sieving gel. The Laemmli system employs chloride leading ions and glycinate trailing ions during the stacking process, with a transition from stacking to separation resulting from the use of a basic separation buffer several pH units higher than the stacking buffer. As the trailing glycinate ions enter the basic environment within the separation gel, their mobility increases substantially, allowing the ions to pass the slower proteins and finally resulting in a uniform separation buffer after stacking. In the microfluidic system, the multifunctional PAAm gels allow specific buffer conditions to be maintained within selected regions of the chip, such as the pH gradient required for the Laemmli buffer system. However, unlike slab gel SDS-PAGE, the 2-D chip does not readily allow for the integration of a large-pore stacking gel between the IEF channel and SDS-PAGE channel array. Furthermore, because of inhomogeneities in the pore size and distribution at the entrance to the photopolymerized

PAAm sieving gel, substantial destacking can occur as sample bands mobilize into the sieving gel. Thus, to maximize separation efficiency in the 2-D chips, it is desirable to perform sample stacking after the SDS-protein complexes have entered the separation gel. To this end, a leading buffer containing chloride ions was placed within the PAAm separation gel, and a trailing buffer containing a low concentration of glycine was placed behind the SDS-complexed proteins during sample injection, with Tris as a common constituent of both solutions which were buffered to pH 6.9 (Table 6). In addition, buffer solution containing a high concentration of glycine, together with the SDS required for the second dimension separation, was placed within the injection channel gel plugs at pH 8.3 to ensure a high initial mobility for glycinate ions within the injection channels. Soon after the SDS-protein complexes enter the separation gel, the high mobility glycinate ions sweep through the sample region, generating a transient electric field gradient which sharpens the individual protein bands. After the leading glycinate ions have traversed the sample region, size-based separation by SDS-PAGE continues within the background buffer containing a lower concentration of glycine. For the buffer conditions given in Table 6, full sharpening of the protein bands was typically observed within 5-10 mm after entering the CGE channels.
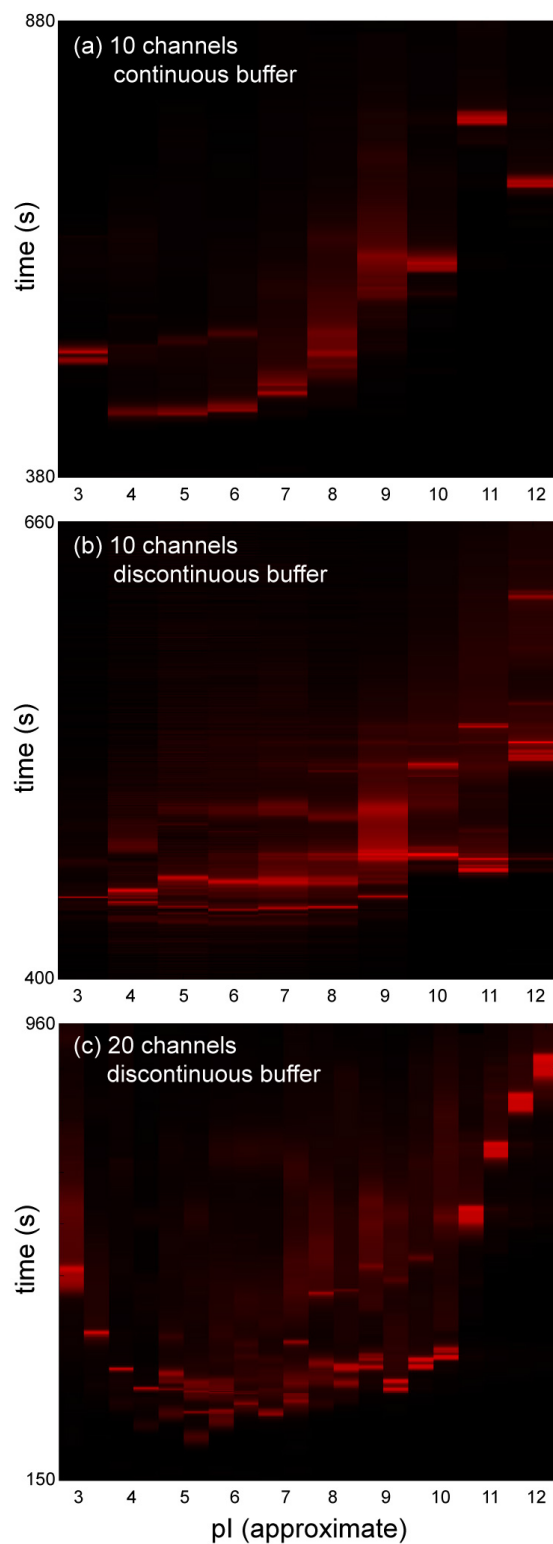
Figure 48. Pseudo-gel images of IEF/SDS-PAGE *E. coli* cell lysate separations using (a) continuous buffers in a 10-channel SDS-PAGE chip, (b) discontinuous buffers in a 10-channel chip, and (c) discontinuous buffers in a 20-channel chip.

The effect of bond sharpening using the heterogeneous buffer system can be seen in the single-dimension SDS-PAGE electropherograms shown in Figure 47. Each of the four model proteins separated in these experiments (parvalbumin, trypsin inhibitor, ovalbumin, and BSA) are resolved in both buffer systems with similar relative elution times, but with significantly higher signal-to-noise ratios when using discontinuous buffers. The peaks are also narrower, leading to a higher peak capacity for the discontinuous SDS-PAGE separation. Defining the width of a sample bond as the time for the half-height full-width of a bond to pass the detector, normalized to the total time between the first and last peaks of each electropherogram, the average peak capacity for the discontinuous buffer separation measured over five runs across all model proteins was 170, an improvement by a factor of 3.4 over the continuous buffer case.

7.2.6   IEF/SDS-PAGE Separations.

Full 2-D separations of *E. coli* cell lysate were performed using both uniform and discontinuous buffer systems. Experiments were first performed using a chip containing 10 parallel SDS-CGE channels, with the results shown in Figure 48 (a-b). In each experiment, electropherogram extracted from the SDS-PAGE channel array were used to generate a pseudo-gel image similar to a conventional 2-D PAGE image revealing MW and pI for each protein peak, but with the MW axis replaced by elution time within the 2-D chip. Using the uniform buffer system, approximately 40 relatively low-intensity peaks were detected, as shown in Figure 48 (a). In contrast, the use of discontinuous buffers provided significantly higher resolving power in the 10-channel chip, with a similar overall peak pattern but approximately twice the number of total peaks as shown in Figure 48 (b). Following background subtraction for both cases, the dynamic range for

the chip employing the discontinuous buffer system is noticeably higher, with 18% higher average peak intensities. Faster SDS-PAGE separations were also realized using the discontinuous buffer system in the 10-channel chip, consistent with the separation results using model proteins (Figure 47).

Table 6. Prepolymer conditions for crosslinked PAAm gel formation, and buffer conditions in injection and SDS-PAGE reservoirs.

	Acid/Base Gel Plugs	SDS-PAGE Gel	SDS-PAGE Reservoirs	Injection Gel Plugs	Injection Reservoirs
AAm (wt %)	3.6	3.6	-	3.6	-
Bis (wt %)	0.4	0.4	-	0.4	-
I2959 (wt %)	0.12	0.12	-	0.12	-
SDS (wt %)	–	0.1	0.1	1.2	0.1
Buffer	5 mM Tris-HCl	5 mM Tris-HCl	125 mM Tris-HCl	25 mM Tris + 192 mM glycine	125 mM Tris + HCl 50 mM glycine
pH	6.9	6.9	6.9	8.3	6.9
UV dose	11 J/cm^2	5.5 J/cm^2	-	11 J/cm^2	-
Gel length	1 mm	6 cm	-	1 cm	-

Further improvements in resolving power were achieved by increasing the density of channels in the second-dimension SDS-PAGE array. Capillary or microchannel IEF is a highly-resolving electrokinetic separation technique, with maximum resolution dictated by precipitation as sample concentration increases during focusing. Typical peak capacities on the order of 60 (based on four model proteins IEF separation) were measured for the relatively short (1.1 cm) IEF channel used in the 2-D chip design. In order to take full advantage of IEF, it may be argued that the focused proteins should be

sampled into the second dimension near the resolution limit of the IEF separation, suggesting that around 60 SDS-PAGE channels would provide optimal peak capacity for the overall separation. However, since detection sensitivity is a function of analyte concentration, it is advantageous to sample the focused proteins below the IEF peak capacity to prevent large numbers of focused sample bands from being split into multiple SDS-PAGE channels, thereby reducing maximum concentration within each channel at the downstream detector. With this constraint in mind, *E. coli* lysate separations were performed using a chip containing 20 SDS-PAGE channels, resulting in the pseudo-gel image shown in Figure 48 (c). The chip design was identical to the 10-channel chip, but an IEF channel twice the overall length compared to the lower density chip. The electric field used for IEF was identical for both cases. Thus the same approximate pI range was sampled by the second-dimension microchannels, but with twice the sampling resolution for the 20-channel design.

The resulting separations using the 20-channel chip reveal a more complex pattern of peaks, with only a few bands which appear to co-elute across adjacent SDS-PAGE channels. It is notable that the 20-channel chip also appears to reveal features at the extreme ends of the pH range which were not apparent in the 10-channel design, suggesting that a wider pH range was sampled for the 20-channel case.

Since the various separation reagents and buffers were stored on-chip within the multifunctional gels, repeated experiments using a single chip could not be performed to evaluate run-to-run reproducibility. Multiple tests performed across different 10-channel chips resulted in similar 2-D peak patterns, but quantitative reproducibility was limited by variations in gel plug lengths, preparation conditions for the discontinuous buffer

components, and channel geometries for the machined chips. Improvements in reproducibility are expected by migrating to polymer chips imprinted from a single mold, and the use of lithographically-defined masks for gel patterning. It should also be noted that the use of chip-based differential gel electrophoresis (DIGE) may ultimately obviate this concern by enabling differential analysis of multiple samples within a single 2-D PAGE separation.

7.2.7 2D-PAGE Reproducibility

The microfluidic 2D-PAGE platform provides an alternative means for proteome analysis. So far, this technique is limited due to irreproducible results caused by many factors. The most critical one is that ion diffusion between IEF and CGE channels, such as high concentration of SDS in injection channel diffusing into IEF channel, and even CGE channel. The SDS binds with proteins and the negatively-charged species migrate towards anode. As a result, certain amount of samples loss during IEF, and IEF focusing pattern will slightly change. There are at least two methods to minimize SDS effect on IEF separation. As shown in Figure 17(a), the 2-mm injection gel plug can completely isolate SDS from IEF channel. The high concentration of SDS is only doped into the injection channel connecting to injection reservoirs. Pre-conditioning of IEF channel using running buffer is another effective approach. Two electrodes are setup between IEF channel inlet and water reservoir. Since SDS is negatively charged molecules, they migrate to positive electrode electrokinetically. The SDS close to IEF channel can be easily cleaned up without making any revision of 2D chip.

Chip dimension plays a role in 2D reproducibility in that inhomogeneous chip thickness tends to change electric field distribution. The 2 *x backbiasing channels* cannot

completely generate uniform current distribution. The uniform channel depth can be achieved by either using uniform thickness of chip, or using imprinting fabrication process. In addition, the IEF channel segment also affects 2D reproducibility. For example, with longer IEF channel segment, less sample loss occurs. Thus the amount of sample separated by IEF is higher. The separated bands in IEF channel should be more repeatable so that improved 2D separation is expected.

7.3   Summary and Conclusions

The presented 2-D microfluidic system combines multifunctional gels, a discontinuous buffer system, and novel chip design elements to achieve high-resolution multidimensional separations of *E. coli* cell lysate proteins. The multifunctional PAAm gels offer several important benefits for the microfluidic platform. Following previous demonstrations of PAAm gels as pressure-blocking elements in complex microfluidic systems, short plugs of *in situ* photopolymerized PAAm gel integrated into selected regions of the chip eliminate unwanted hydrodynamic flow, enabling the various solutions required for both IEF and SDS-PAGE to be isolated until needed during each stage of the separation process. The presented system extends the use of PAAm gel plugs as reagent containers, allowing discrete packets of SDS and discontinuous buffers to be placed on-chip during the fabrication process. This approach to on-chip reagent storage allows a substantial reduction in chip complexity by eliminating the need for separate SDS injection channels as used in our previous work,[179] while also simplifying the system-level operational requirements by integrating all solutions except the sample/ampholyte mixture into the chip. Beyond the present application, gel plugs may also find use as on-chip reagent containers in other microfluidic systems requiring precise

metering of reagents. The PAAm-enabled 2D platform allows upgrading chip density from 5 to 64 channels reliably as shown in Figure 49.
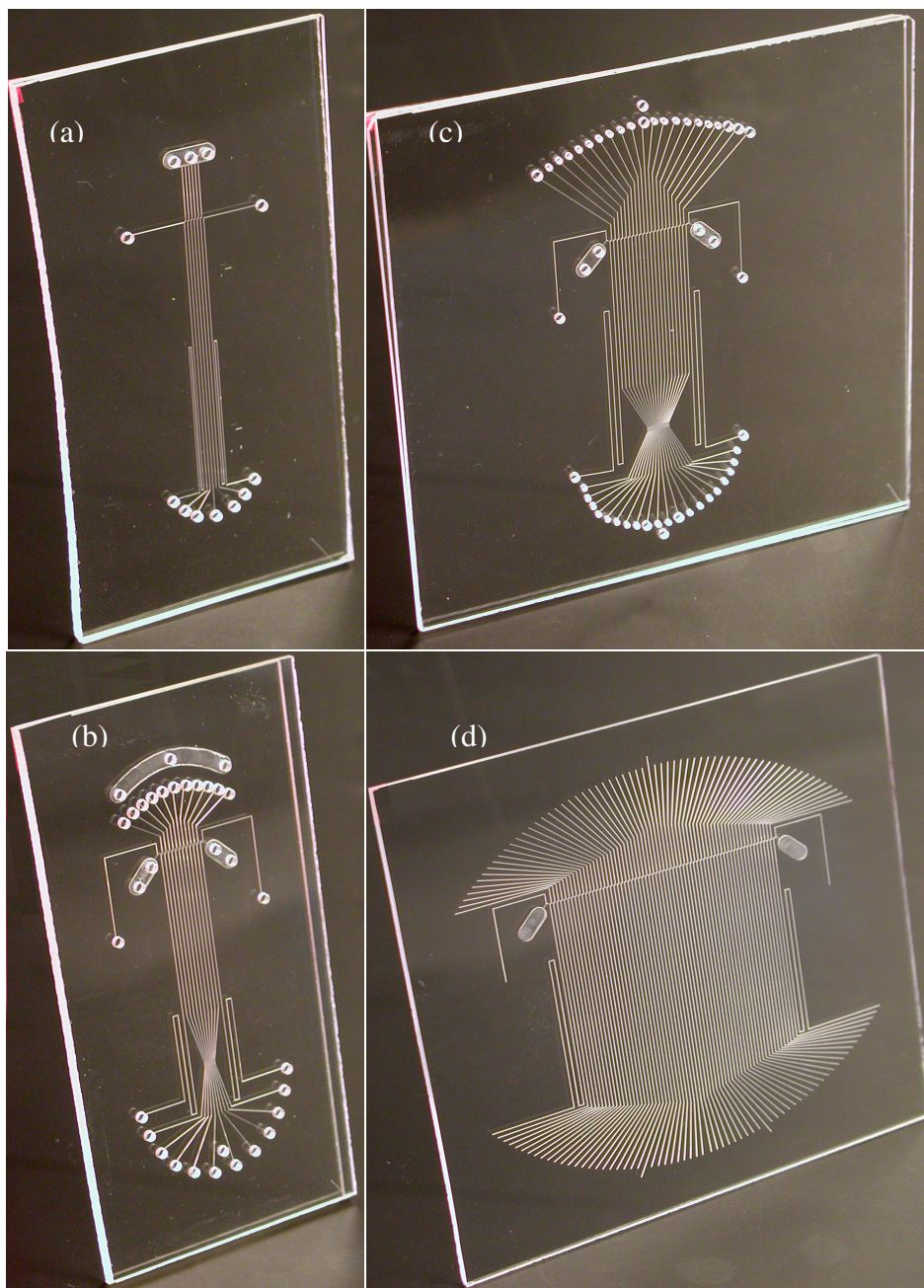
Figure 49. Microchip density upgradeability using PAAm gel-enabled platform. The chip dimension is 100 mm × 100 mm. (a) Five-channel 1D chip; (b) ten-channel 2D chip; (c) 32-channel 2D chip; and (d) 64-channel 2D chip.

The high resolving capacity of slab gel SDS-PAGE is largely due to the use of isotachophoretic stacking of the sample prior to its introduction into the sieving gel. While the traditional Laemmli buffer system cannot be directly applied to the microfluidic platform due to the lack of a stacking gel within the chip, the novel discontinuous buffer system enabled by the on-chip gel plugs provides substantial sharpening of protein bands during SDS-PAGE. The choice of anion and cation species, ion concentration, and buffer pH within each portion of the system was made on the basis of extensive experiments performed over a wide range of conditions. The in-gel bond sharpening is believed to result from a transient electric field or pH gradient generated during the injection of the highly mobile glycinate ions initially maintained at basic pH within the injection gel plugs. Further modeling and optimization of the buffer conditions is needed to fully explore the sharpening effect and yield additional improvements in the peak capacity of the 2-D system.

Because reagents are packaged on-chip using the multifunctional gels, the polymer chips are single-use, and long-terms storage of fabricated chips prior to use is of practical concern. Stability of the on-chip reagent packets is maintained solely by slow diffusion within the fine-pore gel matrix. Separations performed within 1 hour of chip fabrication have shown no significant variations in separation performance, but longer diffusion times are likely to lead to irreproducible results. Improved longevity has been achieved by freezing chips after fabrication. While more rigorous characterization is ongoing to evaluate freezing as a viable method for long-term storage of chips containing PAAm gel plugs, no degradation of the PAAm gels and only minor variations in separation results have been observed for chips exposed to a single 12 h freeze cycle at -20 $^{\circ}$C.

Chapter 8.   Summary and Future Work

This dissertation demonstrates a two-dimensional isoelectric focusing (IEF) – sodium dodecyl sulfate (SDS)/polyacrylamide gel electrophoresis (PAGE) separation on spatially-multiplexed chip platform. The first dimension IEF separates the analytes based on their pI value, and the second dimension SDS/PAGE separates the analytes based on their molecular weight after fully sodium dodecyl sulfate (SDS) denature.

9.1   Conclusion

This dissertation developed an effective approach for plastic surface modification and fabrication. The polymethylmethacrylate (PMMA) is firstly oxidized by UV-ozone to generate hydroxide groups, which then covalently bond to the acrylic groups in the solution. The electroosmotic flow (EOF) is eliminated by coating linear polyacrylamide (LPA) to these acrylic groups on PMMA surface. The LPA coating provides hydrophilic surface to prevent protein non-specific adsorption. The dynamic coating, such as methylcellulose (MC), polyvinyl alcohol (PVA) and bovine serum albumin (BSA), further reduces non-specific protein adsorption to PMMA surface.

In this dissertation, a novel chip design is developed. Application of Pspice and FEMLab simulations, the electrical current distribution is characterized and issues associated with sample transfer are identified, including asymmetrical sample injection, sample leakage, and sample tailing. Proper backbiasing can completely eliminate non-uniformities during sample transfer and 2nd dimension separations, and also prevent leakage of residual sample from the outer regions of the 1st dimension channel. Optimized backbiasing channels, with twice the resistance of a single 2nd dimension channel, can be realized in a number of ways. In the present work, all channels used the

same cross-sectional dimensions, and the length of the backbiasing channels was doubled over the 2nd-D separation channel to implement 2x backbiasing. Alternately, the channel width or depth could have been reduced by half while maintained identical lengths between the backbiasing and 2nd dimension channels. Backbiasing can also be performed by directly applying appropriate biases to each reservoir at the ends of the 1st dimension microchannel. However, this approach requires accurate knowledge of buffer conductivities within both dimensions and thus adds unnecessary uncertainty compared to on-chip backbiasing channels, which ensure uniform injection regardless of the buffer conditions or separation media used in each dimension.

Angled 1st dimension channel segments are also a valuable design element for realizing optimized sample transfer in staggered 2-D microfluidic chips. The angled channel design provides a simple approach for minimizing sample plug tailing and initial sample plug length within the 2nd dimension channels, thereby offering improved peak capacities for the overall system. While this study has focused on the sample transfer process using a single homogeneous analyte, 2-D separations are performed using chips combining both 2x backbiasing and angled channel design elements, using microfluidic isoelectric focusing (μIEF) in the 1st dimension and gel electrophoresis in the 2nd dimension. It is worth noting that the angled channel design does not substantially affect focusing resolution during μIEF. Moreover, the uniform injection and minimized tailing provided by this design feature is providing improvements in the full 2-D separation performance even for relatively complex samples such as cell lysate.

Taking advantage of this unique chip design, this dissertation further developed a novel 2-D separation platform, which combines multifunctional gels, a discontinuous

buffer system, and novel chip design elements to achieve high-resolution multidimensional separations of *E. coli* cell lysate proteins. The multifunctional PAAm gels offer several important benefits for the microfluidic platform. Following previous demonstrations of PAAm gels as pressure-blocking elements in complex microfluidic systems, short plugs of *in situ* photopolymerized PAAm gel integrated into selected regions of the chip eliminate unwanted hydrodynamic flow, enabling the various solutions required for both IEF and SDS-PAGE to be isolated until needed during each stage of the separation process. The presented system extends the use of PAAm gel plugs as reagent containers, allowing discrete packets of SDS and discontinuous buffers to be placed on-chip during the fabrication process. This approach to on-chip reagent storage allows a substantial reduction in chip complexity by eliminating the need for separate SDS injection channels as used in the previous work,[179] while also simplifying the system-level operational requirements by integrating all solutions except the sample/ampholyte mixture into the chip. Beyond the present application, gel plugs may also find use as on-chip reagent containers in other microfluidic systems requiring precise metering of reagents.

The high resolving capacity of slab gel SDS-PAGE is largely due to the use of isotachophoretic stacking of the sample prior to its introduction into the sieving gel. While the traditional Laemmli buffer system cannot be directly applied to the microfluidic platform due to the lack of a stacking gel within the chip, the novel discontinuous buffer system enabled by the on-chip gel plugs provides substantial sharpening of protein bands during SDS-PAGE. The choice of anion and cation species, ion concentration, and buffer pH within each portion of the system was made on the basis

of extensive experiments performed over a wide range of conditions. The in-gel bond sharpening is believed to result from a transient electric field or pH gradient generated during the injection of the highly mobile glycinate ions initially maintained at basic pH within the injection gel plugs. Further modeling and optimization of the buffer conditions is needed to fully explore the sharpening effect and yield additional improvements in the peak capacity of the 2-D system.

Because reagents are packaged on-chip using the multifunctional gels, the polymer chips are single-use, and long-terms storage of fabricated chips prior to use is of practical concern. Stability of the on-chip reagent packets is maintained solely by slow diffusion within the fine-pore gel matrix. Separations performed within 1 hour of chip fabrication have shown no significant variations in separation performance, but longer diffusion times are likely to lead to irreproducible results. Improved longevity has been achieved by freezing chips after fabrication. While more rigorous characterization is ongoing to evaluate freezing as a viable method for long-term storage of chips containing PAAm gel plugs, no degradation of the PAAm gels and only minor variations in separation results have been observed for chips exposed to a single 12 h freeze cycle at -20 $^{\circ}$C.

9.2   Future Work: reproducibility, in situ labeling and MALDI-MS

Future work will focus on: (1) 2-D PAGE reproducibility; (2) in situ labeling of protein during 2D-PAGE; (3) coupling of 2D PAGE with laser desorption ionization (LDI) or matrix-assisted laser desorption ionization (MALDI)/mass spectrometry (MS).

The reproducibility of microfluidic 2-D PAGE needs to be further improved on current platform. It was observed that E.coli mapping is varied run to run, even though all conditions were kept without change, such as gel recipe, buffers, and experimental setup.

Several factors will potentially affect separation repeatability, such as SDS disturbance on IEF, sample loss, sample intrusion into 2nd-D during IEF, channel surface and dimension uniformity etc. During gel preparation, SDS close to 1D-2D intersection might continuously diffuse into IEF buffer. As a result, proteins will migrate towards cathode due to binding with negatively charged SDS. It is recommended to use injection design shown in Figure 17 (a) to replace injection of (b). The short plug in injection channel is able to isolate SDS with protein. Additionally, the sample loss and intrusion during IEF can be alleviated by increasing length of IEF segment and fabricating the front channel near IEF shallow.

In traditional slab-gel 2D-PAGE, the protein is labeled after separation using a variety of staining, such as Coomassie, silver, autoradiography, and fluorescent;[201] the counterpart of labeling in microfluidic 2D-PAGE is use of dyes such as fluorescein isothiocyanate (FITC), Alexa, Sypro dye and etc. This dissertation has demonstrated FITC and Alexa labeling approach, pre-labeled and detected under fluorescent microscope. However, the labeling efficiency on complex proteins may be varied from protein to protein, so that not all proteins can be detected by a single FITC or Alexa dye. The more solid approach seems to *in situ* labeling of protein by Sypro dye. The principle is that Sypro dye can form non-covalent bond with SDS-protein complex, while Sypro dye does not bind to protein self. Since all proteins can form complexes with SDS, the selectivity is not an issue any more for SDS-Sypro *in situ* labeling. In the future work, appropriate Sypro (such as orange, red, ruby etc) will be selected for optimized detection conditions. In addition, design of experiment will be performed to investigate type of Sypro, concentration, and Sypro-gel recipe etc.

Another interesting future work is to deal with protein detection from 2D-PAGE gel, either direct detection by laser desorption ionization (LDI) or indirect by matrix-assisted laser desorption ionization (MALDI). Several studies demonstrated that proteins can be directly ionized by infrared radiation (IR)-MS from PAAm gel.[202,203] Proteins can also be directly detected from ultra-thin layer of PAAm gel, using of UV laser source, by linking to the high throuput and sensitivity of MALDI.[204] However, the detection of protein from gel demands a lot of work, such how to detect protein from gel in microchannel and what protocol is suitable for acquiring signal on higher molecule weight of protein. In literature, the high sensitivity of signal is obtained beyond 10 kDa protein. It may be possible to detect protein by MS since the gel is very thin, down to 10 µm after drying. The success coupling of MS with microfluidic 2-D PAGE will make it possible for clinical proteomics.

Bibliography

1. A. Manz, N. Graber and H. M. Widmer, *Sensors and Actuators B-Chemical*, 1990, **1**, 244-248.
2. Y. Jiang, P. C. Wang, L. E. Locascio and C. S. Lee, *Analytical Chemistry*, 2001, **73**, 2048-2053.
3. D. J. Ehrlich and P. Matsudaira, *Trends in Biotechnology*, 1999, **17**, 315-319.
4. J. Astorga-Wells, H. Jornvall and T. Bergman, *Analytical Chemistry*, 2003, **75**, 5213-5219.
5. M. A. McClain, C. T. Culbertson, S. C. Jacobson, N. L. Allbritton, C. E. Sims and J. M. Ramsey, *Analytical Chemistry*, 2003, **75**, 5646-5655.
6. S. K. Sia and G. M. Whitesides, *Electrophoresis*, 2003, **24**, 3563-3576.
7. S. C. Jakeway, A. J. de Mello and E. L. Russell, *Fresenius Journal of Analytical Chemistry*, 2000, **366**, 525-539.
8. F. Vinet, P. Chaton and Y. Fouillet, *Microelectronic Engineering*, 2002, **61-2**, 41-47.
9. D. R. Meldrum and M. R. Holl, *Science*, 2002, **297**, 1197-1198.
10. L. Marle and G. M. Greenway, *Trac-Trends in Analytical Chemistry*, 2005, **24**, 795-802.
11. E. Verpoorte, *Electrophoresis*, 2002, **23**, 677-712.
12. J. Wang, *Analytica Chimica Acta*, 2004, **507**, 3-10.
13. B. G. Chung, L. A. Flanagan, S. W. Rhee, P. H. Schwartz, A. P. Lee, E. S. Monuki and N. L. Jeon, *Lab on a Chip*, 2005, **5**, 401-406.
14. A. J. de Mello and N. Beard, *Lab on a Chip*, 2003, **3**, 11N-19N.
15. B. M. Paegel, R. G. Blazej and R. A. Mathies, *Current Opinion in Biotechnology*, 2003, **14**, 42-50.
16. C. Yu, M. H. Davey, F. Svec and J. M. J. Frechet, *Analytical Chemistry*, 2001, **73**, 5088-5096.
17. R. S. Foote, J. Khandurina, S. C. Jacobson and J. M. Ramsey, *Analytical Chemistry*, 2005, **77**, 57-63.
18. A. Wainright, U. T. Nguyen, T. Bjornson and T. D. Boone, *Electrophoresis*, 2003, **24**, 3784-3792.
19. S. C. Jacobson, T. E. McKnight and J. M. Ramsey, *Analytical Chemistry*, 1999, **71**, 4455-4459.
20. J. Kobayashi, Y. Mori, K. Okamoto, R. Akiyama, M. Ueno, T. Kitamori and S. Kobayashi, *Science*, 2004, **304**, 1305-1308.
21. J. Khandurina, T. E. McKnight, S. C. Jacobson, L. C. Waters, R. S. Foote and J. M. Ramsey, *Analytical Chemistry*, 2000, **72**, 2995-3000.
22. G. B. Lee, S. H. Chen, G. R. Huang, W. C. Sung and Y. H. Lin, *Sensors and Actuators B-Chemical*, 2001, **75**, 142-148.
23. D. R. Reyes, D. Iossifidis, P. A. Auroux and A. Manz, *Analytical Chemistry*, 2002, **74**, 2623-2636.
24. D. J. Harrison, K. Fluri, K. Seiler, Z. H. Fan, C. S. Effenhauser and A. Manz, *Science*, 1993, **261**, 895-897.

25. A. Manz, D. J. Harrison, E. M. J. Verpoorte, J. C. Fettinger, A. Paulus, H. Ludi and H. M. Widmer, *Journal of Chromatography*, 1992, **593**, 253-258.
26. D. Erickson and D. Q. Li, *Analytica Chimica Acta*, 2004, **507**, 11-26.
27. S. Hjerten, *Chromatographic Reviews*, 1967, **9**, 122-219.
28. S. C. Jacobson, R. Hergenroder, L. B. Koutny and J. M. Ramsey, *Analytical Chemistry*, 1994, **66**, 1114-1118.
29. H. Becker and L. E. Locascio, *Talanta*, 2002, **56**, 267-287.
30. H. Shadpour, H. Musyimi, J. F. Chen and S. A. Soper, *Journal of Chromatography A*, 2006, **1111**, 238-251.
31. S. Z. Qi, X. Z. Liu, S. Ford, J. Barrows, G. Thomas, K. Kelly, A. McCandless, K. Lian, J. Goettert and S. A. Soper, *Lab on a Chip*, 2002, **2**, 88-95.
32. I. Nikcevic, S. H. Lee, A. Piruska, C. H. Ahn, T. H. Ridgway, P. A. Limbach, K. R. Wehmeyer, W. R. Heineman and C. J. Seliskar, *Journal of Chromatography A*, 2007, **1154**, 444-453.
33. H. Becker and C. Gartner, *Electrophoresis*, 2000, **21**, 12-26.
34. A. Muck, J. Wang, M. Jacobs, G. Chen, M. P. Chatrathi, V. Jurka, Z. Vyborny, S. D. Spillman, G. Sridharan and M. J. Schoning, *Analytical Chemistry*, 2004, **76**, 2290-2297.
35. D. Belder and M. Ludwig, *Electrophoresis*, 2003, **24**, 3595-3606.
36. R. A. Zangmeister and M. J. Tarlov, *Langmuir*, 2003, **19**, 6901-6904.
37. J. K. Liu and M. L. Lee, *Electrophoresis*, 2006, **27**, 3533-3546.
38. H. F. Yin, J. A. Lux and G. Schomburg, *Hrc-Journal of High Resolution Chromatography*, 1990, **13**, 624-627.
39. A. S. Cohen and B. L. Karger, *Journal of Chromatography*, 1987, **397**, 409-417.
40. D. Belder, A. Deege, F. Kohler and M. Ludwig, *Electrophoresis*, 2002, **23**, 3567-3573.
41. P. A. Auroux, D. Iossifidis, D. R. Reyes and A. Manz, *Analytical Chemistry*, 2002, **74**, 2637-2652.
42. V. Dolnik, S. R. Liu and S. Jovanovich, *Electrophoresis*, 2000, **21**, 41-54.
43. S. C. Jacobson, R. Hergenroder, L. B. Koutny and J. M. Ramsey, *Analytical Chemistry*, 1994, **66**, 2369-2373.
44. M. Molina and M. Silva, *Electrophoresis*, 2002, **23**, 3907-3921.
45. K. W. Ro, K. Lim, H. Kim and J. H. Hahn, *Electrophoresis*, 2002, **23**, 1129-1137.
46. H. C. Cui, K. Horiuchi, P. Dutta and C. F. Ivory, *Analytical Chemistry*, 2005, **77**, 1303-1309.
47. G. Hunt, K. G. Moorhouse and A. B. Chen, *Journal of Chromatography A*, 1996, **744**, 295-301.
48. J. W. Hong, K. Hosokawa, T. Fujii, M. Seki and I. Endo, *Biotechnology Progress*, 2001, **17**, 958-962.
49. Y. Li, J. S. Buch, F. Rosenberger, D. L. DeVoe and C. S. Lee, *Analytical Chemistry*, 2004, **76**, 742-748.
50. A. Griebel, S. Rund, F. Schonfeld, W. Dorner, R. Konrad and S. Hardt, *Lab on a Chip*, 2004, **4**, 18-23.
51. P. Altenhofer, A. Schierhorn and B. Fricke, *Electrophoresis*, 2006, **27**, 4096-4111.

52. A. E. Herr, J. I. Molho, K. A. Drouvalakis, J. C. Mikkelsen, P. J. Utz, J. G. Santiago and T. W. Kenny, *Analytical Chemistry*, 2003, **75**, 1180-1187.

53. A. V. Hatch, A. E. Herr, D. J. Throckmorton, J. S. Brennan and A. K. Singh, *Analytical Chemistry*, 2006, **78**, 4976-4984.

54. R. Mukhopadhyay, *Analytical Chemistry*, 2006, **78**, 3489-3489.

55. C. M. Wilson, *Plant Physiology*, 1986, **82**, 196-202.

56. M. I. Huber, T. P. Hennessy, D. Lubda and K. K. Unger, *Journal of Chromatography B-Analytical Technologies in the Biomedical and Life Sciences*, 2004, **803**, 137-147.

57. A. J. Link, *2-D Proteome Analysis Protocols*, Humana Press Inc., Totowa, NJ, 1999.

58. J. S. Buch, J. K. Liu, S. Yang, C.-W. Tsao, T. Song, P. Silvanesan, K. Phalnikar, C. S. Lee and D. L. DeVoe, in *the 10th International Conference on Miniaturized Systems for Chemistry and Life Sciences (TAS 2006)*, Tokyo, Japan, 2006, pp. 1579-1581.

59. A. Guttman, J. Horvath and N. Cooke, *Analytical Chemistry*, 1993, **65**, 199-203.

60. PSPICE, Electronics Lab, 2008.

61. FEMLAB, COMSOL, 2008.

62. C. Ajluni, *Electronic Design*, 1995, **43**, 42-44.

63. J. Cheng, M. A. Shoffner, G. E. Hvichia, L. J. Kricka and P. Wilding, *Nucleic Acids Research*, 1996, **24**, 380-385.

64. A. T. Woolley, D. Hadley, P. Landre, A. J. deMello, R. A. Mathies and M. A. Northrup, *Analytical Chemistry*, 1996, **68**, 4081-4086.

65. S. C. Jacobson and J. M. Ramsey, *Electrophoresis*, 1995, **16**, 481-486.

66. H. Nakanishi, T. Nishimoto, A. Arai, H. Abe, M. Kanai, Y. Fujiyama and T. Yoshida, *Electrophoresis*, 2001, **22**, 230-234.

67. K. R. Iler, *The Chemistry of Silica*, John Wiley & Sons, INC., New York, 1979.

68. J. Horvath and V. Dolnik, *Electrophoresis*, 2001, **22**, 644-655.

69. B. C. Giordano, E. R. Copeland and J. P. Landers, *Electrophoresis*, 2001, **22**, 334-340.

70. S. R. Quake and A. Scherer, *Science*, 2000, **290**, 1536-1540.

71. L. Martynova, L. E. Locascio, M. Gaitan, G. W. Kramer, R. G. Christensen and W. A. MacCrehan, *Analytical Chemistry*, 1997, **69**, 4783-4789.

72. J. H. Chan, A. T. Timperman, D. Qin and R. Aebersold, *Analytical Chemistry*, 1999, **71**, 4437-4444.

73. C. Li, Y. N. Yang, H. G. Craighead and K. H. Lee, *Electrophoresis*, 2005, **26**, 1800-1806.

74. B. A. Fogarty, K. E. Heppert, T. J. Cory, K. R. Hulbutta, R. S. Martin and S. M. Lunte, *Analyst*, 2005, **130**, 924-930.

75. T. Koerner, L. Brown, R. X. Xie and R. D. Oleschuk, *Sensors and Actuators B-Chemical*, 2005, **107**, 632-639.

76. I. Grabowska, D. Stadnik, M. Chudy, A. Dybko and Z. Brzozka, *Sensors and Actuators B-Chemical*, 2007, **121**, 445-451.

77. A. Muck and A. Svatos, *Talanta*, 2007, **74**, 333-341.

78. J. Sibarani, M. Takai and K. Ishihara, *Colloids and Surfaces B-Biointerfaces*, 2007, **54**, 88-93.

79. S. L. Llopis, J. Osiri and S. A. Soper, *Electrophoresis*, 2007, **28**, 984-993.
80. K. Obata, K. Sugioka, N. Shimazawa and K. Midorikawa, *Applied Physics a-Materials Science & Processing*, 2006, **84**, 251-255.
81. T. Rohr, D. F. Ogletree, F. Svec and J. M. J. Frechet, *Advanced Functional Materials*, 2003, **13**, 264-270.
82. D. R. Absolom, W. Zingg and A. W. Neumann, *Journal of Biomedical Materials Research*, 1987, **21**, 161-171.
83. G. L. Kenausis, J. Voros, D. L. Elbert, N. P. Huang, R. Hofer, L. Ruiz-Taylor, M. Textor, J. A. Hubbell and N. D. Spencer, *Journal of Physical Chemistry B*, 2000, **104**, 3298-3309.
84. M. P. Richards, *Journal of Chromatography B-Biomedical Applications*, 1994, **657**, 345-355.
85. Y. Wang and P. L. Dubin, *Analytical Chemistry*, 1999, **71**, 3463-3468.
86. C. Stathakis, E. A. Arriaga, D. F. Lewis and N. J. Dovichi, *Journal of Chromatography A*, 1998, **817**, 227-232.
87. E. O. Machiste and G. Buckton, *International Journal of Pharmaceutics*, 1996, **145**, 197-201.
88. F. Q. Dang, K. Kakehi, J. J. Cheng, O. Tabata, M. Kurokawa, K. Nakajima, M. Ishikawa and Y. Baba, *Analytical Chemistry*, 2006, **78**, 1452-1458.
89. B. L. Karger and A. S. Cohen, Univ, Northeastern (US) US, 1989.
90. M. Gilges, M. H. Kleemiss and G. Schomburg, *Analytical Chemistry*, 1994, **66**, 2038-2046.
91. H. J. Tian and J. P. Landers, *Analytical Biochemistry*, 2002, **309**, 212-223.
92. M. Pumera, J. Wang, E. Grushka and R. Polsky, *Analytical Chemistry*, 2001, **73**, 5625-5628.
93. M. Suzuki, A. Kishida, H. Iwata and Y. Ikada, *Macromolecules*, 1986, **19**, 1804-1808.
94. M. L. Steen, A. C. Jordan and E. R. Fisher, *Journal of Membrane Science*, 2002, **204**, 341-357.
95. E. A. S. Doherty, R. J. Meagher, M. N. Albarghouthi and A. E. Barron, *Electrophoresis*, 2003, **24**, 34-54.
96. J. C. Giddings, *Unified Separation Science*, John Wiley & Sons, INC., New York, 1991.
97. D. DeVoe and C. S. Lee, *Multidimensional Microfluidic Systems for Protein and Peptide Separations*, CRC Press Taylor & Francis Group, Boa Raton, 2008.
98. J. C. Giddings, *Analytical Chemistry*, 1984, **56**, 1258-&.
99. P. G. Righetti, C. Simo, R. Sebastiano and A. Citterio, *Electrophoresis*, 2007, **28**, 3799-3810.
100. A. Gorg, C. Obermaier, G. Boguth and W. Weiss, *Electrophoresis*, 1999, **20**, 712-717.
101. B. Bjellqvist, K. Ek, P. G. Righetti, E. Gianazza, A. Gorg, R. Westermeier and W. Postel, *Journal of Biochemical and Biophysical Methods*, 1982, **6**, 317-339.
102. A. Gorg, W. Postel and S. Gunther, *Electrophoresis*, 1988, **9**, 531-546.
103. A. Gorg, C. Obermaier, G. Boguth, A. Harder, B. Scheibe, R. Wildgruber and W. Weiss, *Electrophoresis*, 2000, **21**, 1037-1053.

104. H. C. Cui, K. Horiuchi, P. Dutta and C. F. Ivory, *Analytical Chemistry*, 2005, **77**, 7878-7886.
105. D. Garfin and S. Ahuja, *Handbook of Isoelectric Focusing and Proteomics*, Elsevier Acadamic Press, Amsterdam, 2005.
106. C. Yang, H. C. Liu, Q. Yang, L. Y. Zhang, W. B. Zhang and Y. K. Zhang, *Analytical Chemistry*, 2003, **75**, 215-218.
107. J. W. Albrecht and K. F. Jensen, *Electrophoresis*, 2006, **27**, 4960-4969.
108. Z. Demianova, M. Shimmo, E. Poysa, S. Franssila and M. Baumann, *Electrophoresis*, 2007, **28**, 422-428.
109. Y. C. Wang, M. N. Choi and J. Y. Han, *Analytical Chemistry*, 2004, **76**, 4426-4431.
110. C. Das, J. Zhang, N. D. Denslow and Z. H. Fan, *Lab on a Chip*, 2007, **7**, 1806-1812.
111. D. Mohan and C. S. Lee, *Electrophoresis*, 2002, **23**, 3160-3167.
112. Y. Mao, Y. Li and X. M. Zhang, *Proteomics*, 2006, **6**, 420-426.
113. F. Zhou and M. V. Johnston, *Analytical Chemistry*, 2004, **76**, 2734-2740.
114. Y. J. Wang, B. M. Balgley and C. S. Lee, *Expert Review of Proteomics*, 2005, **2**, 659-667.
115. J. Z. Chen, C. S. Lee, Y. F. Shen, R. D. Smith and E. H. Baehrecke, *Electrophoresis*, 2002, **23**, 3143-3148.
116. F. Giorgianni, D. M. Desiderio and S. Beranova-Giorgianni, *Electrophoresis*, 2003, **24**, 253-259.
117. Q. Tang, A. K. Harrata and C. S. Lee, *Analytical Chemistry*, 1995, **67**, 3515-3519.
118. X. X. Chen, H. K. Wu, C. D. Mao and G. M. Whitesides, *Analytical Chemistry*, 2002, **74**, 1772-1778.
119. L. M. Fu, R. J. Yang, G. B. Lee and H. H. Liu, *Analytical Chemistry*, 2002, **74**, 5084-5091.
120. S. krishnamoorthy and M. G. Giridharan, 2000.
121. S. C. Jacobson, R. Hergenroder, L. B. Koutny, R. J. Warmack and J. M. Ramsey, *Analytical Chemistry*, 1994, **66**, 1107-1113.
122. B. W. Wenclawiak and R. Puschl, *Analytical Letters*, 2006, **39**, 3-16.
123. G. S. Zhuang, G. Li, Q. H. Jin, J. L. Zhao and M. S. Yang, *Electrophoresis*, 2006, **27**, 5009-5019.
124. D. Erickson, *Microfluidics and Nanofluidics*, 2005, **1**, 301-318.
125. D. A. Wolters, M. P. Washburn and J. R. Yates, *Analytical Chemistry*, 2001, **73**, 5683-5690.
126. C. T. Culbertson, S. C. Jacobson and J. M. Ramsey, *Analytical Chemistry*, 1998, **70**, 3781-3789.
127. J. I. Molho, A. E. Herr, B. P. Mosier, J. G. Santiago, T. W. Kenny, R. A. Brennen, G. B. Gordon and B. Mohammadi, *Analytical Chemistry*, 2001, **73**, 1350-1360.
128. Y. Wang, Q. A. Lin and T. Mukherjee, *Lab on a Chip*, 2004, **4**, 453-463.
129. B. M. Paegel, L. D. Hutt, P. C. Simpson and R. A. Mathies, *Analytical Chemistry*, 2000, **72**, 3030-3037.
130. R. S. Lin, D. T. Burke and M. A. Burns, *Analytical Chemistry*, 2005, **77**, 4338-4347.
131. D. P. J. Barz and P. Ehrhard, *Lab on a Chip*, 2005, **5**, 949-958.

132. K. Ueno, H. B. Kim and N. Kitamura, *Analytical Sciences*, 2003, **19**, 391-394.
133. L. M. Fu, R. J. Yang and G. B. Lee, *Electrophoresis*, 2002, **23**, 602-612.
134. W. Thormann and R. A. Mosher, *Electrophoresis*, 2006, **27**, 968-983.
135. W. Thormann, T. M. Huang, J. Pawliszyn and R. A. Mosher, *Electrophoresis*, 2004, **25**, 324-337.
136. R. A. Mosher and W. Thormann, *Electrophoresis*, 2002, **23**, 1803-1814.
137. S. H. Kim, R. Otani, W. Shirai, N. Shibasaki-Kitakawa, A. Kitakawa and T. Yonemoto, *Kagaku Kogaku Ronbunshu*, 2001, **27**, 174-180.
138. Q. L. Mao, J. Pawliszyn and W. Thormann, *Analytical Chemistry*, 2000, **72**, 5493-5502.
139. M. Bier, R. A. Mosher and O. A. Palusinski, *Journal of Chromatography*, 1981, **211**, 313-335.
140. T. L. Sounart and J. C. Baygents, *Journal of Chromatography A*, 2000, **890**, 321-336.
141. M. Pribyl, D. Snita and M. Kubicek, *Computers & Chemical Engineering*, 2006, **30**, 674-685.
142. R. R. Lamonte and D. McNally, *Advanced Materials & Processes*, 2001, **159**, 33-36.
143. C. A. Harper, *Modern Plastics Handbook*, McGraw-Hill, New York, 2000.
144. Z. F. Chen, Y. H. Gao, R. G. Su, C. W. Li and J. M. Lin, *Electrophoresis*, 2003, **24**, 3246-3252.
145. C. W. Tsao, L. Hromada, J. Liu, P. Kumar and D. L. DeVoe, *Lab on a Chip*, 2007, **7**, 499-505.
146. U. Schulz, P. Munzert and N. Kaiser, *Surface & Coatings Technology*, 2001, **142**, 507-511.
147. E. M. Liston, *Journal of Adhesion*, 1989, **30**, 199-218.
148. D. Hegemann, H. Brunner and C. Oehr, *Nuclear Instruments & Methods in Physics Research Section B-Beam Interactions with Materials and Atoms*, 2003, **208**, 281-286.
149. H. Lim, Y. Lee, S. Han, J. Cho and K. J. Kim, *Journal of Vacuum Science & Technology a-Vacuum Surfaces and Films*, 2001, **19**, 1490-1496.
150. R. Bellandi, *Innovative Engineering Technologies for Hazardous Waste Remediation*, Van Nostrand Reinhold, New York, 1995.
151. B. D. Hames and D. Rickwood, *Gel Electrophoresis of Proteins*, Oxford University Press, Oxford, 1998.
152. S. Hjerten and M. D. Zhu, *Journal of Chromatography*, 1985, **346**, 265-270.
153. K. A. Cobb, V. Dolnik and M. Novotny, *Analytical Chemistry*, 1990, **62**, 2478-2483.
154. K. Srinivasan, G. Pohl and N. Avdalovic, *Analytical Chemistry*, 1997, **69**, 2798-2805.
155. L. Gao and S. R. Liu, *Analytical Chemistry*, 2004, **76**, 7179-7186.
156. P. G. Righetti, C. Gelfi and M. Conti, *Journal of Chromatography B*, 1997, **699**, 91-104.
157. S. R. Liu, H. J. Ren, Q. F. Gao, D. J. Roach, R. T. Loder, T. M. Armstrong, Q. L. Mao, I. Blaga, D. L. Barker and S. B. Jovanovich, *Proceedings of the National Academy of Sciences of the United States of America*, 2000, **97**, 5369-5374.

158. M. X. Huang, W. P. Vorkink and M. L. Lee, *Journal of Microcolumn Separations*, 1992, **4**, 233-238.
159. S. R. Liu, L. Gao, Q. S. Pu, J. J. Lu and X. J. Wang, *Journal of Proteome Research*, 2006, **5**, 323-329.
160. R. Westermeier and T. Naven, *Proteomics in Practice*, Wiley-VCH Verlag-GmbH, Weinheim, Germany, 2002.
161. S. Song, A. K. Singh and B. J. Kirby, *Analytical Chemistry*, 2004, **76**, 4589-4592.
162. A. E. Herr, A. V. Hatch, D. J. Throckmorton, H. M. Tran, J. S. Brennan, W. V. Giannobile and A. K. Singh, *Proceedings of the National Academy of Sciences of the United States of America*, 2007, **104**, 5268-5273.
163. A. E. Herr and A. K. Singh, *Analytical Chemistry*, 2004, **76**, 4727-4733.
164. C. Das, C. K. Fredrickson, Z. Xia and Z. H. Fan, *Sensors and Actuators a-Physical*, 2007, **134**, 271-277.
165. M. M. Bradford, *Analytical Biochemistry*, 1976, **72**, 248-254.
166. Y. Li, J. S. Buch, F. Rosenberger, D. L. DeVoe and C. S. Lee, *Anal. Chem.*, 2004, **76**, 742-748.
167. J. M. Peng, J. E. Elias, C. C. Thoreen, L. J. Licklider and S. P. Gygi, *Journal of Proteome Research*, 2003, **2**, 43-50.
168. T. Rabilloud, *Proteome Research: Two-Dimensional Gel Eelctrophoresis and Identification Methods*, Springer, Berlin, 2000.
169. T. Rabilloud, *Analytical Chemistry*, 2000, **72**, 48A-55A.
170. A. Hiratsuka, H. Kinoshita, Y. Maruo, K. Takahashi, S. Akutsu, C. Hayashida, K. Sakairi, K. Usui, K. Shiseki, H. Inamochi, Y. Nakada, K. Yodoya, I. Namatame, Y. Unuma, M. Nakamura, K. Ueyama, Y. Ishii, K. Yano and K. Yokoyama, *Analytical Chemistry*, 2007, **79**, 5730-5739.
171. M. B. Mellott, K. Searcy and M. V. Pishko, *Biomaterials*, 2001, **22**, 929-941.
172. G. Giammona, G. Pitarresi, E. F. Craparo, G. Cavallaro and S. Buscemi, *Colloid and Polymer Science*, 2001, **279**, 771-783.
173. C. F. Ivory, *Electrophoresis*, 2007, **28**, 15-25.
174. H. Y. Tang, N. Ali-Khan, L. A. Echan, N. Levenkova, J. J. Rux and D. W. Speicher, *Proteomics*, 2005, **5**, 3329-3342.
175. R. M. McCormick, R. J. Nelson, M. G. AlonsoAmigo, J. Benvegnu and H. H. Hooper, *Analytical Chemistry*, 1997, **69**, 2626-2630.
176. R. D. Rocklin, R. S. Ramsey and J. M. Ramsey, *Analytical Chemistry*, 2000, **72**, 5244-5249.
177. N. Gottschlich, S. C. Jacobson, C. T. Culbertson and J. M. Ramsey, *Analytical Chemistry*, 2001, **73**, 2669-2674.
178. H. Becker, K. Lowack and A. Manz, *Journal of Micromechanics and Microengineering*, 1998, **8**, 24-28.
179. J. K. Liu, S. Yang, C. S. Lee and D. L. DeVoe, *Electrophoresis in press*, 2008.
180. S. C. Jacobson and J. M. Ramsey, *Analytical Chemistry*, 1997, **69**, 3212-3217.
181. C. S. Effenhauser, A. Paulus, A. Manz and H. M. Widmer, *Analytical Chemistry*, 1994, **66**, 2949-2953.
182. L. M. Fu, R. J. Yang, G. B. Lee and Y. J. Pan, *Electrophoresis*, 2003, **24**, 3026-3032.

183.   Y. J. Pan, J. J. Lin, W. J. Luo and R. J. Yang, *Biosensors & Bioelectronics*, 2006, **21**, 1644-1648.
184.   K. S. Schmitz and M. Lu, *Proceedings of the National Academy of Sciences of the United States of America-Biological Sciences*, 1983, **80**, 425-429.
185.   J. M. Hille, A. L. Freed and H. Watzig, *Electrophoresis*, 2001, **22**, 4035-4052.
186.   M. P. Washburn, D. Wolters and J. R. Yates, *Nature Biotechnology*, 2001, **19**, 242-247.
187.   C. A. Emrich, I. L. Medintz, W. K. Chu and R. A. Mathies, *Analytical Chemistry*, 2007, **79**, 7360-7366.
188.   S. Yang, J. K. Liu and D. L. DeVoe, *Lab on a Chip in press*, 2008.
189.   S. Hu, L. Zhang, L. M. Cook and N. J. Dovichi, *Electrophoresis*, 2001, **22**, 3677-3682.
190.   D. B. Craig, P. M. Polakowski, E. Arriaga, J. C. Y. Wong, H. Ahmadzadeh, C. Stathakis and N. J. Dovichi, *Electrophoresis*, 1998, **19**, 2175-2178.
191.   A. T. Andrews, *Electrophoresis*, Claredon Press, Oxford, England, 1986.
192.   J. J. Lu, S. R. Liu and Q. S. Pu, *Journal of Proteome Research*, 2005, **4**, 1012-1016.
193.   A. E. Herr, D. J. Throckmorton, A. A. Davenport and A. K. Singh, *Analytical Chemistry*, 2005, **77**, 585-590.
194.   B. J. Kirby, A. R. Wheeler, R. N. Zare, J. A. Fruetel and T. J. Shepodd, *Lab on a Chip*, 2003, **3**, 5-10.
195.   O. Smithies, *Archives of Biochemistry and Biophysics*, 1962, 125-131.
196.   D. L. Holmes and N. C. Stellwagen, *Electrophoresis*, 1991, **12**, 612-619.
197.   J. A. Reynolds and C. Tanford, *Proceedings of the National Academy of Sciences of the United States of America*, 1970, **66**, 1002-1007.
198.   U. K. Laemmli, *Nature*, 1970, **227**, 680-685.
199.   L. Ornstein, *Annals of the New York Academy of Sciences*, 1964, **121**, 321-349.
200.   B. J. Davis, *Annals of the New York Academy of Sciences*, 1964, **121**, 404-427.
201.   T. Palzkill, *Proteomics*, Kluwer Academic Publishers, Boston, 2002.
202.   M. Baltz-Knorr, D. R. Ermer, K. E. Schriver and R. F. Haglund, *Journal of Mass Spectrometry*, 2002, **37**, 254-258.
203.   Y. C. Xu, M. W. Little, D. J. Rousell, J. L. Laboy and K. K. Murray, *Analytical Chemistry*, 2004, **76**, 1078-1082.
204.   R. R. O. Loo, T. I. Stevenson, C. Mitchell, J. A. Loo and P. C. Andrews, *Analytical Chemistry*, 1996, **68**, 1910-1917.